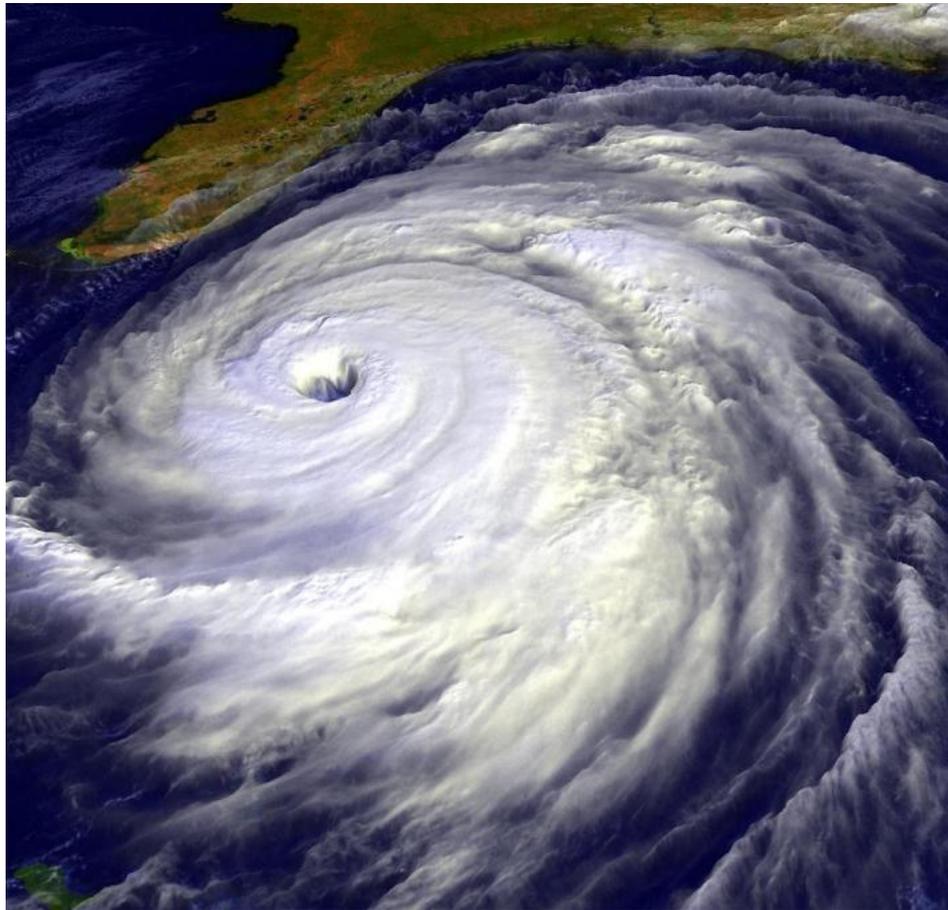Utrecht University

Deltares
Enabling Delta Life

Numerical computation of hurricane-induced saltwater intrusion on fresh groundwater availability in peninsular Florida under different climate scenarios

MSc thesis

Author
Thijs Hendrikx
Student number: 4162498

Supervisors
dr.ir. Gualbert Oude Essink
dr. Derek Karssenberg

MSc programme: Earth Surface and Water
Utrecht University

December 2020

Abstract

Climate change is generally expected to influence hurricane behaviour by supercharging hurricanes through increasingly warmer and moister environments (Trenberth et al., 2018). Climate change projections indicate relatively more extreme hurricane events (Knutson et al., 2015), higher storm-surge values (Lin et al., 2012) and suggest that contemporary storm surge hazard zones could extend further inland while taking sea-level rise into account (Frazier et al., 2010). As storm surge can induce saltwater intrusion into the groundwater system, climate change can threaten fresh groundwater availability in already vulnerable coastal aquifer systems even more. For example, coastal aquifers in south-eastern Florida have been put under increasing pressure due to saltwater intrusion (Sonenshein, 1997). As Florida is more likely to get hit by hurricanes than any other state in the United States (Malmstadt et al., 2009), storm surge increases could have far-reaching consequences in Florida. Due to the vital importance of fresh groundwater availability for population, agriculture and nature, it is important to gain knowledge on the effect of possible climate scenarios on fresh groundwater availability. In this thesis, the following main research question is addressed: How does hurricane-induced saltwater intrusion affect fresh groundwater availability in peninsular Florida under different climate scenarios? To answer this question, a three-dimensional variable-density groundwater flow and coupled salt transport model was developed in iMOD-SEAWAT (i.e. SEAWAT in an iMOD setting; the GUI of MODFLOW by Deltares (Vermeulen et al., 2018)), and climate scenarios were simulated that consist of different hurricane intensities, peak rainfall rates and sea-level rise projections. Model simulations indicate that hurricane intensity has the most pronounced effect on saltwater intrusion and is amplified when sea-level rise projections are considered. Also, the study shows that the surficial aquifer system can nearly always recover in time before another hurricane and related storm surge will strike the shore. However, if the hurricane return period becomes smaller than the flushing period due to climate change, the surficial aquifer system will be put under increasing pressure. Then, this research indicates that strategies that mitigate and reverse saltwater intrusion should be considered timely and carefully. Due to limitations regarding the hurricane-induced storm surge calculations and the hydrogeological model, the findings of this research should be used as an indication of the impact of climate scenarios on fresh groundwater availability. Future research should investigate whether the findings can be reproduced with an accurate storm surge model. Furthermore, climate change effects on hurricane return periods for vulnerable areas should be analysed too.

Acknowledgements

At the beginning of this MSc thesis, I would like to express my gratitude to everyone involved in the project, both directly and indirectly for the support they have given.

First of all, I would like to thank my first supervisor, Gualbert Oude Essink, for his guidance and visions in constructing the models and his views on the thesis; his insightful feedback and enthusiasm brought my work to a higher level. Despite his busy schedule, he was always very interested and supportive, ready to think along and answer my questions. I am very grateful for the many conversations with him in person at the office of Deltares before the pandemic, and the mails, Skype meetings and telephone calls from trains with dropping connection during the pandemic.

I would like to thank Derek Karssenberg for being the second supervisor and reviewing the thesis.

I am also grateful to my brother Niels Hendrikx and Christiaan van Dalum for the feedback on my python scripts and discussions on the thesis.

At last, I want to thank my parents and friends for their support and understanding throughout the thesis.

Table of Contents

List of Figures

List of Tables

1. Introduction

Fresh groundwater resources are essential for coastal populations, since more than 60% of the world's population is living within 100 km of shorelines where fresh groundwater is used for drinking, domestic, irrigation and industrial purposes (Yang et al., 2013). Its presence is of great importance in sustaining economies by contributing to growth and prosperity (Barlow, 2003). However, coastal fresh groundwater resources have been put under increasing pressure due to overexploitation and contamination by saltwater intrusion (Barlow and Reichard, 2010).

1.1. Background

Saltwater intrusion is a natural phenomenon describing the movement of saline water into a freshwater aquifer that can lead to a variety of problems including deterioration of groundwater quality, land salinization and ecosystem degradation (Xiao et al., 2018). Saltwater intrusion can be induced for example by fresh groundwater withdrawals, sea-level rise and hurricane-induced storm surges (Elsayed and Oumeraci, 2018). Sea-level rise and storm surge are linked to climate change. For instance, climate change is generally expected to influence hurricane behaviour by supercharging hurricanes through increasingly warmer and moister environments (Trenberth et al., 2018). Climate change projections predict relatively more extreme hurricane events (Knutson et al., 2015), higher storm-surge values (Lin et al., 2012) and suggest that contemporary storm surge hazard zones could extend further inland while taking sea-level rise into account (Frazier et al., 2010). As storm surge can induce saltwater intrusion into the groundwater system, climate change can threaten fresh groundwater availability in already vulnerable coastal aquifer systems even more. For example, coastal aquifers in south-eastern peninsular Florida have already been put under increasing pressure due to saltwater intrusion (Sonenshein, 1997). As Florida is more likely to become hit by hurricanes than any other state in the United States with return periods of severe hurricanes (categories 3 to 5 on the Saffir-Simpson scale) as short as 13 years in peninsular Florida (Keim et al., 2007; Malmstadt et al., 2009), storm surge increases could have far-reaching consequences in the Florida peninsula. Due to the vital importance of fresh groundwater availability for population, agriculture and nature, it is important to gain knowledge on possible climate scenarios. For instance, the range of its effects can be used for water management strategies: groundwater and surface water withdrawals can be modified and engineered structures can be used to mitigate future impacts of saltwater intrusion (White and Kaplan, 2017).

1.2. Research objective and questions

The main objective of this research is to provide knowledge and insight into consequences of hurricane-induced saltwater intrusion on fresh groundwater availability in peninsular Florida under different climate scenarios. In order to fulfil the research objective, the following main research question was formulated:

How does hurricane-induced saltwater intrusion affect fresh groundwater availability in peninsular Florida under different climate scenarios?

This research question was divided into several sub-questions:

1. How does hurricane-induced saltwater intrusion affect fresh groundwater availability under different hurricane intensities?
2. How does hurricane-induced saltwater intrusion affect fresh groundwater availability under different hurricane peak rainfall rates?
3. How do consequences of hurricane scenarios change when sea-level rise projections are considered?

1.3. Overview

Firstly, a literature review will be presented in which the physical processes are discussed as well as the hydrogeology of peninsular Florida and the modelling software. Afterwards, the methodology will be discussed, followed by the results and the discussion and conclusion.

2. Literature review

To gain knowledge on consequences of climate change on hurricane-induced saltwater intrusion, the general physical processes of saltwater intrusion and storm surge are discussed in this chapter. In addition, an extensive overview of the Floridan hydrogeology is presented to construct the three-dimensional variable-density groundwater flow and coupled salt transport model of the study-area. To gain understanding of the modelling software iMOD-SEAWAT, background theory is given in combination with common approaches to simulate hurricanes into these groundwater models.

2.1. Physical processes

2.1.1. Saltwater intrusion

In coastal aquifers without human activities, fresh groundwater forms a balance (i.e. hydrostatic equilibrium) with saline groundwater. Due to the direction of groundwater flow towards the sea, fresh groundwater is supplied from the inland to the coastal zone. This process can be explained by the present hydraulic gradient: the inland hydraulic heads exceed coastal hydraulic heads due to elevation differences. As groundwater flow is in the direction of the decreasing hydraulic head, fresh groundwater flows from land to sea. Subsequently, fresh groundwater meets saline groundwater that origins from the sea. Due to the higher salinity of saline groundwater than fresh groundwater, another gradient comes into play – the so-called concentration gradient – that causes heavier saline groundwater to flow below the fresh groundwater. As fresh groundwater is less dense than saline groundwater, fresh groundwater will 'float' on top. The result is a dynamical equilibrium between both water bodies that depends on many factors and is prone to change, whilst maintaining a characteristic wedge-shaped transition zone (see Figure 1). In this transition zone, fresh groundwater gradually transitions into saline groundwater due to molecular diffusion and mechanical dispersion, processes that mix the water bodies (Barlow, 2003). By means of simplicity, the transition zone can be assumed to be a sharp boundary (the so-called fresh-saline groundwater interface, see Figure 2). Subsequently, if one assumes hydrostatic conditions, the depth of this conceptual interface can be calculated with the Badon Ghijben-Herzberg equation (see Equation 1). This equation relates the thickness of the fresh groundwater zone above sea-level (h) to the thickness of the zone below sea-level (z) using the densities of freshwater and saline water (Barlow, 2003). This conceptual model, however, is simplified. Therefore, its outcomes should be regarded as an approximation.

The hydrostatic equilibrium between freshwater and saline water zones can change due to natural and anthropogenic factors. If saline water moves into a freshwater aquifer, saltwater intrusion occurs. There are two main types of saltwater intrusion: lateral saltwater intrusion and vertical saltwater intrusion that are described in the following subsections.

$$z = \frac{\rho_f}{\rho_s - \rho_f} * h = 40 * h$$

Equation 1: Badon Ghijben-Herzberg equation, adapted from Barlow (2003).
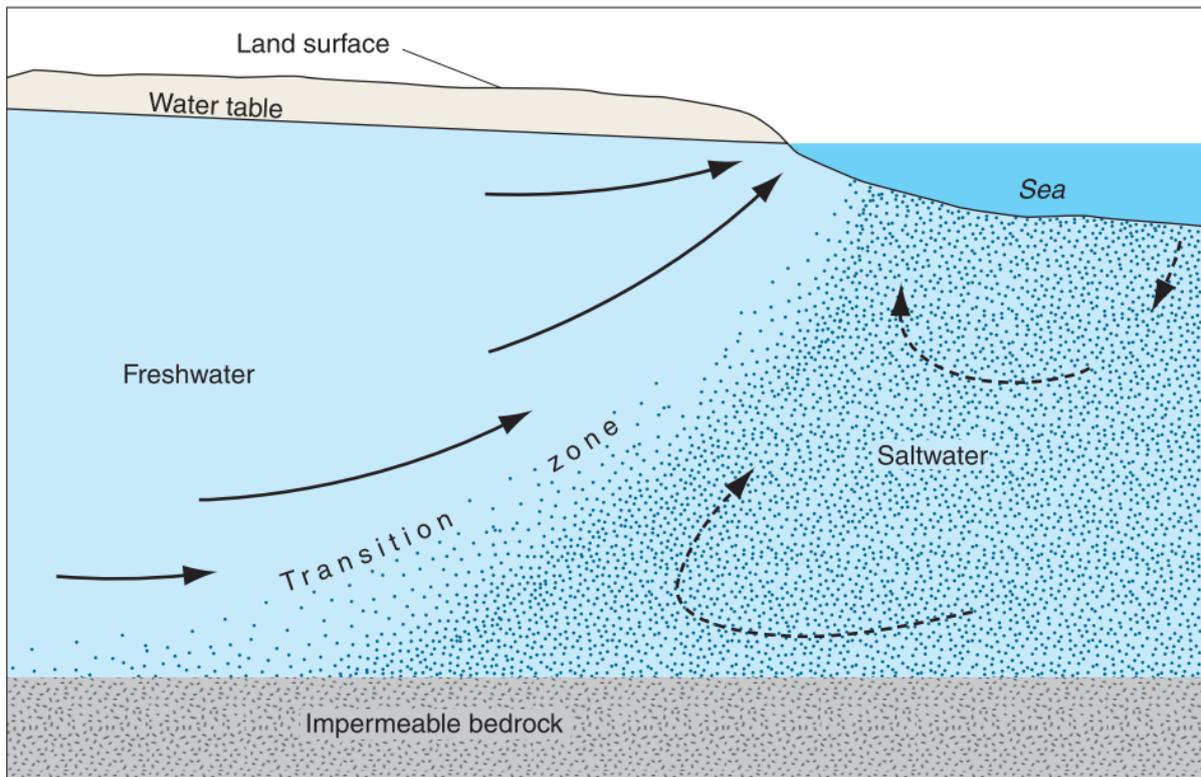
Figure 1: The fresh and saline groundwater bodies gradually transition in the so-called transition zone. This zone does not consist of a simplified sharp boundary (figure by Barlow (2003)).
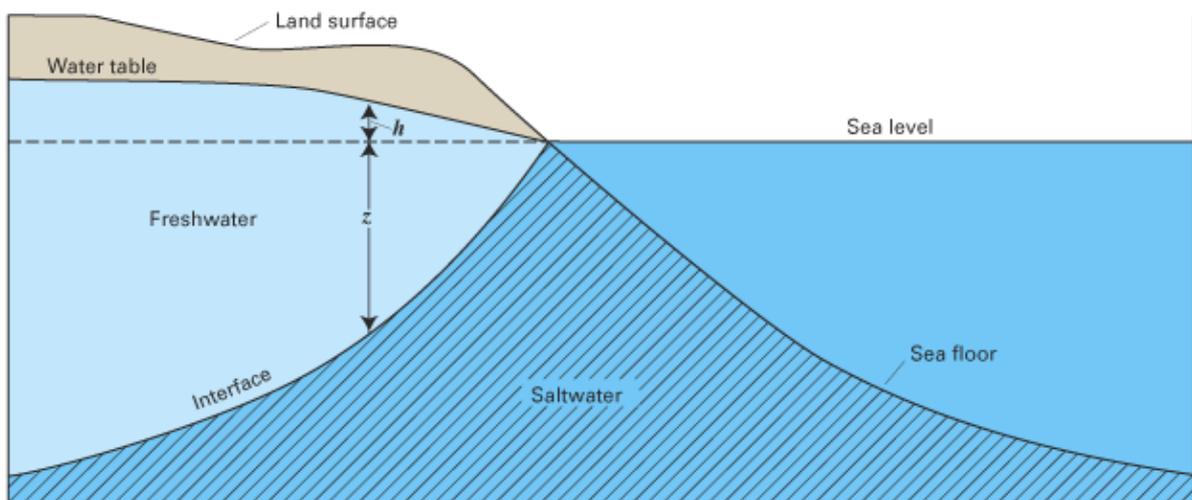
Figure 2: The conceptual fresh-saline groundwater interface showing the fresh groundwater zone thickness above sea-level (h) and the thickness below sea-level (z) that form the input of the Badon Ghijben-Herzberg equation (figure by Barlow (2003)).

2.1.1.1.   Lateral saltwater intrusion

The first type is lateral saltwater intrusion in which the fresh-saline groundwater interface changes laterally and moves inward. According to Elsayed and Oumeraci (2018) lateral saltwater intrusion can be the result of three types of processes: long-term sea-level rise, groundwater table decreases and upconing. For example, long-term sea-level rises would result in an increased pressure head at the seaside boundary of a coastal aquifer (Sherif and Singh, 1999). Because of the additional pressure head that is applied, the hydrostatic equilibrium will change, and new equilibria will develop with the fresh-saline groundwater interface located more inward (see Figure 3).
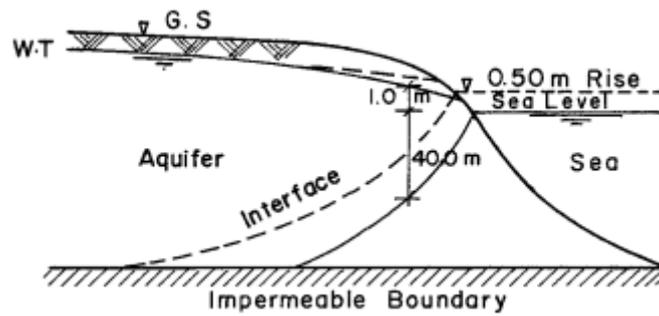
Figure 3: Sea-level rise effect on a fresh-saline groundwater interface (figure by Sherif and Singh (1999)).

Also, human activities such as excessive groundwater pumping and land drainage (e.g. in south-eastern Florida) reduce the groundwater table and the natural groundwater flow to the coast (Barlow, 2003). Hereby, the fresh groundwater pressure head decreases, allowing saline groundwater to intrude the coastal aquifer. The same relationship can be observed when precipitation decreases due to climate change effects (Elsayed and Oumeraci, 2018).

2.1.1.2. *Vertical saltwater intrusion*

The second type considers saltwater intrusion that occurs in the vertical direction. This type of saltwater intrusion can be induced for instance by pumping of groundwater from freshwater aquifers. As a result, saline groundwater underlying the freshwater zone rises upward (this process is often regarded as 'upconing'). In addition, vertical saltwater intrusion can be induced by coastal inundation. In the case of such an event (i.e. storm surges, marine transgression), saline surface water ends up on the land surface where it diffuses into the soil (Yan et al., 2019). When this happens, a density gradient comes into play: 'heavier' saline water resides on top of the 'less dense' freshwater and thus forming an unstable density stratification. In other words, saline water 'wants' to move below the freshwater. Due to density differences, small convective (i.e. unstable) waves start to form in the saline boundary layer (Wooding et al., 1997). Subsequently – once the layer reaches a certain critical thickness – the layer breaks into so-called fingers (i.e. finger instabilities) under the influence of gravity (Yan et al., 2019). The fingers are narrow 'plumes' or 'lobes' of saline water migrating downward, counterbalanced by freshwater moving upward (Ketabchi et al., 2016; Kooi et al., 2000; Simmons et al., 1999). This process is described as convection in groundwater.

Convective flow features (i.e. fingers) can induce relatively more saltwater intrusion than one would expect from molecular diffusion and mechanical dispersion alone (Kooi et al., 2000). However, the exact extent of vertical saltwater intrusion in coastal aquifers (and its recovery) from overwash events is largely determined by the hydrogeological setting that can be defined as the recharge rate, vadose zone thickness, geological heterogeneities and hydraulic properties (Holding and Allen, 2015). For example, horizontally oriented geological heterogeneities with relatively higher hydraulic conductivities than the main aquifer materials can greatly limit saltwater intrusion (Holding and Allen, 2015). Due to the horizontal orientation of a highly permeable zone, saline water will discharge out of the subsurface along this zone, thereby protecting the underlying part of the aquifer from overwash effects (see Figure 4).
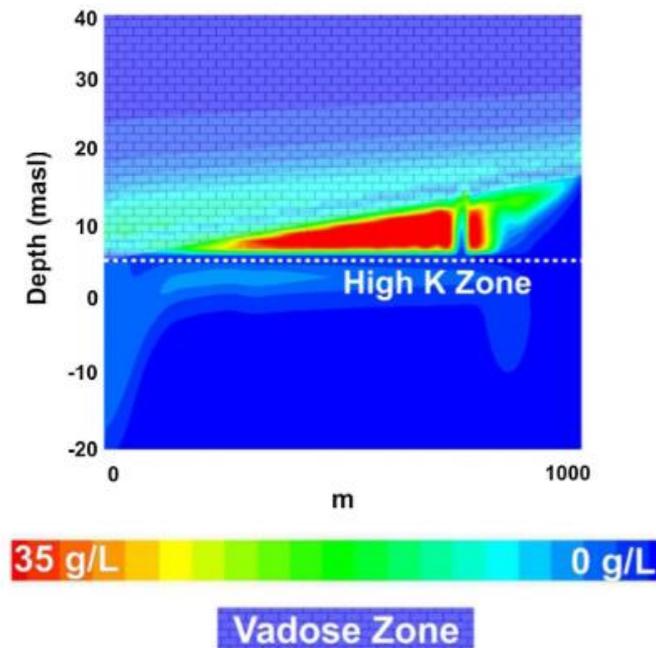
Figure 4: The effect of horizontally oriented geological heterogeneities on the saltwater intrusion extent: relatively higher hydraulic conductivities than the main aquifer materials can greatly limit vertical saltwater intrusion (figure adapted from Holding and Allen (2015)).

2.1.2. Hurricane-induced storm surge

Storm surge is defined as seawater level variations that arise from ocean-atmosphere interactions, i.e., the atmosphere exerts forces on the ocean, whereupon seawater level oscillations are generated. These forces are induced by atmospheric weather systems that pass over the surface of an ocean (Horsburgh et al., 2011). Hurricanes can be considered as rotating atmospheric weather systems with low-pressure centres that exert forces on the ocean surface (and thereby induce storm surge) by two main processes.

Low-pressure systems – such as the centre of a hurricane – are characterized by the rising of warm air. As warm air rises above the surface of an ocean, less atmospheric weight is exerted downward and thereby less force and pressure (NJSGC, 2019). Due to this atmospheric pressure gradient between the ocean's surface and the atmospheric weather system, seawater levels rise in the following manner: pressure reductions of 1 hPa involve seawater levels rises by approximately 1 cm. This process is called the 'inverse barometer effect' or static amplification of the storm surge (Horsburgh et al., 2011; NJSGC, 2019).

The second process considers wind-induced storm surge and forms the dynamic amplification of the storm surge; when a hurricane moves over an ocean, the accompanying winds exert a force (i.e. wind stress) on the ocean's surface. Subsequently, this process pushes seawater towards the coastal zone where the seawater starts to pile up causing the seawater levels to rise (Horsburgh et al., 2011). This process is responsible for the largest part of the storm surge (Horsburgh et al., 2011). When a hurricane makes landfall, one can distinguish between two main wind directions (onshore and offshore winds) dependent on the hurricane side (Figure 5). For example, in the northern hemisphere, onshore winds blow at the right of the hurricane centre path, whereas offshore winds blow at the left of the path (Needham and Keim, 2012). This difference affects the height of the storm surge as well: onshore winds involve higher seawater levels, whereas offshore winds involve lower seawater levels. Furthermore, storm surge levels will be highest close to hurricane centre and decrease with the distance from the path of the hurricane centre (Needham and Keim, 2012).

Alongside these two processes, hurricane-induced storm surge can be influenced by other factors as well, including the astronomical tide, wave setup and wave runup (Hughes, 2016).
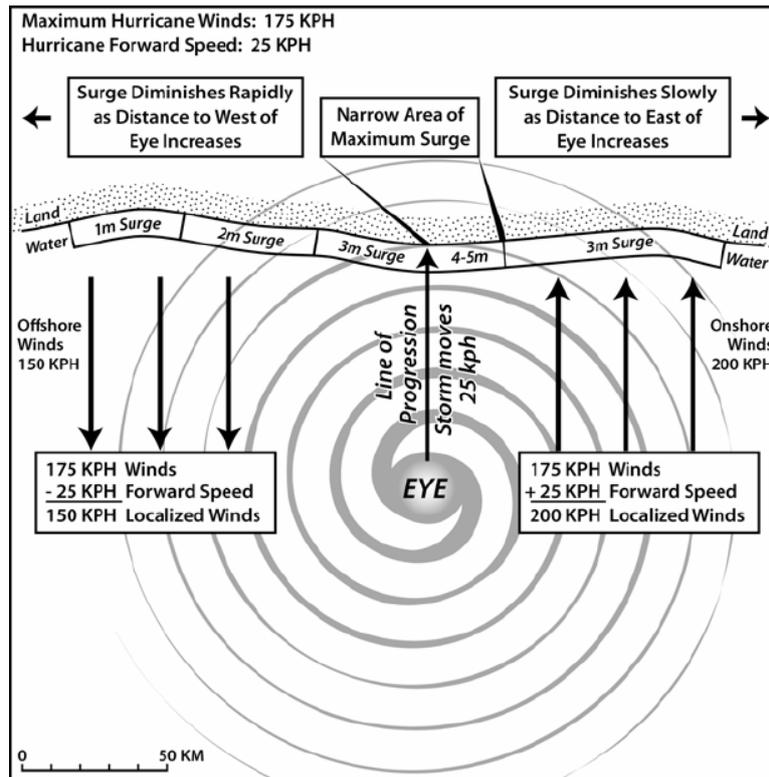
Figure 5: The hurricane-induced storm surge heights depend on wind directions and distance to the hurricane eye (figure by Needham and Keim (2012)).

During a hurricane event, the combination of atmospheric and ocean conditions (e.g. astronomical tide) determines the contribution of the abovementioned processes and thereby the total storm surge. These seawater level variations can be visualized in storm surge hydrographs that represent the rise and fall of seawater-levels with time as the hurricane moves over the hurricane-affected area. Cialone et al. (1993) presented a basic synthetic storm surge hydrograph that incorporates symmetric rising and falling limbs (Xu and Huang, 2014). An example of this basic hydrograph that excludes astronomical tide variations can be seen in Figure 6. Cialone's hydrograph represents the height of the storm surge as a function of time (t) and depends on the storm surge elevation peak height (see Equation 2). The parameter D represents half the storm duration and can be determined by dividing the radius of maximum winds (R) by the hurricane forward speed (F) (Equation 3). The radius of maximum winds is defined as the distance of the hurricane centre to the highest band of strongest winds and the forward speed of the hurricane is defined as the distance the hurricane travels with time. Lastly, the time of landfall and storm surge peak is defined by t_0.

$$H_{storm\ surge}(t) = H_{storm\ surge\ peak}\left(1 - e^{-|D/(t-t_0)|}\right)$$

Equation 2: Cialone's hydrograph equation (adapted from Cialone et al. (1993) and Xu and Huang (2014)).

$$D = \frac{R}{F}$$

Equation 3: Equation of half the storm duration (adapted from Cialone et al. (1993) and Xu and Huang (2014)).

Storm surge hydrograph
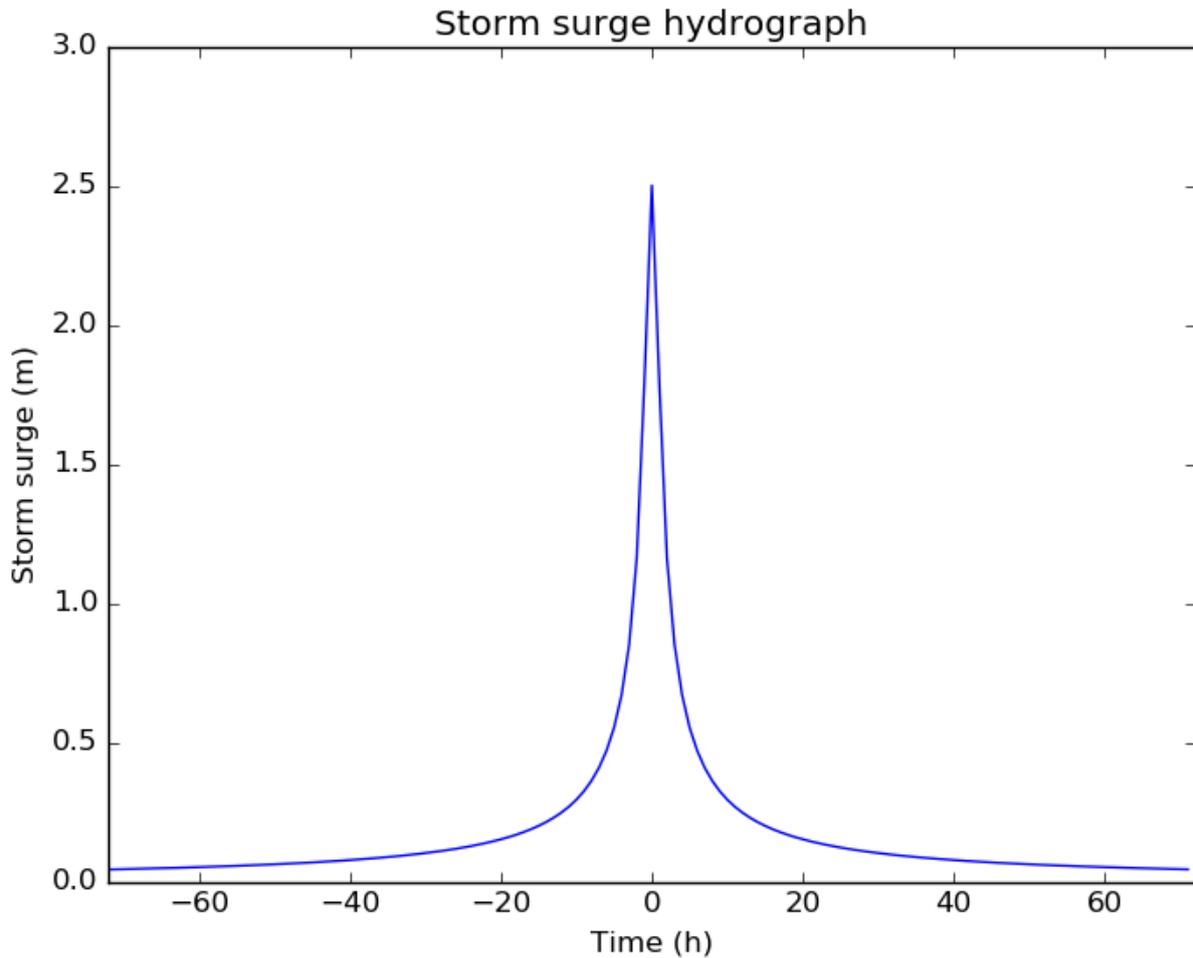
Figure 6: An example of Cialone's storm surge hydrograph with symmetric rising and falling limbs. The graph is obtained by using the following parameters: storm surge peak = 2.5m, hurricane radius of maximum winds = 25km, hurricane forward speed = 20 km/hr and the landfall time = 0 hr.

Since Cialone's hydrograph, several synthetic storm surge hydrographs have been developed. However, these synthetic hydrographs generally do not match hurricane-induced storm surge observations at the falling limbs of certain hurricane categories (e.g. categories 3 and 4 on the Saffir-Simpson scale) (Xu and Huang, 2014). Therefore, Xu and Huang developed a storm surge hydrograph that includes a different approach on the rising and falling limbs. In their research, Xu and Huang proposed an empirical four-parameter synthetic hydrograph with separate equations for the rising and falling limbs including correction parameter. By using this approach, the fitting between the storm surge hydrograph and the seawater level data improved.

2.1.3. Climate change and hurricanes

Over the last three decades, many researches were conducted on the potential influence of climate change on hurricanes. Although still under discussion, it is generally expected that climate change can affect hurricane frequency and intensity (Frazier et al., 2010; Trenberth et al., 2018). This can be explained by the expectation of climate change to lead to warmer and moister environments that 'supercharge' hurricanes. Based on assessments by Knutson et al. (2015), Knutti and Sedláček (2013) and Sobel et al. (2016), Trenberth et al. (2018) concluded that climate change can lead to fewer hurricanes, but also an increase in hurricane intensity (i.e. highest sustained wind speed to be found at the radius of maximum winds). In other words, relatively more 'extreme' hurricane events are expected to occur (i.e. category 4 and 5 on the Saffir-Simpson scale). Also hurricane activity – a broad term for hurricane characteristics such as frequency, size, duration, intensity and track – is expected to increase (Emanuel, 2013; Trenberth and Fasullo, 2008). Furthermore, hurricanes are expected to

slow down; the forward speed of North Atlantic hurricanes is expected to decrease with 20 percent over land areas (Kossin, 2018). As the hurricane forward speed is inversely proportional to the amount of hurricane-related rainfall, local hurricane-induced rainfall totals are expected to increase (Kossin, 2018). Also, Kossin concludes that rainfall rates near hurricane centres are expected to increase as well due to climate change (i.e. warmer environments) based on assessments by Christensen et al. (2013), Kossin et al. (2017) and Walsh et al. (2016). This combination – 'slower' hurricanes with higher rainfall rates near their centres – is expected to increase the total rainfall amounts during hurricane events.

This raises the following question: If climate change can affect above-mentioned hurricane characteristics; how will climate change affect the height of hurricane-induced storm surge? As already explained, the largest part of storm surge levels is determined by wind stress, the dynamical amplification of the storm surge. Based on this theory, one would expect more water to pile up against the coast when hurricane intensities would increase (i.e. higher wind speeds, more wind stress). However, this relationship proved to be not this straightforward. To illustrate this, the well-known Saffir-Simpson scale – the scale that classifies hurricanes into five categories based on hurricane sustained winds (i.e. intensity) – used to include storm surge range for each category, see Table 1. Nowadays, these storm surges are excluded from the scale; the scale led to misconceptions of potential storm surge as hurricanes (such as Katrina (2005)) produced storm surges that exceeded the category ranges (Irish et al., 2008). The scale used to assume storm surge to be a function of the highest sustained wind speed only. In reality, however, the wind speeds cannot predict relatable storm surges, as hurricane size plays an important role in storm surge generation as well (Irish et al., 2008). Irish et al. found that storm surge could vary up to 30% for different hurricane sizes for a specified intensity. Therefore, predictions of the response of hurricane-induced storm surges to climate change become complex. Furthermore, general circulation models – i.e. models that are typically used for climate change predictions – do not simulate hurricane-induced storm surges. Therefore, these models need to be coupled to hydrodynamic models in order to make storm surge predictions (Lin et al., 2012). Using this model combination, Lin et al. (2012) analysed the potential effects of climate change on the storm surge level distribution for New York City: they found storm surge values to increase with a significant amount (e.g. changes that are comparable to sea-level rise projections). One should also take potential sea-level rise into account in storm surge predictions, as sea-level rise could move current existing shorelines more land inward. To illustrate this, Frazier et al. (2010) added sea-level rise to contemporary hurricane-induced storm surge hazard zones and found the storm surge to move further inland. A similar amplification effect was observed in the research of Lin et al. (2012) as well: when including sea-level rise, the return period of storm surge flooding was shortened considerably.

A simplified overview of climate change effects on hurricane behaviour is presented in Table 2.

Saffir-Simpson category	Max 1-min wind speed (m/s)	Storm surge (m)
1	33.0-42.5	1.2-1.5
2	42.9-49.2	1.8-2.4
3	49.6-58.1	2.7-3.7
4	58.6-69.3	4.0-5.5
5	>69.3	>5.5

Table 1: The outdated Saffir-Simpson hurricane scale of the National Weather Service (2006) including storm surge levels (adapted from Irish et al., (2008)).

Hurricane characteristics	Consequence of climate change
Frequency	Decrease
Intensity	Increase
Forward speed	Decrease
Rainfall rates	Increase (near hurricane centres)
Total rainfall	Increase
Storm surge levels	Increase
Storm surge hazard zones	Increase

Table 2: A simplified overview of consequences of climate change on hurricane characteristics.

2.2. Study area

Two major aquifer systems can be found in the Florida peninsula: the surficial aquifer system and the Floridan aquifer system. These aquifer systems interact with each other (i.e. groundwater can flow from one to the other system) and this interaction is controlled by the presence of a less permeable hydrogeological unit – referred to as the upper confining unit – that separates the aquifer systems (Williams and Kuniansky, 2016). In other words, this lower permeable hydrogeological unit restricts the vertical groundwater flow between both aquifer systems (Miller, 1986). The surficial aquifer system is unconfined, whereas the Floridan aquifer system is confined with the exception of locations where there is no upper confining unit and the Floridan aquifer system is at the land surface. The extent to which the hydrogeological units are exposed at the land surface is visualized in Figure 7. Below the Floridan aquifer system is the hydrogeological base that consists of lowly permeable limestone and dolomite and is defined as the bottom of the Floridan groundwater flow system (Spechler and Halford, 2001).
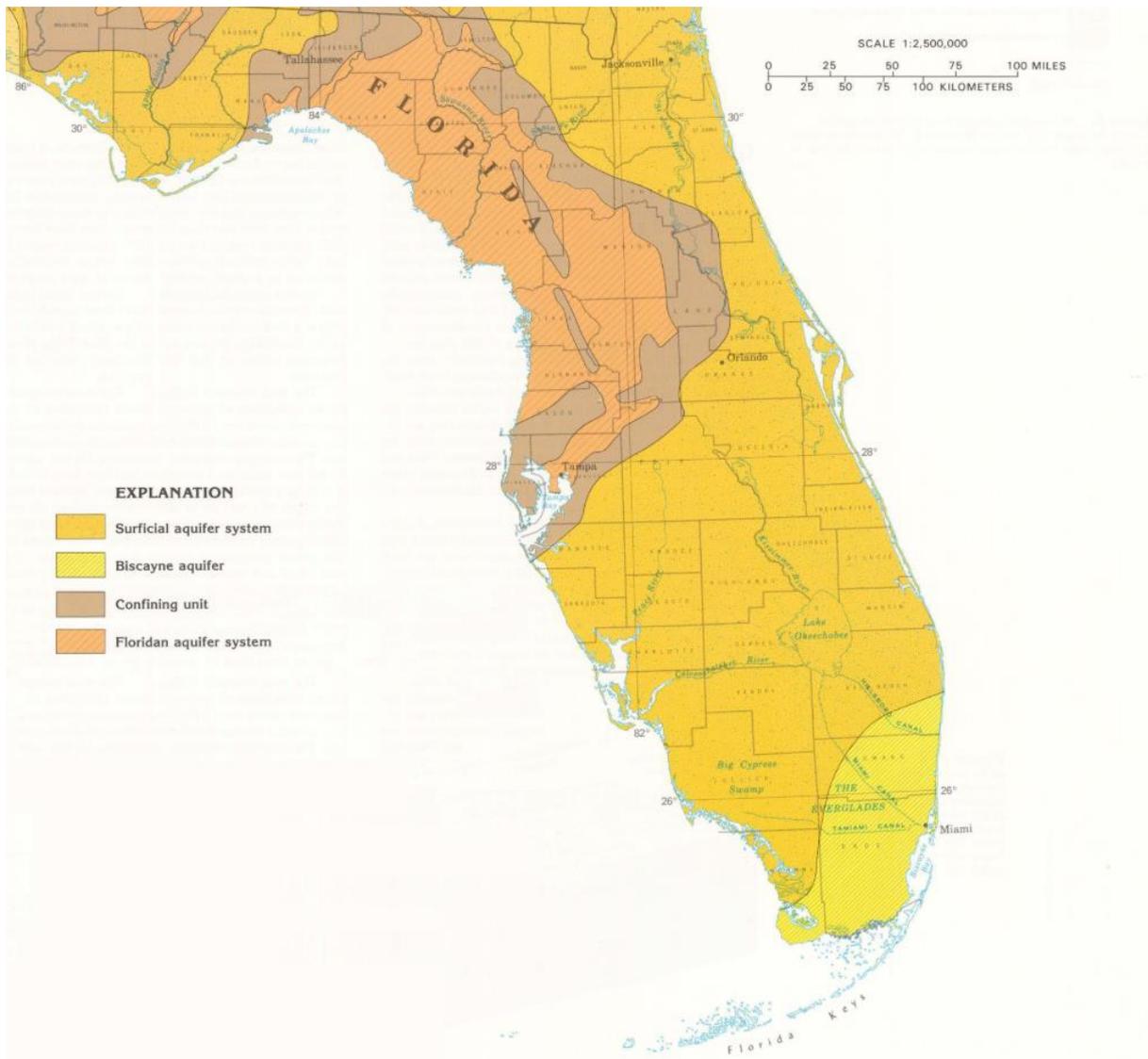
Figure 7: The distribution of various Floridan hydrogeological units at the land surface (figure adapted from Miller (1986)).

The general groundwater movement of the Floridan groundwater flow system is visualized in Figure 8. First of all, surface water (e.g. precipitation) percolates into the surficial aquifer system. Afterwards, the groundwater can either move laterally or vertically, depending on the presence of the upper-confining unit. Where the upper-confining unit is thick and/or where clay is mostly prevalent, groundwater in the overlaying surficial aquifer system is forced to flow laterally and thereby to discharge in surface water bodies (e.g. lakes, rivers and sea). In these zones, groundwater cannot percolate from the surficial aquifer system through the impermeable upper confining unit to recharge the Floridan aquifer system (Miller, 1986). Where the upper-confining unit is breached, thin or absent, groundwater from the surficial aquifer system can flow through the Floridan aquifer system only. Therefore, the Floridan aquifer system is recharged by leakage from the overlying aquifer systems only (Marella and Berndt, 2005). The opposite movement has been observed as well; in these cases groundwater is found to leak upwards from the Floridan aquifer system towards the surficial aquifer system (Miller, 1990). This movement can be explained by the difference in terms of hydraulic heads: when the hydraulic head of the Floridan aquifer system exceeds the hydraulic head of the surficial aquifer system, the groundwater will flow upwards. Both aquifer systems as well as the upper-confining unit are further elaborated upon in this section in terms of appearance, thickness, materials and accompanying hydrogeological properties and groundwater usage. Also, the appearance of hurricanes in Florida is discussed.
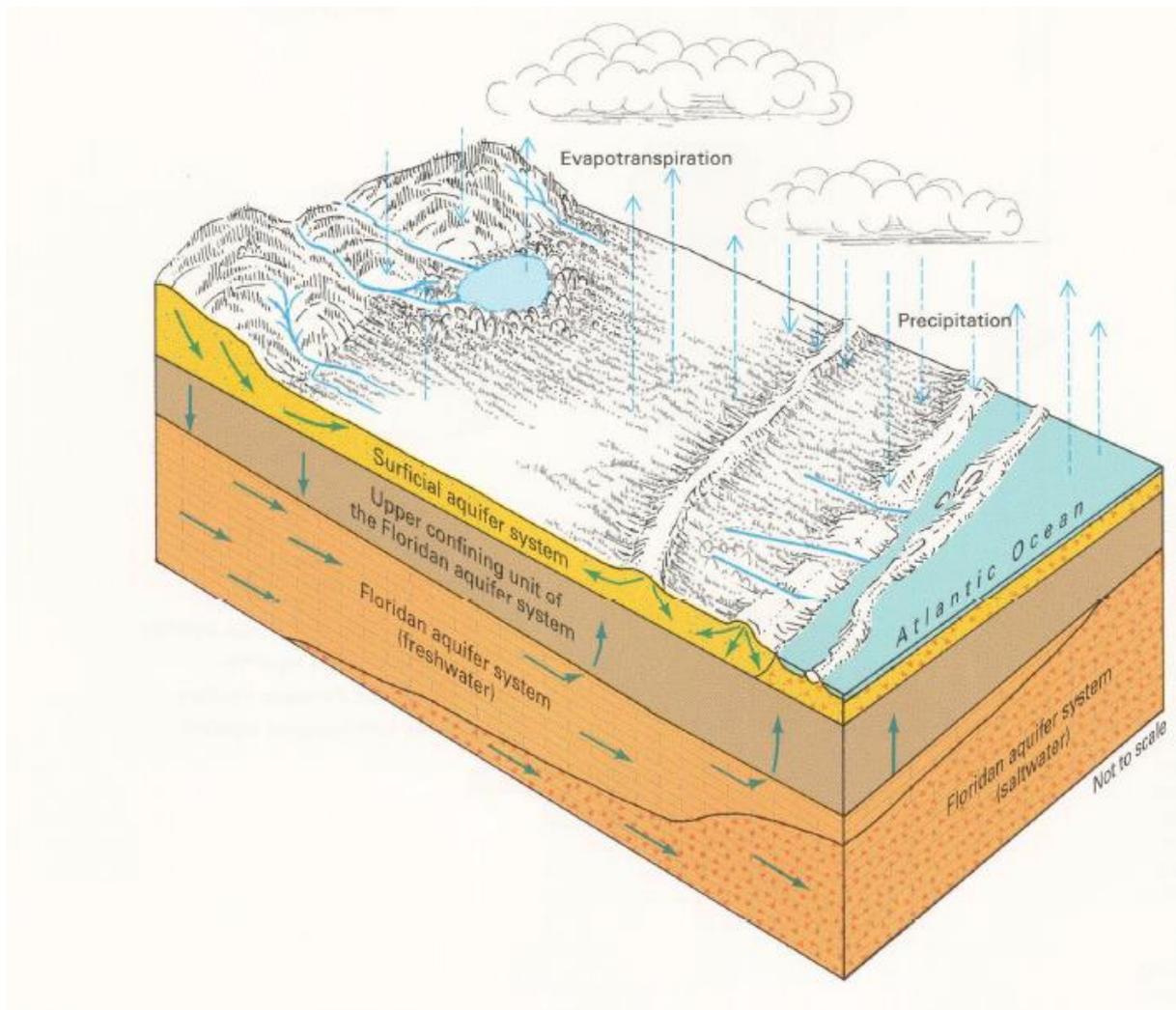
Figure 8: General groundwater movement in hydrogeological units of Florida (figure adapted from Miller (1986)).

2.2.1. Surficial aquifer system

The surficial aquifer system is the topmost located hydrogeological unit in the majority of peninsular Florida. The thickness of this aquifer varies among the area: thicknesses up to around 60 m can be found in southern and eastern peninsular Florida, whereas in north-western peninsular Florida the aquifer is relatively small (e.g. smaller than 3 m) or even entirely absent (Williams and Kuniansky, 2016).

The aquifer composition varies throughout peninsular Florida; the majority of the aquifer consists of sandy materials whereas carbonate rocks (e.g. sandy limestone) are encountered in south-eastern Florida. As these carbonate rocks are relatively thick and highly permeable, this part is the most permeable zone of the surficial aquifer system. Due to this difference with the rest of the surficial aquifer system, this zone of the surficial aquifer system has been assigned a different name to distinguish it from the rest of the system: the Biscayne aquifer system (see Figure 9) (Williams and Kuniansky, 2016). The Biscayne aquifer is characterized by its sensitivity to external stresses (e.g. drainage, recharge, evapotranspiration, groundwater extraction and subsurface movement of seawater) on the groundwater system; this response can be seen in terms of swiftly changing water-levels and saltwater intrusion, threatening the aquifer's freshwater resources (Sonenshein, 1997).

As the surficial aquifer system material varies among peninsular Florida, accompanying hydrogeological properties are variable as well. For example, most reported transmissivity values range between $1x10^2$ to $1x10^3$ m^2/d, whereas locally (e.g. in the presence of limestone, i.e. the Biscayne aquifer) values between $2.3x10^3$ to $4.6x10^3$ m^2/d have been reported (Miller, 1990).

The surficial aquifer system and Biscayne aquifer system serve as important water resources for the Floridan population; the Biscayne aquifer system is used to supply water for large municipalities, whereas the surficial aquifer system is used to supply water for smaller municipalities (Miller, 1990).
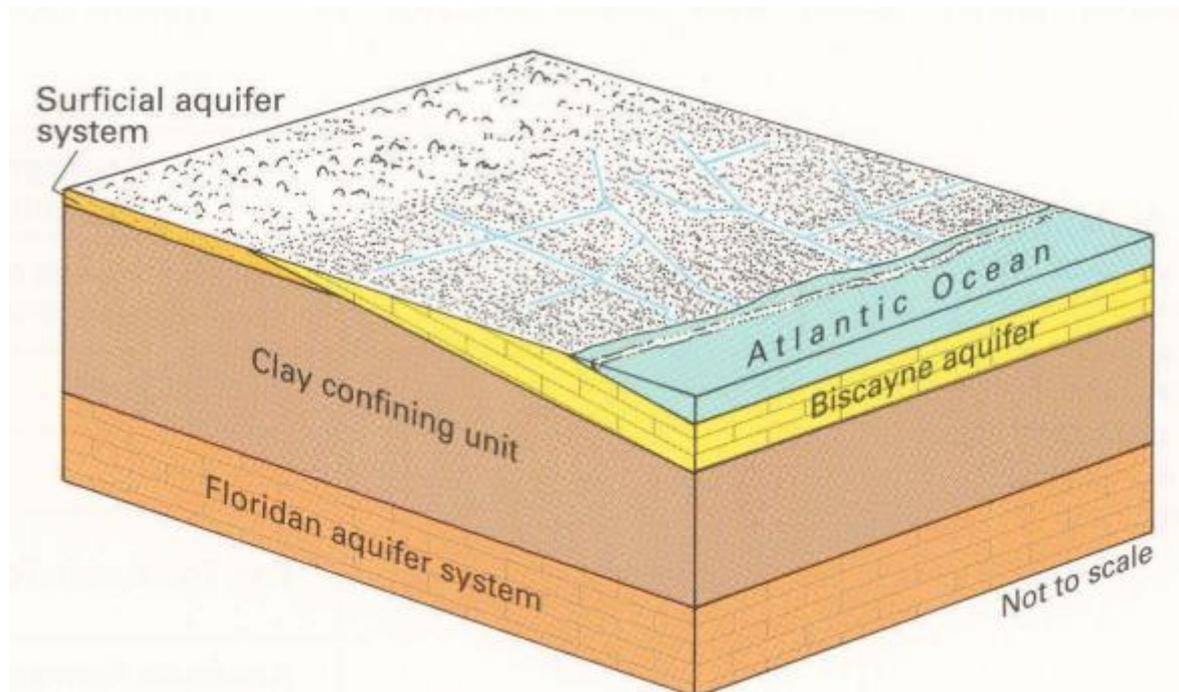
Figure 9: Cross-section of Floridan hydrogeological units including the Biscayne aquifer (figure adapted from Miller (1986)).

2.2.2. Upper-confining unit

Below the surficial aquifer system lays the upper confining unit upon the Floridan aquifer system. As is indicated by its name, this hydrogeological unit confines the Floridan aquifer system. The level of confinement depends on two parameters: the thickness and the vertical hydraulic conductivity of the upper-confining unit (Williams and Kuniansky, 2016).

The thickness of the upper-confining unit is described thoroughly by the research of Williams and Kuniansky (2016). Based on data from their research and results of the research by Miller (1986), they constructed a map depicting the variable thickness of the upper confining unit throughout Florida. In southern Florida, the hydrogeological unit is most pronounced; thicknesses greater than 30 m are reported. If we move in northern direction – towards the centre of peninsular Florida– smaller values are obtained. The hydrogeological unit is also reported to be breached in places due to sinkholes (Miller, 1986), thereby establishing a direct hydrogeological connection of the surficial aquifer system with the underlying Floridan aquifer system. In north-western peninsular Florida, the upper confining unit is very thin or even absent. In this zone, the hydrogeological unit is removed partly by erosion, leaving the Floridan aquifer system in direct contact with the surface or separated only by a very small layer of sand of the surficial aquifer system (Miller, 1986). The upper confining unit is composed of low-permeable plastic clays, whereas locally beds consisting of clayey sand, limestone, dolostone and silty clay are reported (Williams and Kuniansky, 2016). The upper confining unit is known to include a local aquifer system; in south-western peninsular Florida the intermediate aquifer system is encountered that is formed in thick and permeable sandy beds (Williams and Kuniansky, 2016).

The hydrogeological properties of the upper confining unit involve broad ranges in clayey zones, vertical hydraulic conductivities between 2.4×10^{-7} to 4.6×10^{-3} m/d are observed (Miller, 1986), whereas clay situated in the western panhandle of Florida involved a range of 3×10^{-8} to 3×10^{-5} m/d (Maslia and Hayes, 1988). For sandy zones, obviously much higher values are encountered, transmissivities up to 1.2×10^{3} m^2/d are reported (Miller, 1986). As these estimations vary greatly, they should serve as an indicator only. Therefore, it is valuable to investigate actual hydrogeological properties that are used already in local groundwater flow models. An example is the research of Spechler and Halford (2001) concerning the Seminole and Vicinity counties. In their research, Spechler and Halford divided the vertical hydraulic conductivity of the upper confining unit into four separate groups based on thickness and level of karstification (i.e. the process by which soluble rocks are dissolved and a subterranean drainage network is established). Where the upper confining unit exceeded a thickness of 30 m, the hydraulic conductivity was set to 3.4×10^{-4} m/d. For thicknesses between 15 to 30 m slightly higher values were assigned of 2×10^{-3} m/d and for relatively thin layers (smaller than 15 m) two groups were defined of 0.02 m/d for karstic areas and 0.0020 m/d for non-karstic areas.

2.2.3. Floridan aquifer system

The Floridan aquifer system is the deepest situated aquifer system of Florida and covers Florida entirely as well as parts of adjacent states. Three separate hydrogeological units can be distinguished within the aquifer system: the upper Floridan aquifer system (the top permeable zone), the middle confining unit and the lower Floridan aquifer system. Wherever the middle confining unit is absent, the upper and lower Floridan aquifer system are considered as one.

The lower Floridan aquifer system overlays the so-called lower confining unit that forms the base of the hydrogeological system in Florida (Williams and Kuniansky, 2016).

The level of confinement of the Floridan aquifer system depends on the thickness of the overlaying upper confining unit. As already mentioned, the upper confining unit is (almost) absent in northwest peninsular Florida, causing the Floridan aquifer system to be present at or close to land surface, resembling unconfined conditions (see Figure 7). The thickness of the Floridan aquifer system varies among the state. For example, in southern peninsular Florida the aquifer system is thickest (exceeding 1125 m) whereas the system is considerably thinner in the northern part (up to around 425 m) (Williams and Kuniansky, 2016).

The Floridan aquifer system consists mainly of carbonate rocks: thick layers of limestone and dolomite are reported. Due the composition of these rocks, the permeability of the Floridan aquifer system is several orders of magnitude larger than the permeability of the upper and lower hydrogeological units (Miller, 1986). The permeability and porosity vary highly within the Floridan aquifer system. For example, Kuniansky and Bellino (2016) reported transmissivities of the upper Floridan aquifer system that range in the order of 6 magnitudes (0.7 to 860000 m^2/d). For the lower Floridan aquifer system, similar ranges are encountered (12 to 420000 m^2/d). These high-order magnitudes ranges are characteristic for carbonate rock aquifers due to the natural karstification of these aquifers (see Subsection 2.2.3.1 for an overview of karstification of the Floridian aquifer system).

The Floridan aquifer system is considered one of the world's most productive aquifer systems: it provides water for up to 10 million people and it is of vital importance for agriculture, industry and tourism in Florida (Marella and Berndt, 2005; Miller, 1990). The Floridan aquifer system is extensively used in different ways depending on groundwater salinity. For example, where freshwater is prevalent, water is extracted for water supply, whereas where saline water is prevalent, treated sewage and industrial wastes often are injected (Miller, 1990). Other usages of the aquifer include water extraction for cooling and desalinization purposes.

The upper Floridan aquifer system is considered the most productive part of the Floridan aquifer system: large zones of the system contain mainly freshwater that is below the 0.250 kg/m^3 drinking-water threshold (Barlow, 2003; Kuniansky and Bellino, 2016). These zones coincide with the degree of confinement: where the upper-confining system has thin or absent, the aquifer transmissivity is considerably high and therefore the groundwater salinity is relatively low (i.e. lower than the drinking-water threshold) (Barlow, 2003). The majority of the lower Floridan aquifer system exceeds the threshold and freshwater is limited to zones that lay relatively far from the coast (Kuniansky and Bellino, 2016).

2.2.3.1. *Karstification of the Floridan aquifer system*

Karst can be defined as a distinctive topography type characterized by sinkholes and caves and indicates dissolution of underlying dissolvable rocks (e.g. carbonate rocks) by surface water or groundwater (Alpha et al., 1997). It is well-developed in the Floridan carbonate platform (e.g. Floridan aquifer system and the Biscayne aquifer system) and was formed in the most recent geologic period by various processes (Tihansky, 1999). The first process involves sea level fluctuations that have alternately exposed and submerged the carbonate platform to seawater inundations, leading to dissolution and weathering (Tihansky, 1999). Nowadays, geochemical processes continue to dissolve carbonate rocks by slightly acidic groundwater flow (i.e. resulting from slightly acidic precipitation) through the carbonate aquifer systems. In doing-so, considerable conduits (e.g. caves and channels), cavities and pores have been formed or enlarged, involving groundwater to flow at higher paces (Kuniansky and Bellino, 2016; Miller, 1990; Tihansky, 1999). Transmissivity rates are closely related to the presence of the upper confining unit (Williams and Kuniansky, 2016). For example, the highest transmissivities are observed in the zones of the Floridan aquifer system where the upper-confining unit is mostly absent or relatively thin. In these zones, solution openings are well-developed and prevalent, allowing infiltrating rainwater to move rapidly into the subsurface and thereby dissolving carbonate rock (Miller, 1990; Tihansky, 1999). In areas where the upper-confining unit is more pronounced and the Floridan aquifer system more confined, less dissolution occurs and therefore the transmissivity tends to be lower (Williams and Kuniansky, 2016).

2.2.4. Hurricanes in Florida

Florida is more likely to become hit by a hurricane than any other state in the United States with a three-year return period of tropical storms and hurricanes and a 13 to 15 years return period of category 3 to 5 hurricanes for southern Florida (Keim et al., 2007; Malmstadt et al., 2009). In their research, Keim et al. analysed tropical storms and hurricanes strikes at coastal locations along the Floridan peninsula over a period of 105 years (1901–2005) (see Figure 10), however, without including potential climate change effects on hurricane return periods. Therefore, the suggested return period can be affected as climate change projections indicate relatively more extreme hurricane events. For instance, climate change projections indicate fewer hurricanes, but also an increase in hurricane intensity (Knutson et al., 2015).
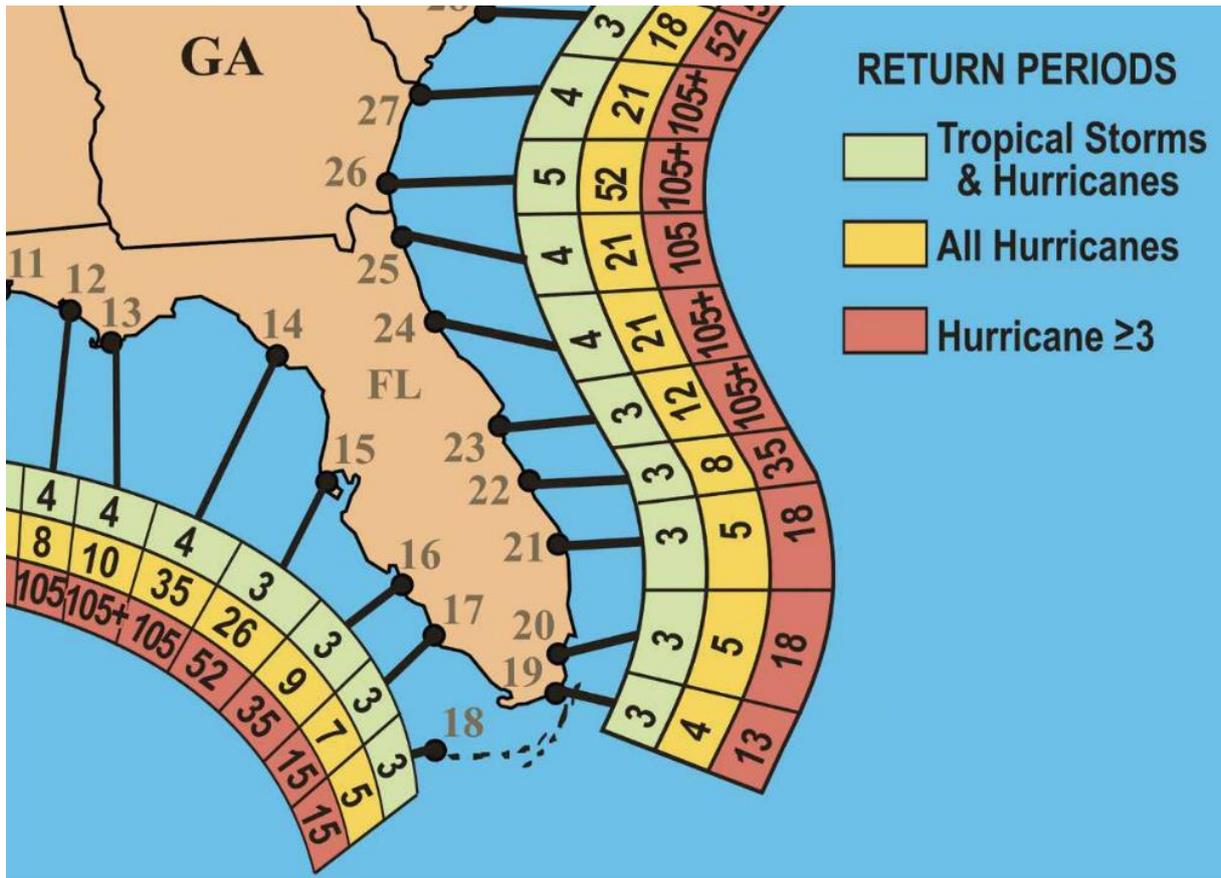
Figure 10: The return periods of tropical storms and hurricanes in peninsular Florida (figure by Keim et al. (2007)). In the figure, tropical storms are defined as storms with a 1-minute maximum sustained wind speed smaller than 33 m/s, whereas hurricanes are categorized using the Saffir-Simpson scale (see Table 1).

2.3. Modelling software iMOD-SEAWAT

The three-dimensional variable-density groundwater flow and coupled salt transport model was constructed using iMOD-SEAWAT (i.e. SEAWAT in an iMOD setting). The iMOD-software (interactive MODeling) is the graphical user interface (GUI) and accelerated version of MODFLOW developed by Deltares (Vermeulen et al., 2018). SEAWAT is a coupled version of MODFLOW and MT3DMS and is used to simulate three-dimensional variable-density saturated groundwater flow and coupled salt transport (Langevin et al., 2007). In the following subsections, the functioning of the software is described based on the governing equations, equations of state, boundary and initial conditions and modelling schemes. Subsequently, the accompanying packages of iMOD-SEAWAT are described.

2.3.1. Governing equations

The core of the iMOD-SEAWAT code is based on governing equations on groundwater flow and solute transport that need to be solved to determine the hydraulic head and fresh-saline groundwater distribution over time. The first governing equation (Equation 4; tensors shown in bold) shows the (constant density) groundwater flow equation and is derived from Darcy's law. The change of hydraulic head over time (i.e. groundwater flow) depends on the three-dimensional hydraulic head change and is related to the hydraulic conductivity (K) – a heterogeneous characteristic of the medium. Sinks and sources of water are represented by a volumetric flux (q) and the specific storage by S_s (i.e. the amount of water that is released from the aquifer storage per unit change in hydraulic head).

$$\nabla \cdot (\mathbf{K}\nabla h) = S_s \frac{\partial h}{\partial t} - q$$

Equation 4: The constant density groundwater flow equation (adapted from McDonald and Harbaugh (1988)).

$$\nabla = \left(\frac{\partial}{\partial x}, \frac{\partial}{\partial y}, \frac{\partial}{\partial z}\right)$$

As SEAWAT takes variable-density groundwater flow into account, the accompanying governing equation differs from the constant density governing equation as used in the MODFLOW code (McDonald and Harbaugh, 1988). Equation 5 shows the equation for transient three-dimensional groundwater flow in a heterogeneous and anisotropic medium and is derived by combining the equation of continuity (i.e. mass balance) with Darcy's law. The governing equation of variable-density groundwater flow is significantly more complex as one now distinguishes between the fluid density (ρ) and the reference fluid density (ρ_0).

$$\nabla \cdot \left[\rho \frac{\mu_0}{\mu} \mathbf{K_0} \left(\nabla h_0 + \frac{\rho - \rho_0}{\rho_0} \nabla z\right)\right] = \rho S_{s,0} \frac{\partial h_0}{\partial t} + \theta \frac{\partial \rho}{\partial C} \frac{\partial C}{\partial t} - \rho_s q'_s$$

Equation 5: The variable-density groundwater flow equation (Langevin et al. (2007)).

To derive Equation 4 from Equation 5, one uses the following assumptions:

- one concentration species ($\rho=\rho_s$; $q=q_s$ and $S_{s,0}=S_s$)
- constant density ($\rho=\rho_0$)
- constant dynamical viscosity ($\mu=\mu_0$)
- constant hydraulic head ($h=h_0$)

This results into the following equation:

$$\nabla \cdot \left[\rho \frac{\mu}{\mu} \mathbf{K_0} \left(\nabla h + \frac{\rho - \rho}{\rho} \nabla z \right) \right] = \rho S_s \frac{\partial h}{\partial t} + \theta \frac{\partial \rho}{\partial C} \frac{\partial C}{\partial t} - \rho q$$

Now, one assumes a constant porosity (θ) and fluid density.

$$\frac{\partial \rho}{\partial t} = \frac{\partial \rho}{\partial x} = \frac{\partial \rho}{\partial y} = \frac{\partial \rho}{\partial z} = 0$$

This results into the following equation.

$$\rho \nabla \cdot [\mathbf{K_0}(\nabla h)] = \rho S_s \frac{\partial h}{\partial t} - \rho q$$

$$\nabla \cdot [\mathbf{K_0}(\nabla h)] = S_s \frac{\partial h}{\partial t} - q$$

The second governing equation (Equation 6; tensors shown in bold) involves the (constant density) solute transport equation. This equation shows fate and transport of contaminants in three-dimensional groundwater flow systems and involves the transport mechanisms advection and dispersion (as well as sinks and sources and reactions) (Zheng and Wang, 1999).

$$\frac{\partial(\theta C^k)}{\partial t} = \nabla \cdot (\theta \mathbf{D} \cdot \nabla C^k) - \nabla \cdot (\theta \boldsymbol{v} C^k) - q'_s C_s^k + \sum R_n$$

Equation 6: The constant density solute transport equation (adapted from Zheng and Wang (1999)).

The constant density solute transport equation can be rewritten by multiplying the groundwater velocity tensor with the porosity to obtain the Darcy flux tensor (**q**) and by assuming no reaction.

$$\frac{\partial(\theta C^k)}{\partial t} = \nabla \cdot (\theta \mathbf{D} \cdot \nabla C^k) - \nabla \cdot (\mathbf{q} C^k) - q'_s C_s^k$$

As SEAWAT involves variable-density solute transport, the accompanying equation is more complex:

$$\left(1 + \frac{\rho_b K_d^k}{\theta} \right) \frac{\partial(\theta C^k)}{\partial t} = \nabla \cdot (\theta \mathbf{D} \cdot \nabla C^k) - \nabla \cdot (\mathbf{q} C^k) - q'_s C_s^k.$$

Equation 7: The variable-density solute transport equation (retrieved from Langevin et al. (2007)).

This can be rewritten to:

$$\frac{\rho_b K_d^k}{\theta} \frac{\partial(\theta C^k)}{\partial t} + \frac{\partial(\theta C^k)}{\partial t} = \nabla \cdot (\theta \mathbf{D} \cdot \nabla C^k) - \nabla \cdot (\mathbf{q} C^k) - q'_s C_s^k.$$

To derive Equation 6 from Equation 7, one assumes constant density:

$$\frac{\partial \rho_b}{\partial t} = 0$$

this gives:

$$\frac{\partial(\theta C^k)}{\partial t} = \nabla \cdot (\theta \mathbf{D} \cdot \nabla C^k) - \nabla \cdot (\mathbf{q} C^k) - q'_s C_s^k.$$

2.3.2. Equation of state

In order to solve the governing equations, one needs to solve the equation of state. This equation is of essential importance as it links the governing equations to each other, by connecting the fluid density (ρ) to the solute concentration (C). Based on some assumptions, one can write a general equation of state for fluid density:

$$\rho = \rho_0 \, exp[\beta_C(C - C_0) + \beta_T(T - T_0) + \beta_P(P - P_0)].$$

Equation 8: The exponential equation of state (Langevin et al. (2007)).

The volumetric expansion coefficients equations for solute concentration, temperature and pressure, are defined as follows (Langevin et al., 2007):

$$\beta_C = \frac{1}{\rho}\left(\frac{\partial \rho}{\partial C}\right)_{T,P},$$

$$\beta_T = \frac{1}{\rho}\left(\frac{\partial \rho}{\partial T}\right)_{C,P},$$

$$\beta_P = \frac{1}{\rho}\left(\frac{\partial \rho}{\partial P}\right)_{C,T}.$$

This exponential equation of state can be linearized and simplified to the following linear equation of state that is used in iMOD-SEAWAT (Guo and Langevin, 2002):

$$\rho = \rho_f + EC.$$

Equation 9: the linear equation of state (Guo and Langevin (2002)).

The equation represents an empirical relation between density and concentration of saline water and is developed by Baxter and Wallace (1916); ρ_f equals the freshwater density (1000 kg/m³) and E is a dimensionless constant with a value of 0.7143:

$$E = \frac{\partial \rho}{\partial C} = \frac{1025 - 1000 \left(\frac{kg}{m^3}\right)}{35 - 0 \left(\frac{kg}{m^3}\right)} \approx 0.7143.$$

This value can be calculated by taking the derivative of Equation 9 and by using salt concentrations from freshwater (assumed to be 0 kg/m³) and seawater (assumed to be 35 kg/m³) (Guo and Langevin (2002)).

2.3.3. Boundary conditions (and initial conditions)

To solve the governing equations, three types of boundary conditions can be used, these include Dirichlet (first type) boundary conditions, Neumann (second type) boundary conditions and Robin or mixed (third-type) boundary conditions (Winston, 2019a). An example of a Dirichlet boundary condition is a fixed value of a variable; therefore, it is mentioned as a specified variable boundary. Neumann boundary conditions are often referred to as specified flux boundaries. The last-mentioned boundary conditions, the Robin or mixed form, is known as the head-dependent flux boundary. An example is the drainage system of an area (i.e. the outflow (flux) from the drains depends on the water level (head)).

2.3.4. Numerical schemes

In iMOD-SEAWAT, several numerical schemes can be used to solve the governing equations, including the finite-difference method, the method of characteristics, the hybrid method of characteristics and the total variation diminishing scheme. The options are defined in the MT3DMS ADVection (ADV) package (Zheng and Wang, 1999).

2.3.5. Parallel modelling

To limit large computation times, the Parallel Krylov Solver (PKS) package can be used. This package facilitates running large models on multi-core computers (Vermeulen et al., 2020). The package divides the model domain vertically into four subdomains and assigns each subdomain to a core. Subsequently, the model can be simulated on all cores. To keep all subdomains interconnected, a few rows are shared by the subdomains (i.e. results in subdomain 1 can affect results in subdomain 2).

2.3.6. Packages

The packages that are used in the iMOD-SEAWAT software are MODFLOW, MT3DMS and SEAWAT packages. The MODFLOW packages can be subdivided into groundwater flow (process) packages, boundary condition packages and solver for the groundwater flow equation packages. The MT3DMS packages are subdivided into a basic transport package, transport component packages and a solver package for solute transport. In this subsection, packages that are relevant for this research are described briefly.

2.3.6.1.   Groundwater flow package (MODFLOW)

The discretization (DIS) package forms the MODFLOW model base as it specifies the spatial and temporal model discretization. The model is spatially discretized by the number of layers, rows and columns. Afterwards, the top elevation of the model layer can be implemented (parameter TOP) and the bottom of each model layer (parameter BOT). Subsequently, the model can be discretized temporarily by defining the number of stress-periods, the number of time-steps and the length of the stress period. Furthermore, for each stress-period it can be specified whether the simulation is transient (TR) or steady-state (SS).

In groundwater flow process basic (BAS6) package, the role that grid-cells play in participating model calculations considering hydraulic heads is defined. For example, grid-cells can either be active or inactive based on the value of the IBOUND parameter. Another option is that grid-cells have a fixed hydraulic head; in that case the hydraulic head of the specified grid-cells does not change throughout the model simulation (e.g. sea-cells). The starting hydraulic head can be defined by the parameter STRT.

Whereas the DIS and BAS6 constructs the model body, the layer property flow (LPF) package defines the hydrogeological characteristics for each grid-cell. These characteristics include the horizontal and vertical hydraulic conductivity (parameters HK and VKA respectively) and the specific storage (parameter SS).

2.3.6.2.   Boundary condition packages (MODFLOW)

The boundary conditions packages consist of packages that simulate specified flux boundary conditions and head-dependent flux boundary types. The packages include the drain package, the general head boundary condition package, the river package and the recharge package.

The drain (DRN) package simulates head-dependent flux boundaries. Just like real-life drains, the model drain serves as a drainage system that removes groundwater from an area where an excess of water is present. The height of the drain is specified in the parameter ELEVATION. If the hydraulic head in a specific model-cell exceeds the drain elevation, water leaves the groundwater through the drain boundary (i.e. drainage). If the hydraulic head in this cell is lower than this threshold, the flux

from the drain drops to zero (Winston, 2019a, 2019b). The flowrate of the drain is proportional to the difference between the hydraulic head and the drain elevation in the cell. This relationship is controlled by the drain conductance, the higher the drain conductance; the more active the drain will work. The drain conductance can be calculated using Equation 10. In this cell, the hydraulic conductivity of a certain cell is multiplied with the area of the cell and divided by the thickness of the sediment in which the drain resides.

$$conductance(x, y) = \frac{K(x, y) * L(x, y) * W(x, y)}{M(x, y)}$$

Equation 10: The conductance equation (adapted from Winston, 2019b).

The general head boundary (GHB) package is another package that is used to simulate head-dependent flux boundaries. The package consists of four parameters: the boundary head (HEAD), the concentration (CONC), the density (DENS) and the conductance (COND). Whenever a general head boundary is applied to a cell, it simulates a groundwater flux that flows either towards or from a model cell (i.e. drainage). This groundwater flux is proportional to the difference in hydraulic head between the model cell and the assigned boundary head within the cell and this relationship is determined by the conductance (Winston, 2019b). The higher the conductance, the higher the flux and the better the hydraulic characteristics (hydraulic head, concentration and density) resemble the conditions of the general head boundary. In other words, when relatively high conductance values are maintained throughout a model simulation; the general head boundary mimics a constant head, constant concentration and constant density.

The last head dependent flux boundary package is the river (RIV) package that allows for drainage and infiltration, depending on the difference between the hydraulic head within the model-cell and the river stage (parameter STAGE) in the model-cell (Vermeulen et al., 2001). When the groundwater level (i.e. hydraulic head) exceeds the stage of the river, drainage occurs, inducing the groundwater flux discharge and groundwater level will fall as a result. Whenever the groundwater level is lower than the river stage and higher than the bottom of the river bed, the flux appears in the opposite direction and infiltration occurs. The flowrate of this flux is proportional to the head-difference between these two variables. This relationship is controlled by the conductance (Winston, 2019b): the higher the conductance, the stronger the process will be (i.e. the stronger the infiltration or drainage becomes). Whenever the groundwater level is lower than the bottom of the river bed, infiltration occurs as well, albeit at a constant rate (Winston, 2019a).

Another boundary condition is the recharge (RCH) that is defined in the specified flux boundary package. Unlike the previous boundary conditions recharge is independent of the hydraulic head of a model-cell. For each cell of the top layer recharge values can be assigned that simulate a specified flux (Winston, 2019a).

2.3.6.3. Solver package (MODFLOW)

In MODFLOW, several solvers can be used for example the Preconditioned Conjugate-Gradient (PCG) solver. This solver can be used to solve finite difference equations for each time-step in a stress-period (Winston, 2019a). If parallel modelling is considered, the Parallel Krylov Solver (PKS) is used instead of the PCG-solver.

2.3.6.4. Basic Transport package (MT3DMS)

The basic transport (BTN) package forms the base of the MT3DMS software. In this basic package, concentration boundary and initial conditions are defined based on the ICBUND parameter. This parameter specifies whether model cells play an active or inactive role in concentration calculations. For example, when model cells are set to inactive, the model-cells are excluded from the governing equations. Another ICBUND option considers the fixed concentration. If this option is selected for a grid-cell, the concentration remains constant throughout all calculations. After defining the ICBUND, concentration values are applied using the parameter SCONC. Other functions of this package include

setting the cell thickness, porosity and the maximum transport steps that is allowed in one flow time-step (Zheng and Wang, 1999).

2.3.6.5. Transport component packages (MT3DMS)

The transport component packages refer to the main processes that occur inside the governing equation for solute transport. These processes are divided into three packages and include the advection (ADV) package, the dispersion (DSP) package and the sink and source mixing (SSM) package.

In the advection package, the advection solution option is defined; in this package one of the numerical schemes can be chosen. Also, the Courant number is defined as the number of cells (or fractions of cells) in which a substance can be transported by advection in one transport step (Zheng and Wang, 1999).

The dispersion (DSP) package includes dispersion and diffusion parameters, for example the longitudinal dispersivity and the ratio of the horizontal and vertical transverse dispersivity to the longitudinal dispersivity. Also, this package includes the molecular diffusion coefficient.

The last package is the sink and source mixing (SSM) package in which the maximum number of all point sinks and sources is defined (parameter MXSS). Furthermore, this package defines the concentration of the recharge flux and the rivers.

2.3.6.6. Solver package (MT3DMS)

MT3DMS uses the generalized conjugate gradient (GCG) package as solver. In this package, the matrix equations that arise from the implicit solution of the solute transport equation are solved (Zheng and Wang, 1999).

2.3.6.7. Solver package (SEAWAT)

The variable-density flow (VDF) package is a SEAWAT package that is based on the MODFLOW methodology and is developed to solve the variable-density groundwater flow equation (Langevin et al., 2007). The package defines the minimum and maximum occurring fluid density (DENSEMIN and DENSEMAX respectively) and incorporates the linear equation of state and the accompanying constant (DENSESLP).

2.4 Hurricane simulation approach in MODFLOW models

In three-dimensional variable-density groundwater flow and coupled salt transport models, hurricane-events can be implemented as variations of surface water-levels (i.e. sea-levels and coastal land inundation levels), concentrations and densities. These variations are either caused by hurricane-induced storm surge (saline water) or by hurricane-induced rainfall (freshwater). These variations depend on time and hurricane position. For instance, if a hurricane makes landfall in the coastal zone, storm surge inundation occurs (increase in hydraulic head and concentration), whereas further inland freshwater accumulates by excessive rainfall (increase in hydraulic head only). After the hurricane-event (during the so-called recovery or flushing period), surface water-levels will decrease again.

Variations of surface water levels, concentration and densities can be applied through various boundary conditions. For example, Xiao et al. (2019) simulated hurricane-induced saltwater intrusion in coastal east-central Florida using time-variant specified head boundaries and obtained water-levels from the storm surge ADCIRC model. Elsayed and Oumeraci (2018) used river boundaries to model marine flooding effects on saltwater intrusion near Bremerhaven (northern Germany) and used the XBeach model for simulation of storm surge inundation. By doing so, a saline-water layer can be applied on the top model layer that causes saline water to infiltrate (i.e. head-dependent flux boundary) to the groundwater system. This interaction is controlled by river conductance factor. Another option is the recharge boundary that applies a specified flux with a specific concentration. The last option is the general head boundary condition that applies a flux based on the applied (general head boundary) hydraulic head and the hydraulic head in the accompanying grid-cell. This method allows for implementing hydraulic head and concentration variations and its functioning strength can be easily modified by the conductance factor.

3. Methodology

In this chapter, the methodology of the research is presented. First, the stationary model and the accompanying tuning are described, followed by the description of the transient model. Thereafter, the hurricane-tool – the input of the transient model – is described. At last, the scenarios and data-analysis are described.

3.1. Stationary model

The main purpose of the stationary model was to establish the steady-state hydraulic head distribution and fresh-saline groundwater distribution of the Florida peninsula. Subsequently, the steady-state hydraulic heads and concentration values were tuned and implemented in the transient models.

3.1.1. Spatial discretization

The three-dimensional variable-density groundwater flow and coupled salt transport model was constructed using iMOD-SEAWAT to represent the Florida peninsula that covers southern Florida and part of northern Florida. The model extent covers a total area of 750km x 500km and is visualized in Figure 11. The domain was discretized into cells of 1000m x 1000m and is divided into 14 vertical layers of uniform thickness. The first six layers cover a total thickness of 30m (each layer is 5m thick), followed by a sequence of six layers with a total thickness of 60m (each layer is 10m thick). The last two layers cover 30m each; a total of 60m. The total thickness of the model extent is 150m (see Table 3 for an overview of the model layers). This model thickness was maintained as it allows to research the surficial aquifer system, the Biscayne aquifer system, the upper confining unit and the upper part of the Floridan aquifer system that are all approximately located within 150m below the land surface (see Section 2.2).

The Digital Elevation Model (DEM) of the ground surface and bathymetry were based on the GEBCO_2014 Grid (30 arc-second global grid of elevations). The elevations of the land surface ranged between 0 and 113m. As one can see from Figure 11, most of the Florida peninsula is low-lying; especially in southern Florida elevations of smaller than 10m are common and can pose a threat for inundation during a hurricane-event.

3.1.2. Temporal discretization

Initially, the model faced completely saline conditions and the fresh-saline groundwater distribution was undeveloped (see Subsection 3.1.4). Over time, processes such as recharge were applied to freshen up the model domain. Due to the large extent of the model, the model was simulated with relatively large stress-periods (i.e. 100 years) with 10 time-steps each. In other words, each time-step represents a 10-year period. Due to the large model extent, the groundwater flow model reached a steady-state fresh-saline groundwater distribution after a relatively long model simulation period: 3000 years. However, this approach is rather simplified. In reality, one should take variations in the geological setting, sea-level, groundwater recharge and rivers etc. (i.e. changes in boundary conditions) into account for each stress period. The latter is done during a paleo-hydrogeological reconstruction of the fresh-saline groundwater distribution.
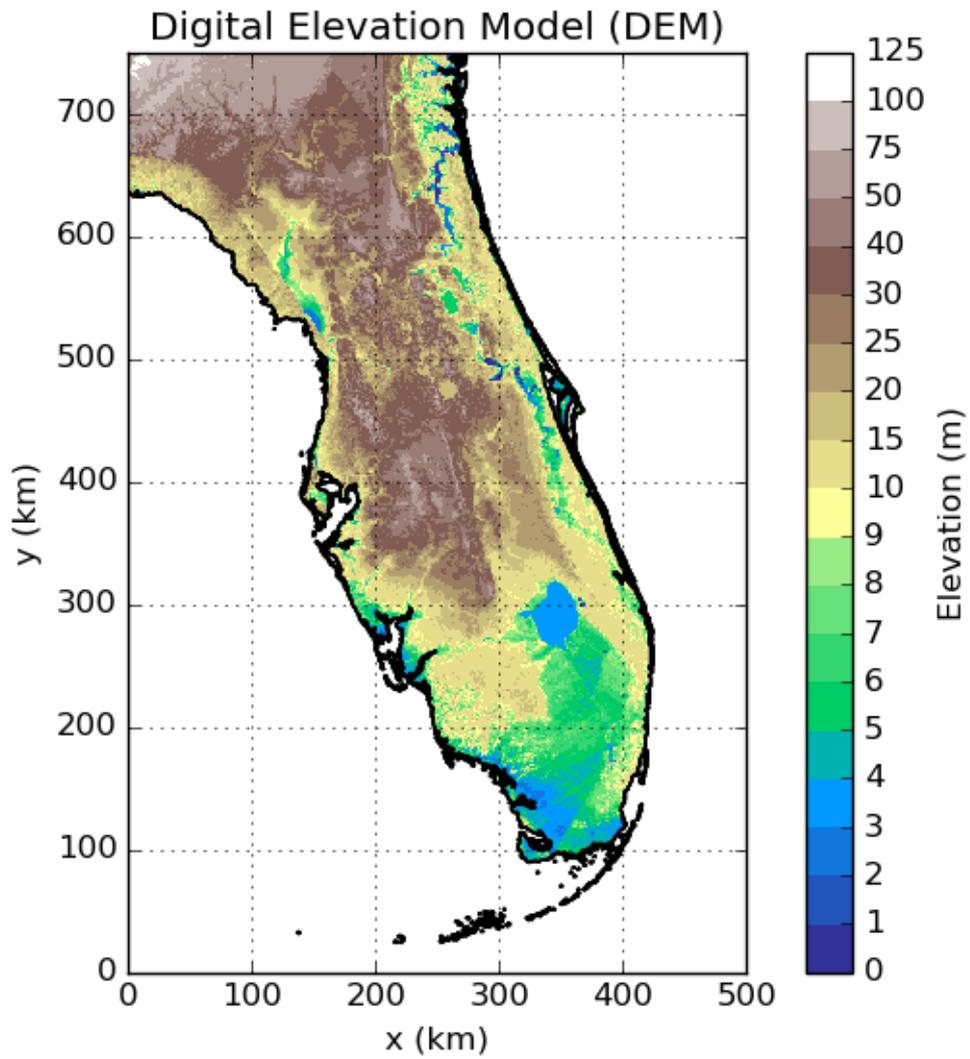
Figure 11: The Digital Elevation Model (DEM) of the Florida peninsula.

Layer number	Thickness (m)
1	5
2	5
3	5
4	5
5	5
6	5
7	10
8	10
9	10
10	10
11	10
12	10
13	30
14	30

Table 3: An overview of the 14 vertical layers of the model.

3.1.3. Hydrogeological parameters

In the model, the Floridan hydrogeology was simplified as such that the major hydrogeological units were highlighted only. The presence and locations of these units for each model layer were based on data from Miller (1990) and Williams and Kuniansky (2016). Local differences in hydrogeology (for instance, an intermediate aquifer system located in the upper confining unit) were omitted, as it is out of the scope of this research to produce a detailed hydrogeological map. Also, all hydrogeological units were assumed to have one value of the hydraulic conductivity only based on the material of the hydrogeological unit. Subsequently, for each material type, typical values for the hydraulic conductivity were assigned, see Table 4. These values were based on the ranges as provided by Heath (1983), see Figure 12. This approach resulted in various (horizontal) hydraulic conductivity zones that are plotted in Figure 13. The vertical hydraulic conductivity was set to 1/10th of the horizontal hydraulic conductivity, as a rule of thumb.

Hydrogeological unit	Material	Horizontal hydraulic conductivity (m/d)
Surficial aquifer system	Sand	10
Biscayne aquifer system	Carbonate rocks	1000
Upper confining unit	Clay	0.001
Upper Floridan aquifer system	Carbonate rocks	1000

Table 4: The Floridan hydrogeological units and their material and accompanying horizontal hydraulic conductivity.
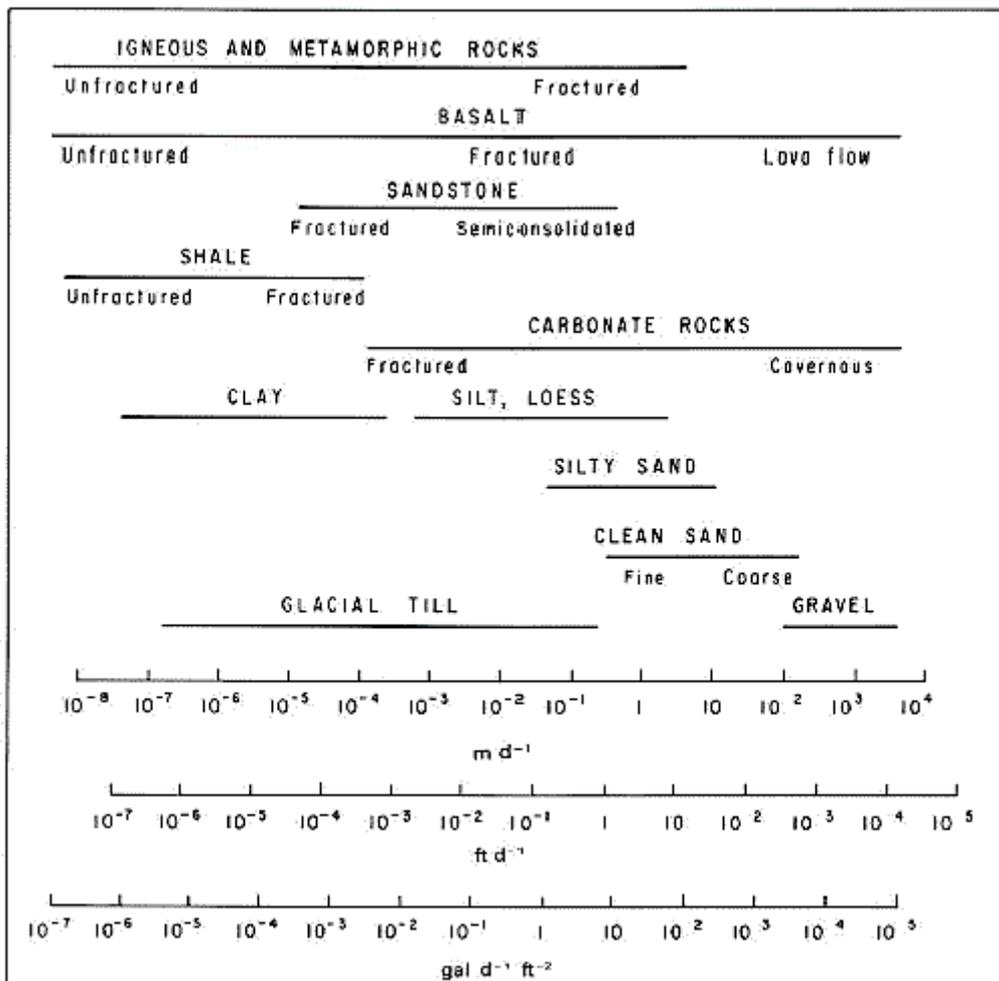
Figure 12: The hydraulic conductivity depends on the rock-type and ranges through 12 order of magnitude among the different rock-types (figure by Heath (1983)).

Hydraulic conductivity zones
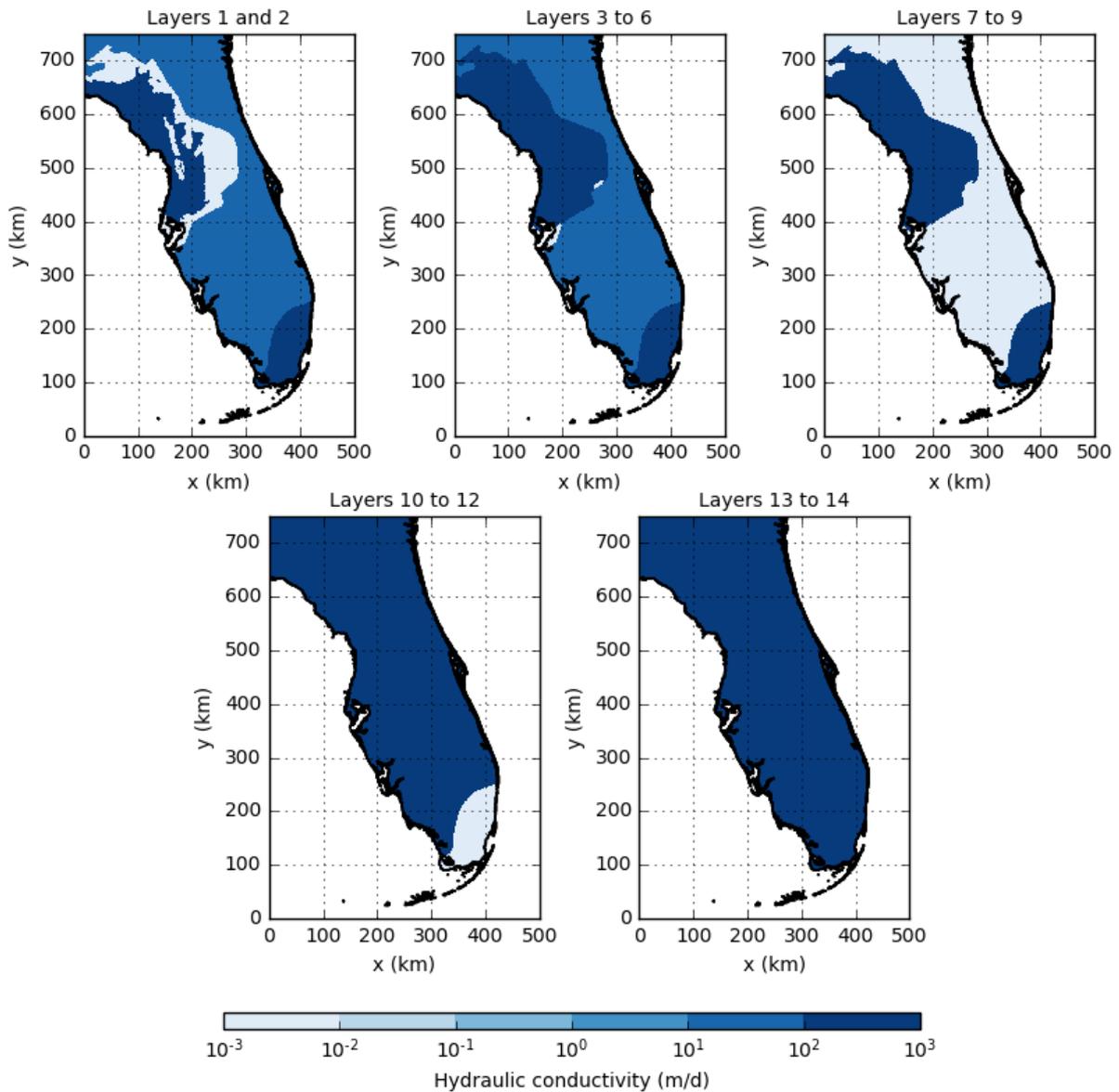
Figure 13: The horizontal hydraulic conductivity per model layer varies among the Floridan peninsula surface and depth, dependent on the occurring rock-types.

For reasons of simplicity, the porosity is assumed to be constant throughout the complete model domain. In reality, the porosity will vary among the different rock-types. Therefore, this assumption might have consequences for the steady-state hydraulic head distribution. As it is out of this research's scope to create a steady-state distribution that matches local measurements (the model is too coarse), this assumption is considered valid.

The specific storage differs for the uppermost layer and the lower layer: the uppermost layer has a higher value (0.150) than the lower layers (0.001); i.e. the uppermost layer can store relatively more water than the lower layers. These values are assumed as a rule of thumb (Oude Essink, personal communication, 2019). For the density and concentration of the freshwater and seawater, the molecular diffusion coefficient and dispersivities, common default values were used (see Table 5).

Hydrogeological parameters	Value	Unit
Porosity	0.3	-
Specific storage (upper layer)	0.150	-
Specific storage (lower layers)	0.001	-
Freshwater density	1000	kg m^{-3}
Seawater density	1025	kg m^{-3}
Freshwater concentration (TDS)	0	kg m^{-3}
Seawater concentration (TDS)	35	kg m^{-3}
Molecular diffusion coefficient	0.0000864	m^{2}d^{-1}
Longitudinal dispersivity	10	m
Horizontal transverse dispersivity	1	m
Vertical transverse dispersivity	1	m

Table 5: In the stationary model, common default values were used for various hydrogeological parameters.

3.1.4. Boundary and initial conditions

Model boundary conditions referring to the hydraulic heads are based on the coastline of Florida. This was accomplished by setting all cells that represent land to 'active' using the IBOUND package. In other words, these cells are active in the calculations and participate in the groundwater flow equations. All cells that that represent the sea are also active but are set to constant via the IBOUND package, implying that the hydraulic head remains constant throughout all model calculations. Subsequently, initial conditions are assigned to the active model cells. As for the hydraulic head values on land-cells of the upper layer and lower layers, the initial values were set to 1m below the land surface. All sea-values were set to 0.

Also, concentrations boundary conditions are defined using the ICBUND package. The same approach is maintained for all layers except the bottom layer. For the upper layers, the land-cells are set to active cells (i.e. the concentration is allowed to vary in these cells during the model calculations), whereas the sea-cells were set to constant concentration model-cells. The starting concentration of all cells is 35 kg/m^3. Therefore, the model starts under completely saline conditions. If the model would be simulated this way, the model would not be able to reach a proper fresh-saline groundwater distribution that is in equilibrium; rainfall would basically 'flush' the groundwater of the model to unrealistic completely fresh conditions; in reality a saline source from below would be present (e.g. see the situation in the Nile Delta, Egypt (van Engelen et al., 2018; 2019). Therefore, for the bottom layer, a different approach is used. To force the model to create a fresh-salt water distribution that is in equilibrium, the land-cells of the bottom layer are assigned fixed concentration values (see Figure 14). These boundary concentration values are based on the fresh-saline groundwater distributions by Barlow (2003) that represent the concentration values for the upper part of the Upper Floridan Aquifer system and the upper part of the Lower Floridan Aquifer system. As the depth of this research's bottom layer does not match the depths of the distributions by Barlow, the average of Barlow's fresh-saline groundwater distributions is calculated. The resulting values are assigned to the lowest layer and should be regarded as a rough estimation only. With a fixed concentration boundary layer at the bottom, the model can be freshened up by molecular diffusion and mechanical dispersion from the bottom layer and by recharge (0.001m/d) applied to the upper layer. By simulating these processes, a steady-state fresh-saline groundwater distribution is created. A similar procedure has been executed by Mabrouk et al. (2019).

Concentration (bottom layer)
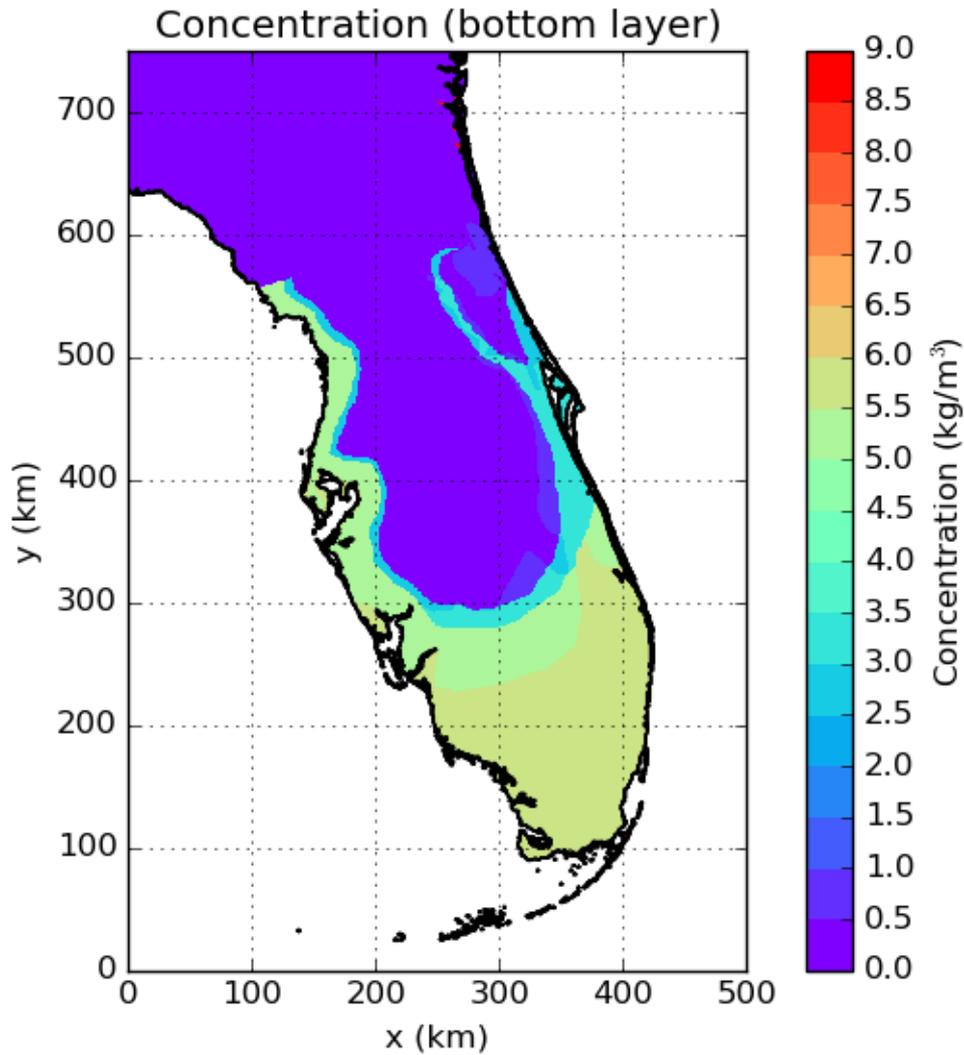
Figure 14: The concentration of the stationary model bottom layer was calculated by averaging data on the groundwater concentration of the upper part of the Upper Floridan Aquifer system and the upper part of the Lower Floridan Aquifer system (data adapted from Barlow (2003)).

The head-dependent flux boundary conditions consist of river systems and drains. Data on river stages is obtained by the GEBCO dataset and data on the river locations and accompanying river bottom elevations are retrieved from the GAIA-dataset. The river water head, the difference between the river stage and the river bottom is plotted in Figure 15. The river width is obtained from the same dataset and is used in calculation of the river conductances. As can be seen from Figure 15, river systems are not present in every grid-cell, whereas in reality small rivers and ditches may be present as the cell-size is relatively large. As river systems control the model drainage capability, the absence of river systems can lead to insufficient drainage. To construct an adequate drainage system, drains were applied to the land-surface; causing the drainage system to be present in each cell. Initially, the drainage conductance is set to 1000 m²/d.

Also, recharge (a specified flux boundary) is applied to the land-surface and considers 0.001 m/d.
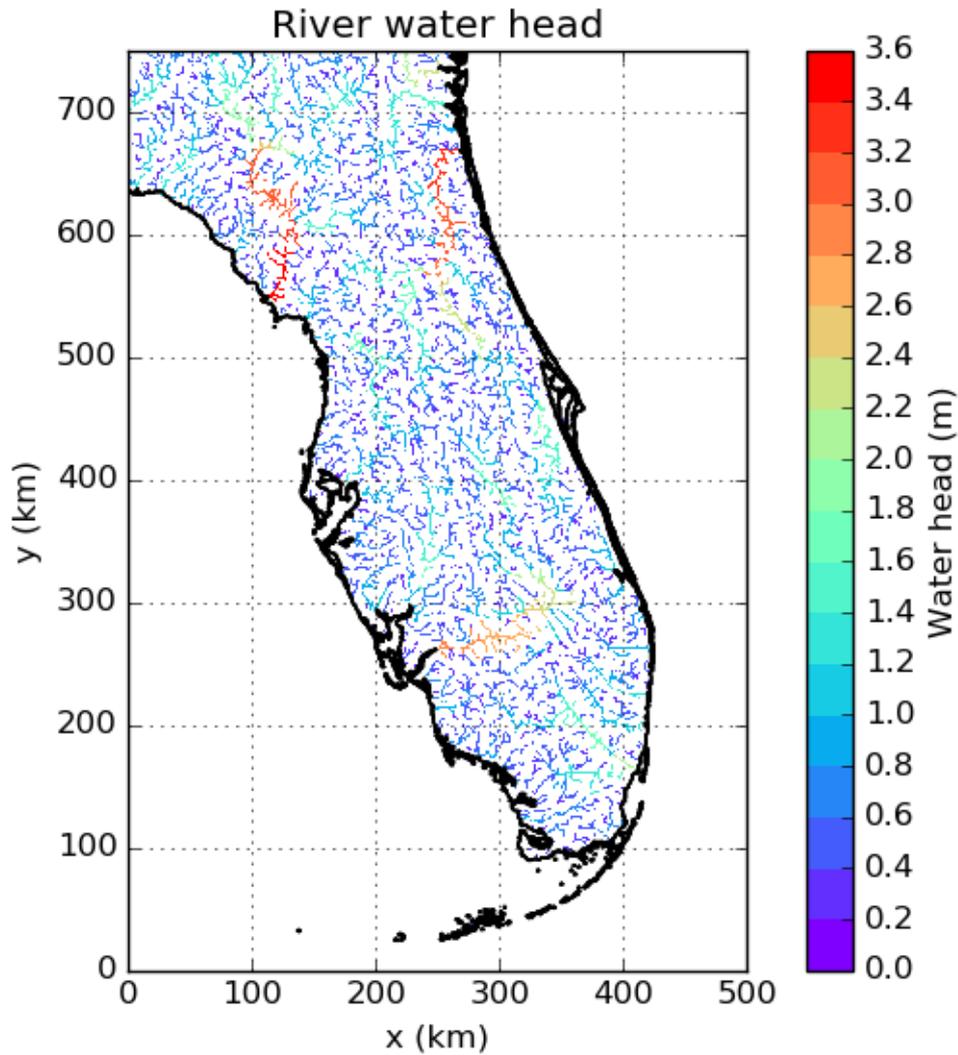
Figure 15: The river water head (relative to Mean Sea Level) of the Floridan peninsula was calculated by subtracting the river stage data (GEBCO-dataset) by the river bottom data (GAIA-dataset).

3.1.5. Numerical settings

Due to the large extent of the model, the model faces large runtimes. To limit these computation times, the Parallel Krylov Solver (PKS) package was implemented. The Parallel Krylov Solver divides the domain vertically into four subdomains and assigns each subdomain to a core (an overview of the subdomains is presented in Figure 16). The implicit solution of the solute transport equation was solved using the third-order TVD numerical scheme and a Courant number of 0.75.
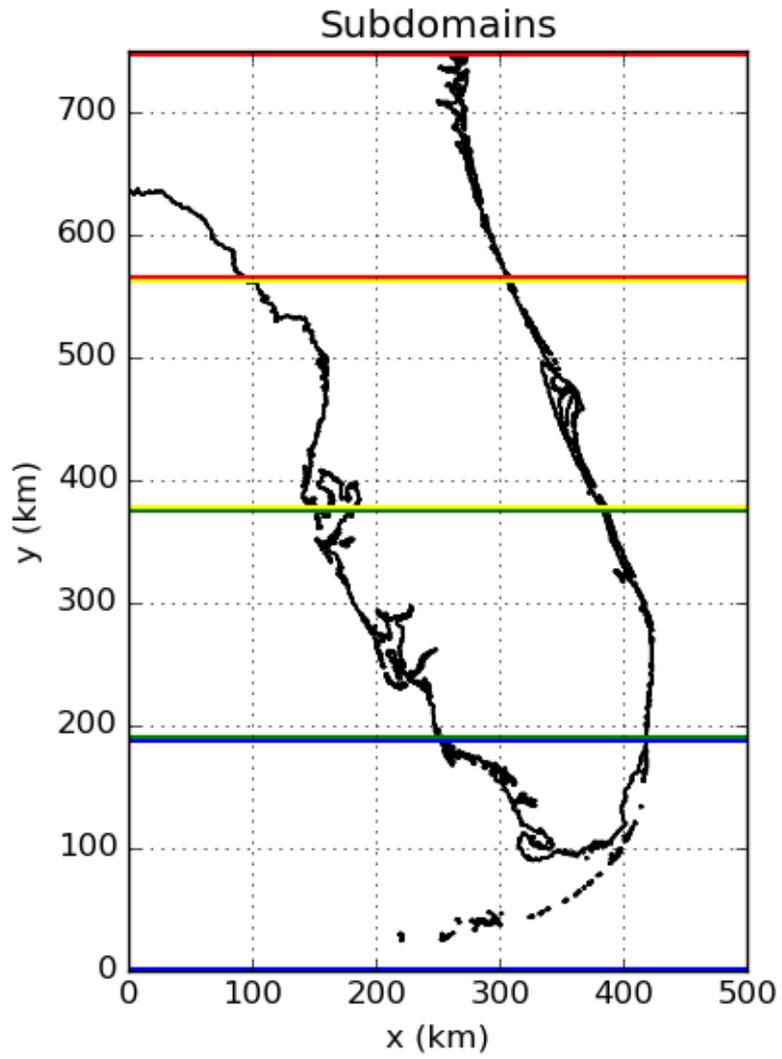
Figure 16: An overview of the four subdomains in the model, on the y-axis from up to down: p000, p001, p002 and p003.

3.2. Tuning of the stationary model

Before the steady-state hydraulic head distribution was implemented in the transient model, the distribution was re-evaluated as the model results showed hydraulic heads that rose severely above the land surface (see Figure 17). These exceedances indicate that the drainage system of the model is insufficient, leading to relatively high hydraulic heads as the water cannot be drained away properly. Therefore, tuning of the stationary model (by varying drainage system parameters) is required to make the model output more realistic. Therefore, we need to take a closer look at the drainage system of the stationary model.

In groundwater modelling, river system parameters amongst other parameters such as drainage system parameters and hydrogeological parameters (i.e. storage coefficients and hydraulic conductivity) are responsible for groundwater drainage (i.e. water in cells near the river can leave the groundwater system when the hydraulic head exceeds the river stage). Therefore, implementation of an appropriate river system is important for an adequate drainage system. In the stationary model, rivers were implemented using the GAIA dataset. This dataset allows relatively large rivers to be present in the model (see Figure 15) but excludes small rivers and/or ditches. In the cells that were left out, no 'river' was allocated using the RIV-package, whereas, in reality, it is plausible to assume these cells to have a small river/ditch as the grid cells are relatively large (i.e. 1000x1000m grid-cells). In other words, usage of the GAIA dataset underestimates the total river presence and the accompanying groundwater drainage.

To compensate this underestimation, one can assign relatively small rivers to cells that are left out in the GAIA dataset approach. By assigning smaller widths and lengths, the river conductance becomes lower than the conductance of larger river cells (see Equation 10). Therefore, groundwater will be drained to a lesser extent than for larger rivers. Another approach is to implement drains from the DRN-package in every land-cell. This approach was used in this research by implementing drains at 0.50m below land surface level using a drainage conductance of 1000 m^2/d. In doing so, every land-cell is participating in the groundwater drainage (this method affects all land-cells directly, whereas increasing the river conductance only affects cells near the river). However, as groundwater levels exceed the land surface, the drainage system is still not capable to drain most of the water properly. Therefore, the drainage conductance is adapted manually (see Figure 17). By increasing the drain conductance, the effect of the drains becomes more pronounced. However, for drainage conductances up to 10000 m^2/d, water levels are still locally exceeding the surface level up to 10m. Therefore, the drainage conductance is increased until the hydraulic head reaches the drain elevation. Using the drainage conductance of 25000 m^2/d, most cells could drain away the water. The effect of increasing the drainage conductance can also be observed from the mass budget table (see Table 6). For instance, the percentage of water that leaves the model via the drains increases from 0.10% to 0.12% when increasing the conductance from 1000 to 25000 m^2/d. In addition, the interaction between the groundwater system and the river system changes (i.e. drainage or infiltration, see Subsection 2.3.6.2). Initially, the drainage conductance was set to 1000 m^2/d and river drainage occurred. In other words, water flows from the groundwater system into the river system. However, the drainage conductance of 25000 m^2/d lowered the groundwater level below the river stage, allowing infiltration to occur. This process can be seen for the drainage conductance of 25000 m^2/d: surface water infiltrates into the groundwater system via the river system (i.e. the river leakage becomes an input). At last, drainage occurred via the constant head boundary for the drainage conductance of 1000 m^2/d. This flux is determined by the hydraulic head difference between the constant head and the groundwater level. With the conductance of 25000 m^2/d, the groundwater level lowers (as the groundwater is more actively drained from the model) and thus the hydraulic head difference becomes smaller. As a result, the drainage flux towards the constant head decreases (from 0.02 to 0.01%).

	DRNCD = 1000 m^2/d		DRNCD = 25000 m^2/d	
	In (%)	Out (%)	In (%)	Out (%)
Recharge	0.12	0	0.12	0
Constant head	0	0.02	0	0.01
Drains	0	0.10	0	0.12
River leakage	0	0.01	0.01	0

Table 6: A summary of inflows and outflows of water in (mass) percentage of the total water budget of the model. The sources and sinks included are stresses such as recharge, rivers and drains. In addition, constant-head flow is included. For reasons of simplicity, the other processes are excluded from the table. The stresses and constant-head flow represent flow into or out of the simulated flow system (Langevin et al., 2020). The contribution of the sinks and sources is presented for two drainage conductances (abbreviated as DRNCD).
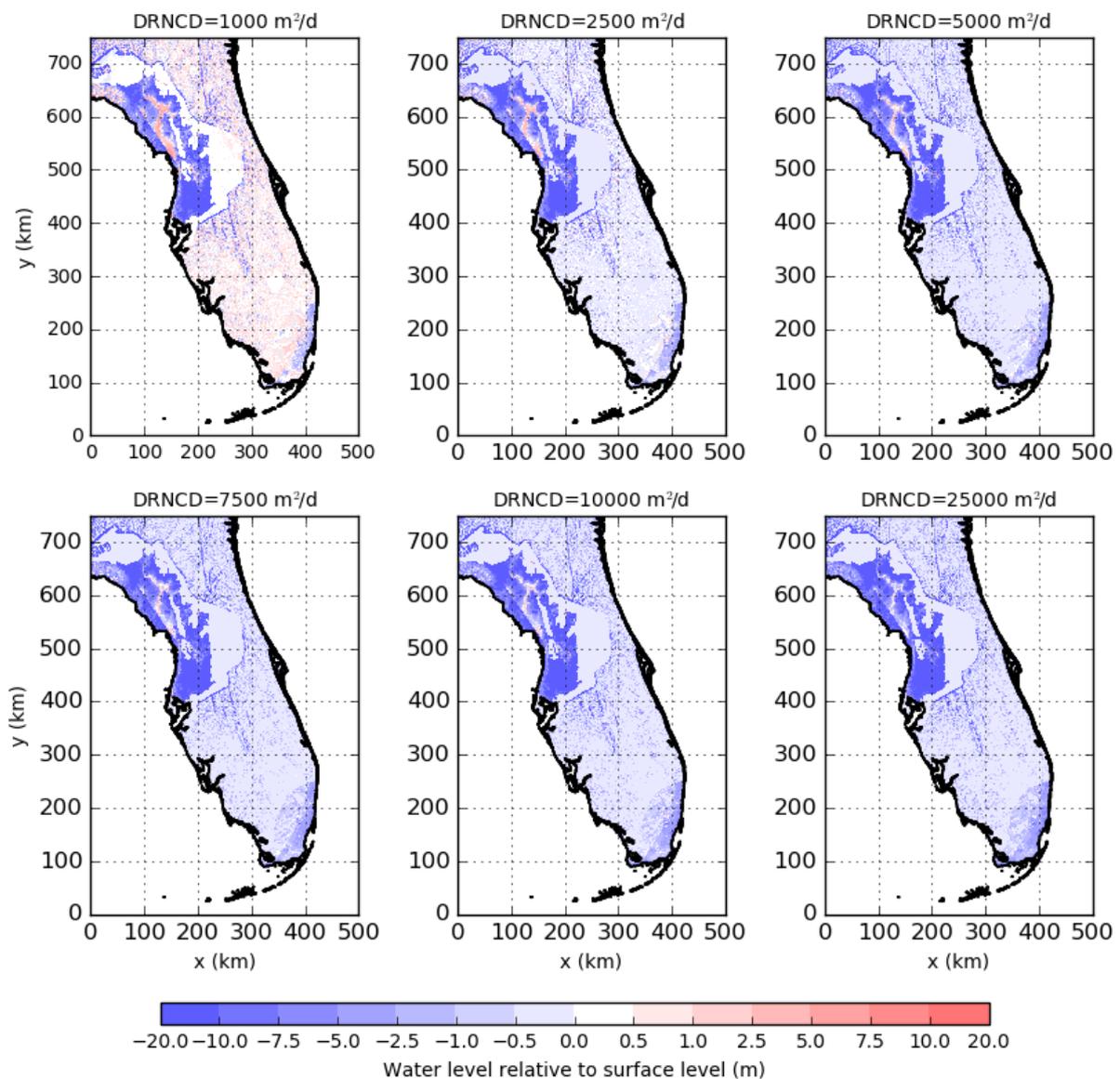
Figure 17: The water level relative to the surface level is plotted for various model runs with different drainage conductances (abbreviated as DRNCD). During the tuning of the stationary model it can be observed that a high drainage conductance is required to obtain realistic results (i.e. water levels that do not exceed the surface level).

3.3. Transient model

The transient model was constructed to simulate the hurricane event. The model uses as input the results from the stationary model (e.g. the steady-state hydraulic head distribution and the fresh-salt water distribution of the Florida peninsula). The core of the hydrogeological model is the same for the stationary and the transient model; however, adaptations were made with regards to the spatial and temporal discretization and the boundary conditions of the model.

3.3.1. Spatial discretization

Whereas the first layer of the stationary model considered a 5m thick layer, in the transient model this upper layer was divided into two separate layers with a thickness of 1m and 4m, respectively. The remainder of all model layers remains the same for the stationary and transient model. This adjustment was made to apply general head boundaries to a thin layer (i.e. 1m) instead of a 'thick' layer (i.e. 5m). In doing so, the boundary is forced over 1m thickness and affects only a relatively smaller part of the model.

3.3.2. Temporal discretization

To simulate the hurricane, relatively small time-steps are required. Therefore, the transient model uses 144 stress-periods of 1 hour (i.e. 6 days), followed by 20 stress-periods of 1 day (i.e. 20 days). During the first 6 days, the hurricane arrives and leaves, inducing the storm surge, followed by percolation of storm surge in the next 20 days (the length of this period is explained in Subsection 3.4.1). After 26 days, the storm surge was assumed to have either percolated or evaporated. Afterwards, the transient model was simulated for 25 years (25 stress-periods of 1 year) to recover from the hurricane-induced storm surge. All stress-periods were set with 10 time-steps each.

3.3.3. Hydrogeological parameters

The same hydrogeological parameters were used as in the stationary model. The first and second layers have the same hydrogeological parameters as the first layer in the stationary model.

3.3.4. Boundary and initial conditions

The transient model uses the same boundary conditions as the stationary model, except for the general head boundary conditions that were applied to the transient model only. These boundary conditions were applied to the upper layer (1m thick) to simulate the hurricane event in terms of hydraulic head, concentration, density and conductance. During the flushing period, that is to say 25 years, no general head boundary conditions were applied on top of the surface water system (only recharge, drain and river boundary conditions were used).

First, the (general head boundary) head is defined. When the hurricane travels over sea, the seawater elevation was assumed to increase only by the height of the storm surge. The contribution of rainfall was then incorporated in this (general head boundary) head and thus set to zero. Therefore, the sea boundary head at the location and in the neighbourhood of the storm surge equals the storm surge:

$$ghb\_head\_sea(x, y, t) = H_{storm\ surge}(x, y, t).$$

Equation 11: the general head boundary head equation for sea-cells of the uppermost model layer.

How the storm surge and storm rainfall elevations are calculated, is described in Section 3.4.

When the hurricane arrives on land, inundation occurs. Here, the total water elevation on the land surface was assumed to be a superposition of the storm surge water elevation and the storm rainfall level. For the head, the total inundation level was added directly to the hydraulic head of the first layer of the tuned stationary model:

$$ghb\_head\_land(x, y, t) = H_{tuned}(x, y, t) + H_{storm\,surge}(x, y, t) + H_{storm\,rainfall}(x, y, t).$$

Equation 12: The general head boundary head equation for land-cells of the uppermost model layer.

In doing so, the water was applied directly into the groundwater system. Therefore, there is no lag; the water does not have to percolate downward. In reality, however, surface water needs time to percolate towards the groundwater system and effects on the groundwater table are not directly visible. Therefore, the approach of this research can be regarded as a worst-case scenario with directly visible effects.

As the model considers peninsular Florida in its whole area, many places will be unaffected by a hurricane event. To this end, land-cells beyond the reach of influence of storm surge were set to the tuned stationary hydraulic head, whereas unaffected sea-cells maintained a constant seawater level of 0m.

Secondly, (general head boundary) concentrations were calculated. When the hurricane arrives on land, the inundation concentration will be calculated based upon the contribution of the storm surge and the accompanying storm rainfall to the total level of inundation:

$$ghb\_conc\_land(x, y, t) = \frac{H_{storm\,surge}(x, y, t) * 35 + H_{storm\,rainfall}(x, y, t) * 0.001}{H_{storm\,surge}(x, y, t) + H_{storm\,rainfall}(x, y, t)}.$$

Equation 13: The general head boundary concentration equation for land-cells of the uppermost model layer.

All general head boundary conditions are applied directly to the uppermost layer (1m thick). In reality, inundation water would mix with the groundwater present in the first layer. In this model, however, this initial mixing process was omitted. Therefore, this model's results can be assumed to be like a worst-case scenario: the simulated concentration would be somewhat higher than in reality.

The (general head boundary) density was applied in the same way as the boundary concentration was defined:

$$ghb\_dens\_land(x, y, t) = \frac{H_{storm\,surge}(x, y, t) * 1025 + H_{storm\,rainfall}(x, y, t) * 1000}{H_{storm\,surge}(x, y, t) + H_{storm\,rainfall}(x, y, t)}.$$

Equation 14: The general head boundary density equation for land-cells of the uppermost model layer.

Therefore, the boundary density was assumed to be constant for seawater: 1025 kg/m³. When the hurricane makes landfall, the density was calculated based on the level of saline water (storm surge) and freshwater (rainfall). For land-cells that are out of hurricane reach, density values were assigned based on the salinity distribution of the tuned stationary model.

At last, the (general head boundary) conductance were defined. These conductance values were set such that the cells of the uppermost layer were forced to be equal to the general head boundaries conditions. This approach overwrites the initial hydraulic head and concentration values and replaces them with general head boundary conditions. In other words, this approach implements the hurricane directly on the top layer of the model.

3.3.5. Numerical settings

The transient model employed the same numerical settings as the stationary model.

3.4. Hurricane tool

During this research, a hurricane tool was developed that makes hurricane-induced storm-surge and rainfall predictions for the Florida peninsula for various hypothetical hurricanes based on the Sea, Lake, and Overland Surge from Hurricanes (SLOSH) model data. The hurricane tool produces hurricane storm surge and rainfall data that were used in the general head boundary conditions calculations. In this section, the tool development is described.

First, it was assumed that the hypothetical hurricane centre size equalled the grid-size (i.e. 1000x1000m) and one row or column was selected among which the hurricane centre travels in a specific direction. Subsequently, the hurricane was assigned a radius (i.e. set number of rows or columns) that was based on the radius of maximum winds. In doing so, the hurricane reach was defined that distinguishes between zones affected and unaffected by the hurricane (see Figure 18). The hurricane reach formed the basis of storm surge and inundation level calculations that were calculated only inside the reach. An overview of these conceptual hurricane characteristics and their definitions is presented in the table below.

Conceptual hurricane characteristic	Model definition
Hurricane centre path	Fixed row or column
Hurricane centre size	Grid-size (1000x1000m)
Hurricane radius (of maximum winds)	Fixed number of rows or columns
Hurricane reach	Centre path ± hurricane radius
Hurricane direction	North, south, east or west

Table 7: An overview of the various conceptual hurricane characteristics and their definitions.
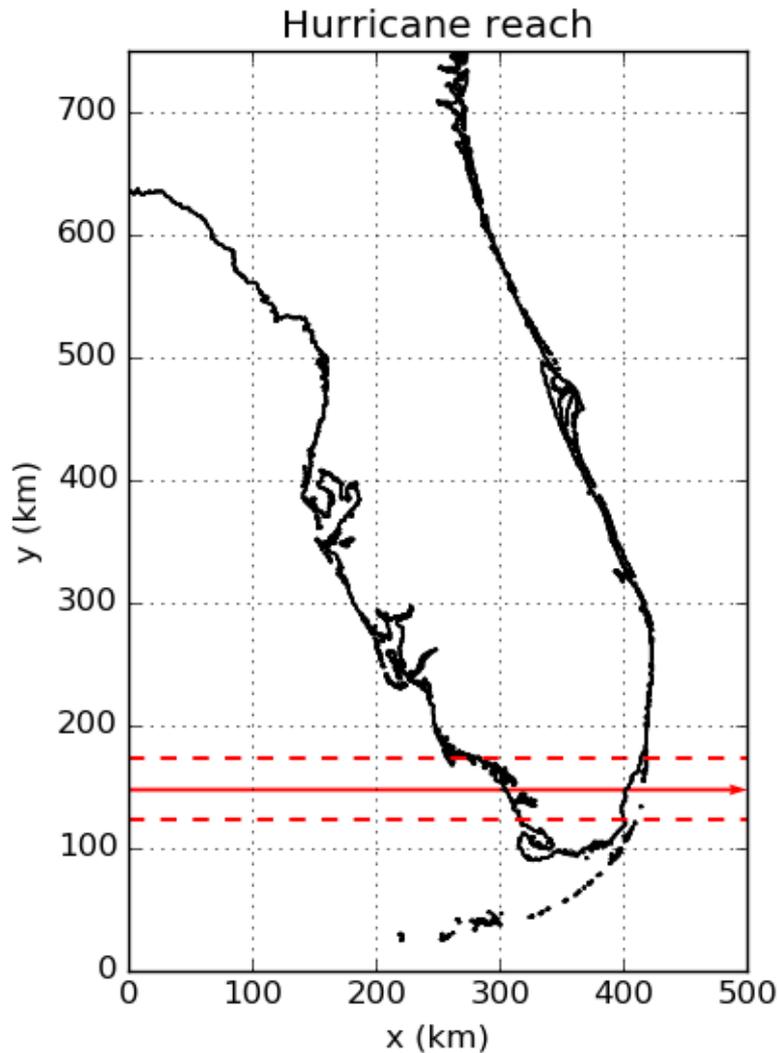
Hurricane reach

Figure 18: The hypothetical hurricane reach was defined by addition and subtraction of the radius of maximum winds by the hurricane centre path. An example of a hurricane centre path (arrow) and its reach (dashed lines) is shown.

3.4.1. Storm surge hydrographs

The storm surge head was calculated using Cialone's storm surge hydrograph equation and these calculations required data on storm surge peak elevations.

Cialone's hydrograph cannot be used directly in this research as it was designed for coastal storm surge only (Xu and Huang, 2014) whereas in this research varying seawater levels and inundation-levels are required. Therefore, assumptions regarding the hydrograph were made to make it applicable for this research purposes.

Firstly, t_0 in Equation 2 was redefined. For example, t_0 was previously defined as the hurricane landfall time (Xu and Huang, 2014) whereas in this research, t_0 does not only represent the hurricane landfall time but the hurricane arrival time among the entire hurricane centre track. To illustrate this: for a sea-location among the hurricane track, the arrival time t_0 is assumed to be the time at which the hurricane arrives at this specific point. It was defined as the distance from starting position of the hurricane centre (e.g. the west model boundary) to this specific point in sea, divided by the forward speed of the hurricane. The arrival time was calculated for any location on the hurricane centre track that resulted into an array of arrival times for a specific hurricane forward speed.

Secondly, the storm surge head and storm surge peak variables were assumed to be dependent on three dimensions (x,y,t) instead of only one (i.e. time). Afterwards, the hydrograph was rewritten as such that it can be assigned to each individual model-cell inside the hurricane reach:

$$H_{storm\ surge\ on\ sea}(x, y, t) = H_{storm\ surge\ peak\ on\ sea}(x, y) \left(1 - e^{-\left| \frac{D}{(t - t_0)} \right|} \right)$$

Equation 15: The adapted storm surge hydrograph equation for sea-cells.

where the storm duration (D) is based on the radius of maximum winds (RMW) and the forward speed (F):

$$D = \frac{RMW}{F}$$

and where t_0 is the hurricane arrival time (at location x_0) that is based on the location (x) of the hurricane and the forward speed (F):

$$t_0 = \frac{x - x_0}{F}.$$

Using these assumptions, storm surge hydrographs can be developed for any location inside the hurricane reach on sea, once the hurricane storm surge peak values were defined (how these storm surge peak values were calculated is discussed later in this section).

For storm surge levels on land, a different approach was used. As it is out of scope of this research to model the relation between the surface water system and the groundwater system extensively (e.g. the pace at which inundation levels decline and vanish), simplifications regarding these dynamics were made. Therefore, data was retrieved from the USGS that shows the response of the Floridan surficial groundwater system to Hurricane Irma (2017) and was used an indicator of the behaviour of the inundation levels (see Figure 19). As one can see from the figure, the groundwater level rises exponentially as the hurricane makes landfall, followed by a more or less linear decrease. After approximately 20 days after hurricane landfall, groundwater levels had ceased to pre-hurricane conditions. Then, the groundwater system has recovered from the hurricane event in terms of hydraulic head, indicating that the inundation levels have ceased.

The storm surge head and the related general head boundary conditions in this research were assumed to follow the same groundwater behaviour as the observation in Figure 19. However, as the groundwater recovery pace depends on soil characteristics, this assumption may not be accurate (i.e. the actual groundwater recovery may vary). Therefore, Figure 19 was merely used as an indicator.
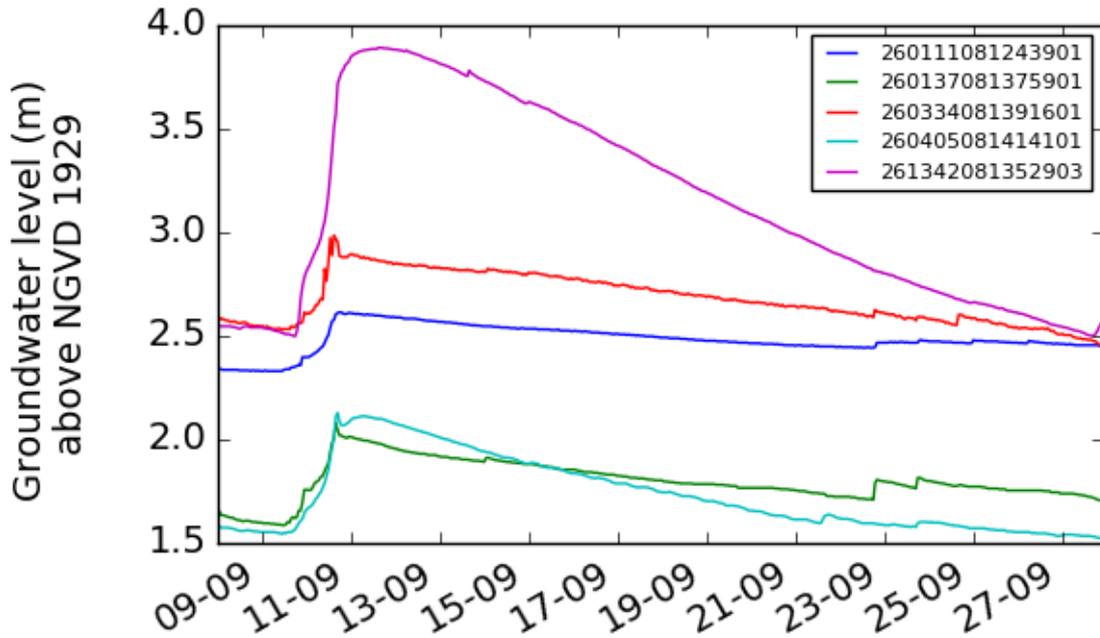
Figure 19: Groundwater observations in wells in Collier County (Florida) during Hurricane Irma in 2017. The corresponding USGS well numbers are presented in the legend.

If one would use Cialone's hydrograph to model land inundation levels, the groundwater system would have recovered too fast (see green line in Figure 20 and Equation 16). If one were to use a complete linear relationship, it looks too unnatural compared to the observed data in Figure 19 (see red line in Figure 20 and Equation 17). Therefore, an average of the exponential and linear approach was used (see blue line in Figure 20) that can be quantified with Equation 18. The first term in the equation is the exponential decreasing term (Cialone's hydrograph) and the second term is the linear decreasing term. The recovery time was set to 20 days and based on the data of Figure 19.

$$H_{storm\ surge\ land}(x, y, t) = H_{peak}(x, y)\left(1 - e^{-\left|\frac{D}{(t-t_0)}\right|}\right)$$

Equation 16: The adapted storm surge hydrograph equation for land-cells in the exponential form.

$$H_{storm\ surge\ land}(x, y, t) = H_{peak}(x, y) - \frac{H_{peak}(x, y)}{t_{recovery}} * t$$

Equation 17: The adapted storm surge hydrograph equation for land-cells in the linear form.

$$H_{storm\ surge\ land}(x, y, t) = \frac{H_{peak}(x, y)\left(1 - e^{-\left|\frac{D}{(t-t_0)}\right|}\right) + H_{peak}(x, y) - \frac{H_{peak}(x, y)}{t_{recovery}} * t}{2}$$

Equation 18: The adapted storm surge hydrograph equation for land-cells in the average form.
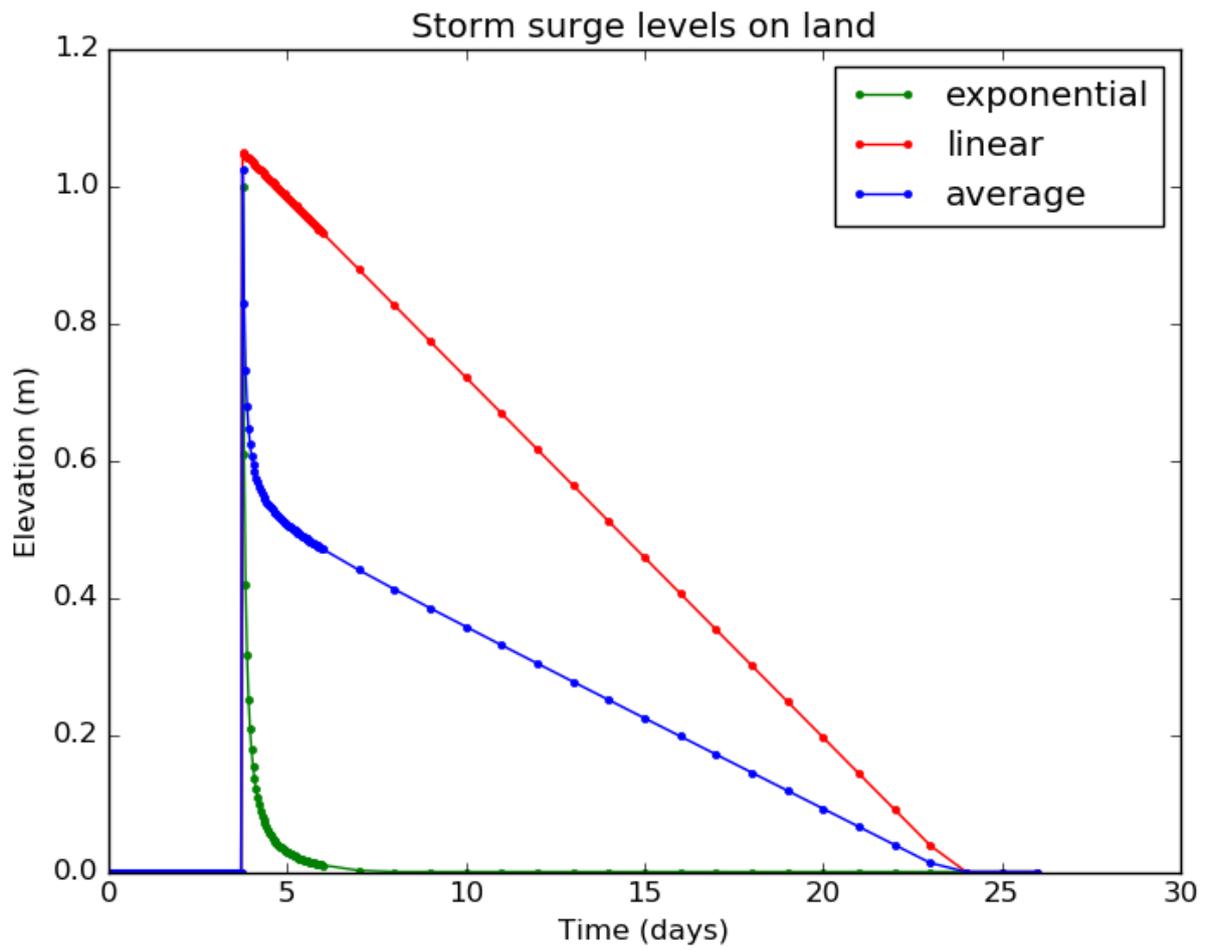
Figure 20: The storm surge levels on land for three storm surge hydrograph equations (i.e. the exponential, linear and average form).

3.4.2. Storm rainfall hydrograph

As the prediction of hurricane-induced rainfall is out of the scope of this research, hurricane-induced rainfall was assumed to follow the same behaviour of storm surge. Therefore, Cialone's hydrograph was adapted:

$$H_{rainfall}(x,y,t) = H_{maximum\ rainfall\ per\ hour}(x,y)\left(1 - e^{-\left|\frac{D}{(t-t_0)}\right|}\right).$$

Equation 19: The storm rainfall hydrograph equation has the exponential form based on Cialone's hydrograph.

3.4.3. Hurricane characteristics

As one can see from storm surge hydrograph equations, hurricane characteristics such as half of the storm duration (D), the radius of maximum winds (RMW) and the forward speed (F) are necessary to calculate the storm surge head. As it is out of the scope of this research to examine these variables extensively, averages of these parameters were obtained, that serve as an indicator on the size of the input parameters of the models of this research.

For example, hurricane forward speed data were obtained from Dorst (2019) who averaged the forward speed of Atlantic hurricanes for specific latitude bins using the HURDAT database of the Hurricane Research Division of NOAA. In Table 8, data on three latitudes bins (5 degrees) are provided. The Florida peninsula corresponds approximately with the latitude bin 25°-30°N.

Latitude bin	Forward speed (km/hr)	Number of cases
20°-25°N	17.5	8602
25°-30°N	20.1	6469
30°-35°N	27.1	3397

Table 8: The forward speed varies with latitude (data obtained from Dorst (2019)).

Data on maximum winds radii were obtained from the research by (Bell and Ray, 2004). In their research, Bell and Ray provide statistics on major north Atlantic hurricanes from 1977 – 1999, distinguishing for so-called hurricane quadrants (see Table 9). Based on their data, the radius for a hypothetical hurricane was set to 25km: 25 model rows or columns width.

Hurricane	RMW (km)	Standard deviation (km)	Median (km)
Left rear	25.10	9.96	23.50
Left front	25.77	10.10	25.50
Right front	24.73	9.29	23.75
Right rear	26.45	10.00	26.25
Front	25.95	9.89	24.00
Right	25.54	9.77	25.50
Left	25.25	9.90	25.00
Rear	25.41	9.86	23.25

Table 9: The radius of maximum winds varies with the hurricane quadrant (data obtained from Bell and Ray (2004)).

3.4.4. Storm surge peak values

Storm surge peak elevations were required to obtain the storm surge hydrograph of interest. Storm surge peak elevations can be determined by various models such as ADCIRC, SLOSH and XBeach (Elsayed and Oumeraci, 2018; NHC, 2019a; Xiao et al., 2019). For this research the SLOSH model was selected. This numerical model was developed by the National Weather Service (NWS) in order to predict storm surges when a hurricane is approaching.

The working of SLOSH can be described as follows: SLOSH estimates storm surge for hypothetical hurricanes based on the wind field that is determined by related variables such as the atmospheric pressure, hurricane size, hurricane forward speed, hurricane intensity (i.e. Saffir Simpson categories) and the tidal phase during the hurricane (NHC, 2019a, 2019b). Subsequently, these variables are used in the core-set of equations that are applied to grid-cells that form the so-called SLOSH basin (i.e. a grid definition that is centred on the area of interest (Conver et al., 2008)). Furthermore, SLOSH takes, next to the DEM, physical features into account, such as local shorelines, water depths, bridges, roads and levees (NHC, 2019a).

The output of SLOSH is based on up to 100000 hurricane simulations with varying conditions and landfall points (NHC, 2019b). Subsequently, based on these runs so-called Maximum Envelope of Water (MEOW) composites are constructed. These composites show the maximum storm surge that are observed in each grid cells of the basin of interest for all the hurricanes runs. The SLOSH output, however, is not directly compatible with the models in the research due to the differences in the nature of the models. First of all, there are differences in mesh grid shape and model resolution and SLOSH does not take sea-level rise into account. However, the major obstacle is that SLOSH does not represent storm surge peak values for individual hurricanes whereas in this research individual hurricanes were simulated. Therefore, to implement SLOSH output in this research's models, the SLOSH output was adapted in this subsection; an operation that involves losing quality of the SLOSH output.

3.4.4.1. *Adaptations model grid and resolution*

SLOSH makes uses of curvilinear, elliptical and hyperbolic telescoping mesh grid shapes for the model calculations (NHC, 2019b). These mesh grid-shapes complicate direct implementation in the groundwater model that is used in this research; this model consists solely of rectangular grid-cells. Also, the model resolution is different: the resolution of SLOSH ranges from 10m up to more than 1000m (NHC, 2019b) whereas this research's model employs a fixed resolution of 1000m – relatively coarse in comparison to SLOSH. Similarly, SLOSH employs a relatively accurate DEM with a resolution of 1 arc second (approximately 30m) (Zachry et al., 2015) whereas this research's model employs a DEM with a resolution of 1000m.

To cope with these differences the SLOSH's data was moulded into a rectangular form and was scaled up to a new resolution of 1000m. In doing so, the data quality of SLOSH was deteriorated as the original data became aggregated and averaged out. After these conversions, both models are in line with respect to mesh grid-shape and resolution (see Figure 21); however, the inundation values cannot be implemented directly yet as SLOSH uses a different DEM to compute these values. By using a different DEM than this research's model, SLOSH would predict certain cells to be inundated while the DEM of research would be too high to become inundated. In other words, the combination of SLOSH data with this research's DEM would create unrealistic inundation situations: inundation would occur at cells of the groundwater model that do not allow for inundation due to their elevation. To illustrate this problem, Table 10 was constructed.
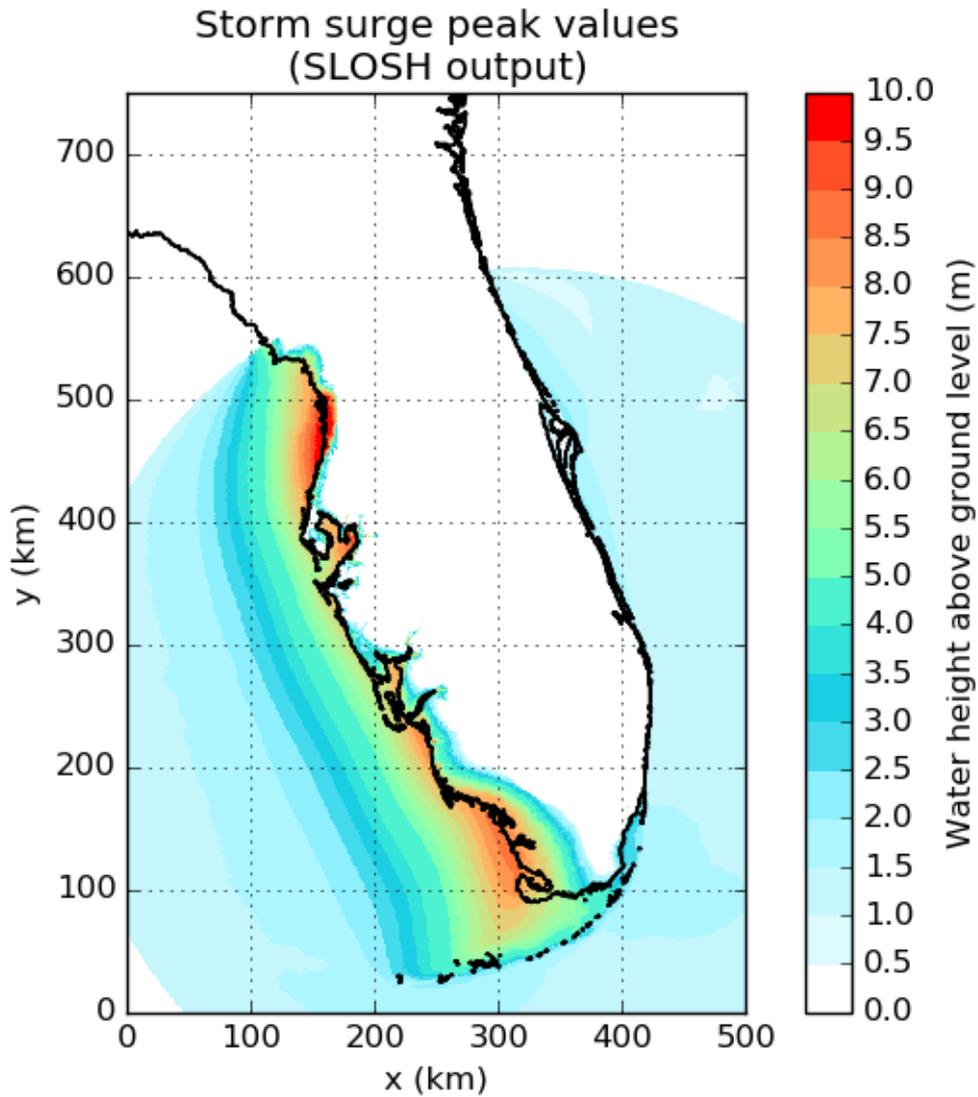
Figure 21: The SLOSH output for an eastward moving category 5 hurricane. The output consists of water heights above groundwater level.

Variable	Value (m)
SLOSH's DEM	4
SLOSH's water head	1
SLOSH's total head (DEM + water head)	5
Research's DEM	6

Table 10: Example of an unrealistic inundated cell: according to the SLOSH data, the cell should be inundated with 1 m water and the DEM should be equal to 4 m. However, the DEM in this cell is 6 m in this research. In other words, the cell cannot be inundated as this research's DEM (6 m) exceeds the total head provided by SLOSH (5 m).

To cope with this problem of unrealistic inundation, the SLOSH data was adapted such that unrealistic inundation values were removed. If the total head that SLOSH predicts exceeds the DEM of this research, the cell remains inundated with the original total head. However, if the total head of SLOSH is lower than the DEM, the cell does not get inundated: the storm surge peak value is set to 0 instead. As a result, unwanted inundated cells were removed (Figure 22).
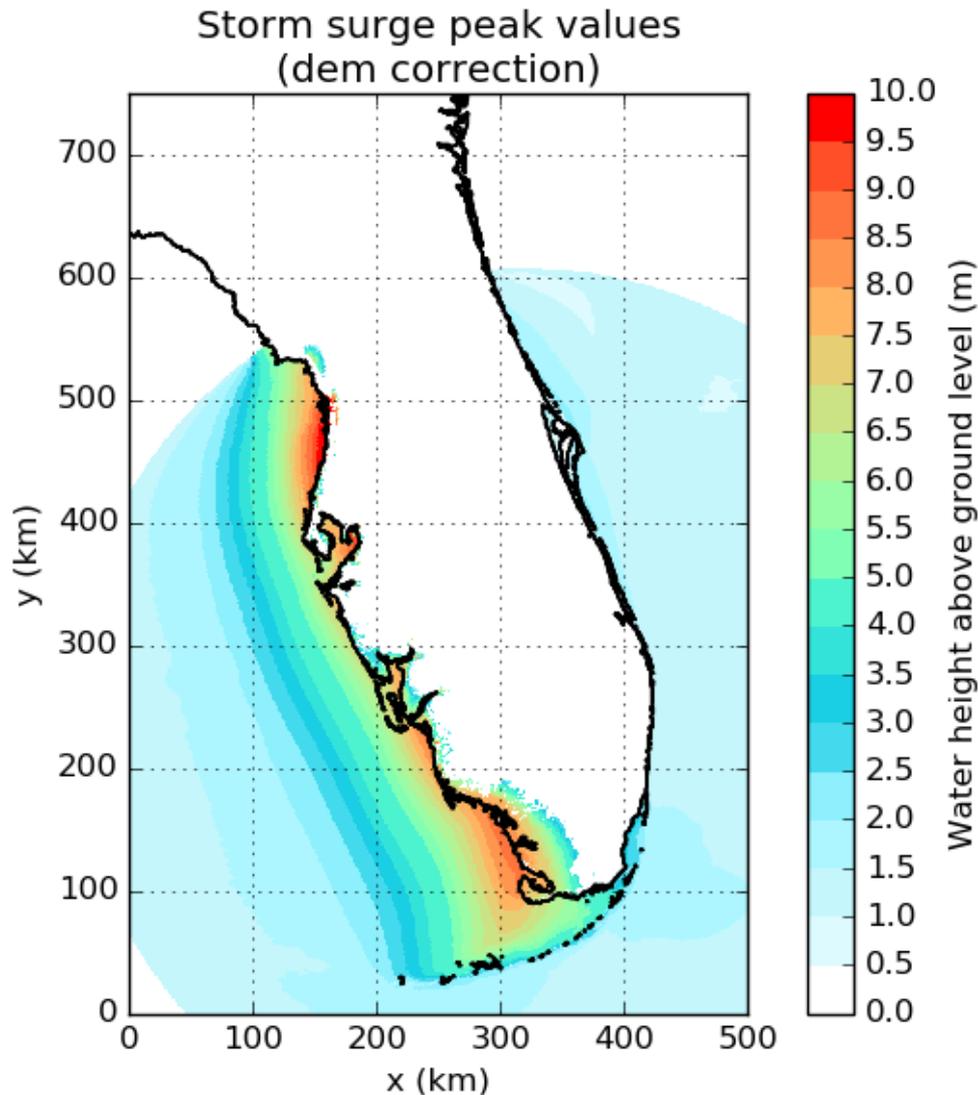
Figure 22: Storm surge peak values after correcting the SLOSH output for DEM-differences. As can be seen after comparison with Figure 21, some land cells are not inundated anymore.

Although this method removes unwanted inundated cells, it does not completely solve all problems yet; it creates new problems. In some areas – especially in the more inland located inundation zones – the inundation zones are connected to the sea by a few so-called pathway cells. Due to the correction method, some of these cells were removed that served as a pathway of the flood to the inland inundation zones. Because of the removal of these pathway cells, inundation zones were left behind, and so-called isolated inundation cells come into being. However, as the pathway cannot be inundated with the DEM of this research, these connected inundation zones cannot be inundated as well. Therefore, the isolated inundation zones were removed based on the principle that all inundated cells must have an established connection with the sea. In doing so, this approach removes all inundated-cells that have lost their pathway to the sea (see Figure 23).
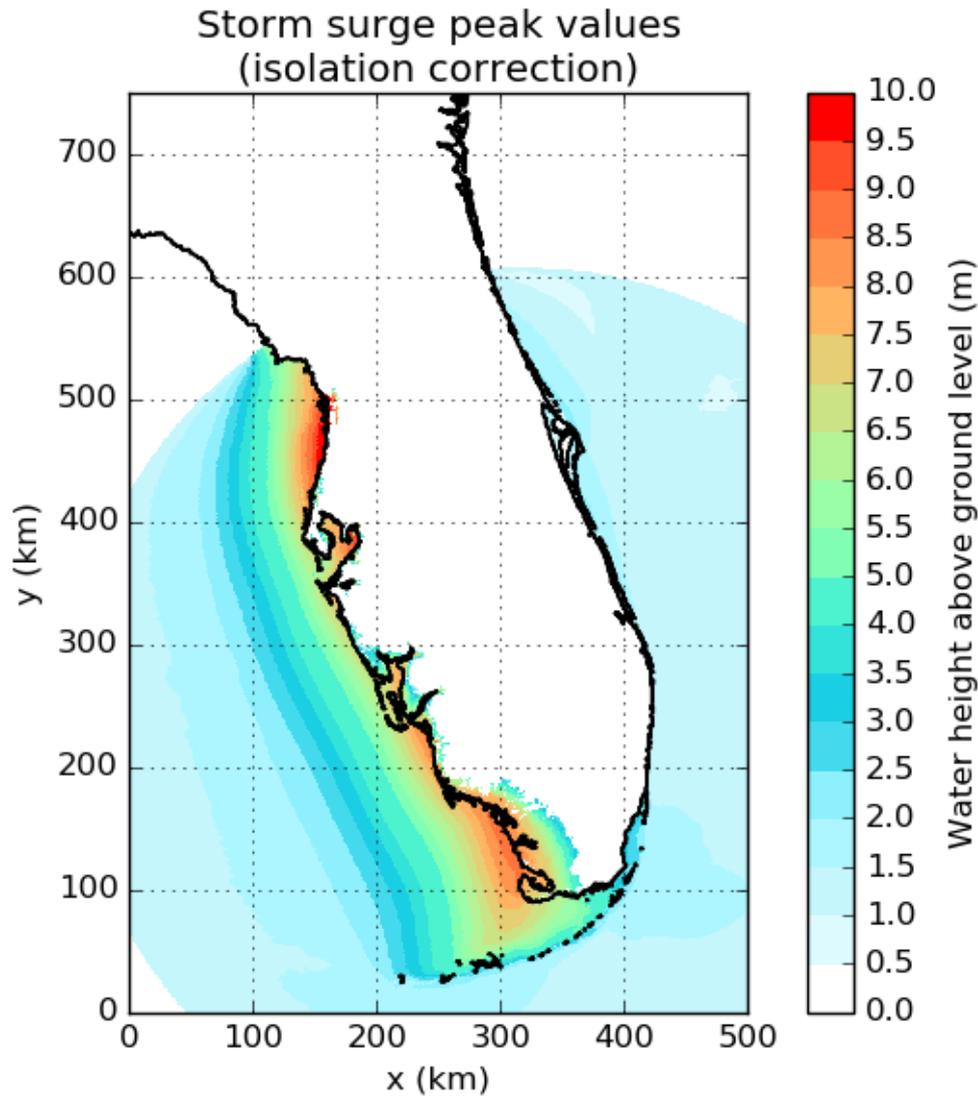
Figure 23: Storm surge peak values after removing isolated inundation cells. As can be seen after comparison with Figure 22, some land cells are not inundated anymore (a small difference only).

3.4.4.2.   Adaptations sea-level rise

To account for sea-level rise effects on hurricane-induced storm surge, the SLOSH data was modified as SLOSH does not take these effects into account. In order to combine sea-level rise SLOSH, Maloney and Preston (2014) added sea-level rise projections to hurricane-induced storm surge data obtained from SLOSH. This approach was adopted in this research. First, the sea-level rise projection of 1m was added to the storm surge data by SLOSH (see Figure 24).
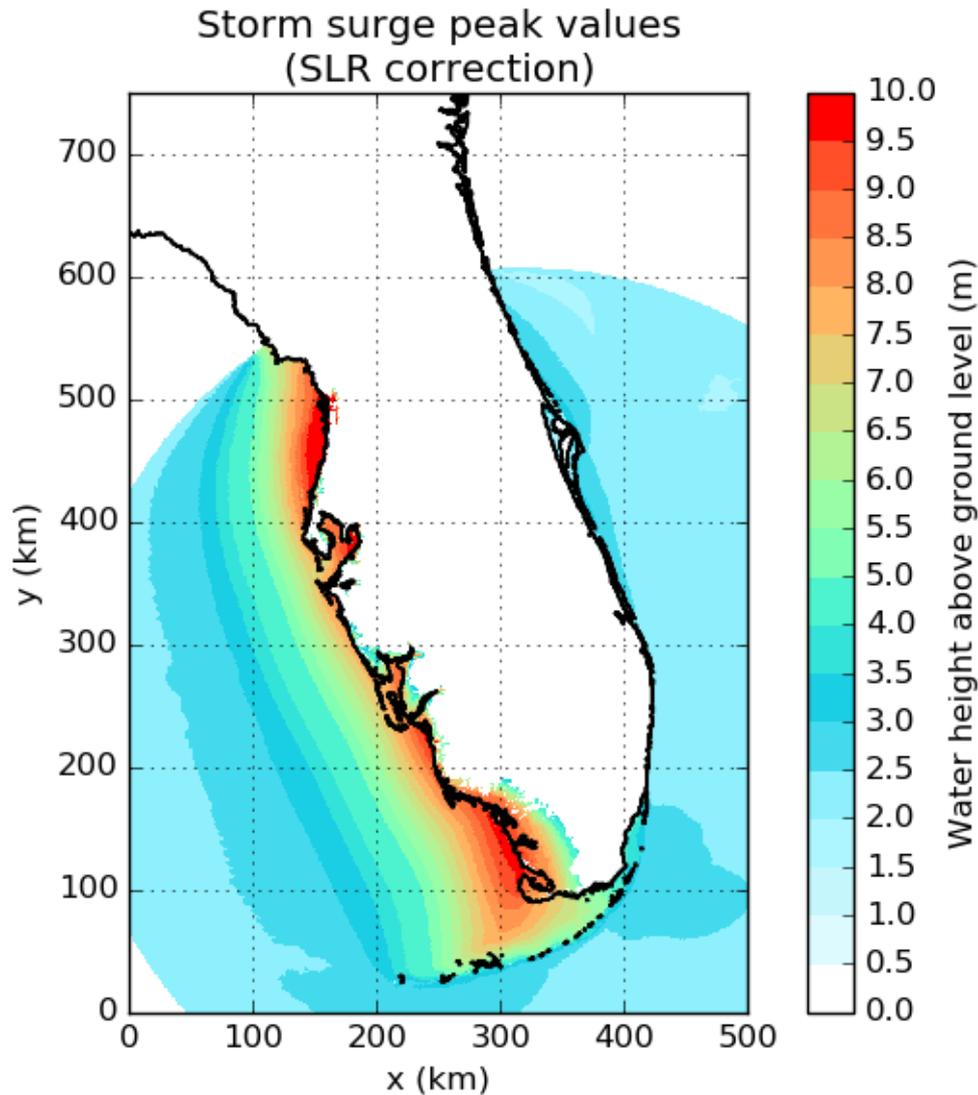
Figure 24: A sea-level rise of 1m was added to the storm surge peak values from the SLOSH output.

Afterwards, the DEM of non-inundated grid cells was compared with the total heads (DEM + water-level) of neighbouring inundated cells. If the non-inundated cell has a lower elevation than an inundated cell, the non-inundated cell gets inundated with a water depth equalling the difference between the two cells (see visualization in Figure 25). Afterwards, this difference was multiplied with a factor of 0.95 to maintain a negative head-gradient (inland decreasing head). This procedure was repeated until no cells become inundated anymore (see Figure 26). The major disadvantage of this method is that valuable information of the SLOSH data is lost. For example, SLOSH includes natural barriers (e.g. levees, houses and forests) in model flow calculations. By using this sea-level rise approach however, this barrier accuracy could not be maintained anymore, and the quality of the SLOSH data slightly deteriorated (Maloney and Preston, 2014).
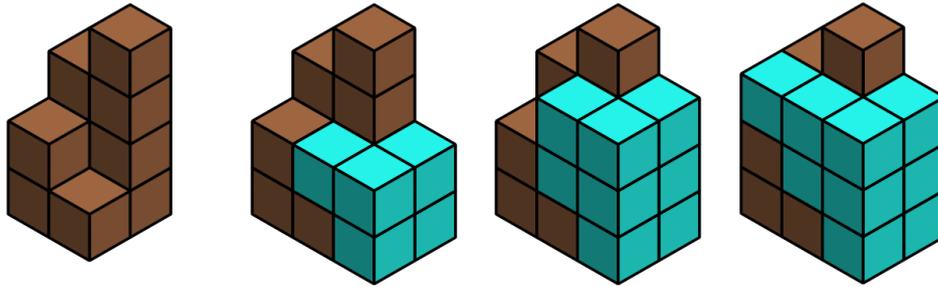
Figure 25: Scheme illustrating the sea-level rise procedure, from left to right: DEM only, DEM and storm surge peak values, DEM and storm surge peak values + SLR, and lastly inundation of a previously non-inundated cell due to the sea-level rise projection (note that the factor of 0.95 is not included in this picture).
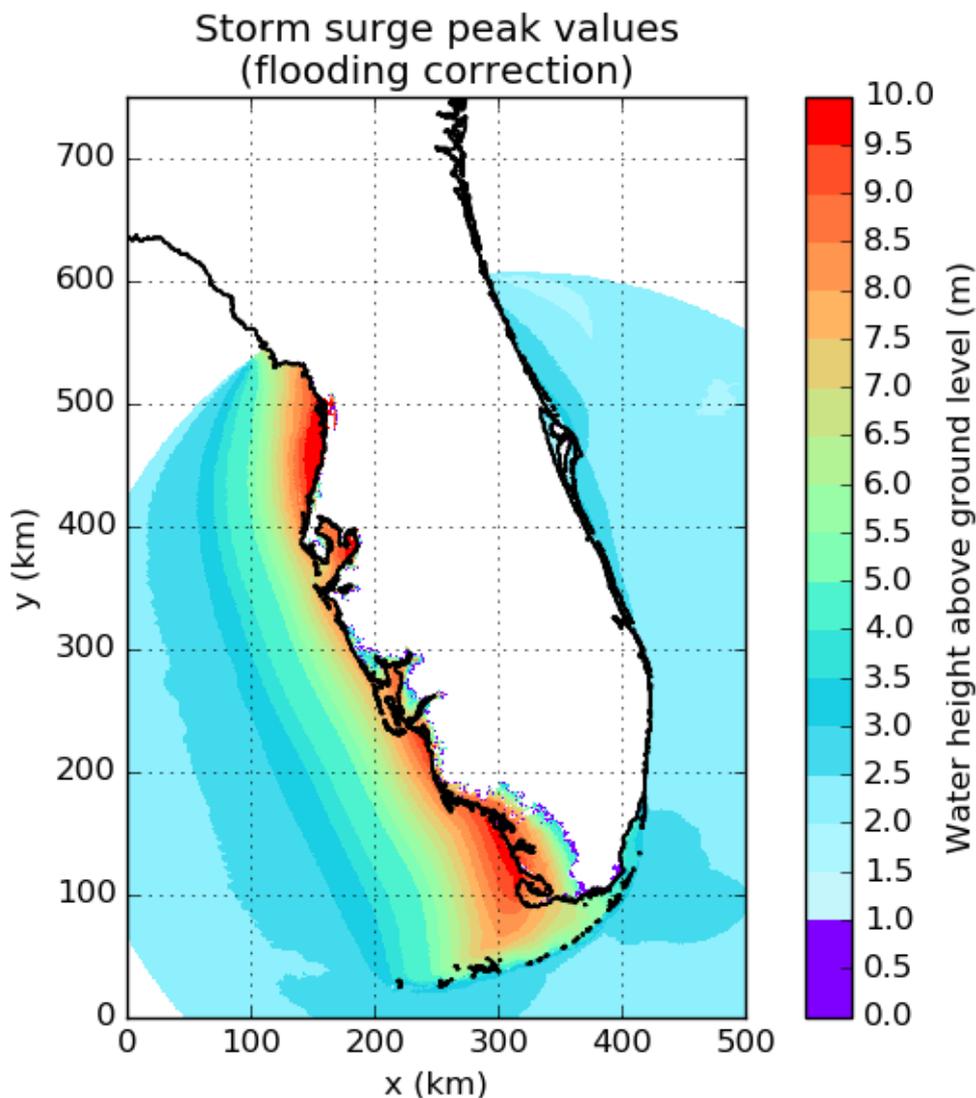
Figure 26: Storm surge peak values including the additional flooding related to the imposed sea-level rise (accentuated with purple). As can be seen after comparison with Figure 24, extra land cells are inundated.

3.4.4.3. Adaptations individual hurricane

As already stated, the major drawback is that the SLOSH output does not represent storm surge peak values for individual hurricanes. If one would apply the SLOSH data directly in the groundwater model, a large part of the Floridan coast would be flooded (see Figure 21).

Furthermore, there would be a severe overestimation as the SLOSH output (MEOW) consists of the highest simulated storm surge values only; these worst-case values are not representative for

individual hurricanes (NHC, 2019b). In order to continue to incorporate the SLOSH output in this research, the data needs to be adapted as such that it represents one single hurricane that induces storm surge elevations that are as realistic as possible.

To this end, the SLOSH output was adapted according by the following approach. First of all, only the storm surge peak values of the centre hurricane path were selected (i.e. one row) followed by all the data that is located within the radius of maximum winds (i.e. rows above and under the hurricane centre row). Afterwards, the values of one coast-side were selected (i.e. the west-coast only) (see subplot "hurricane extraction" in Figure 27).
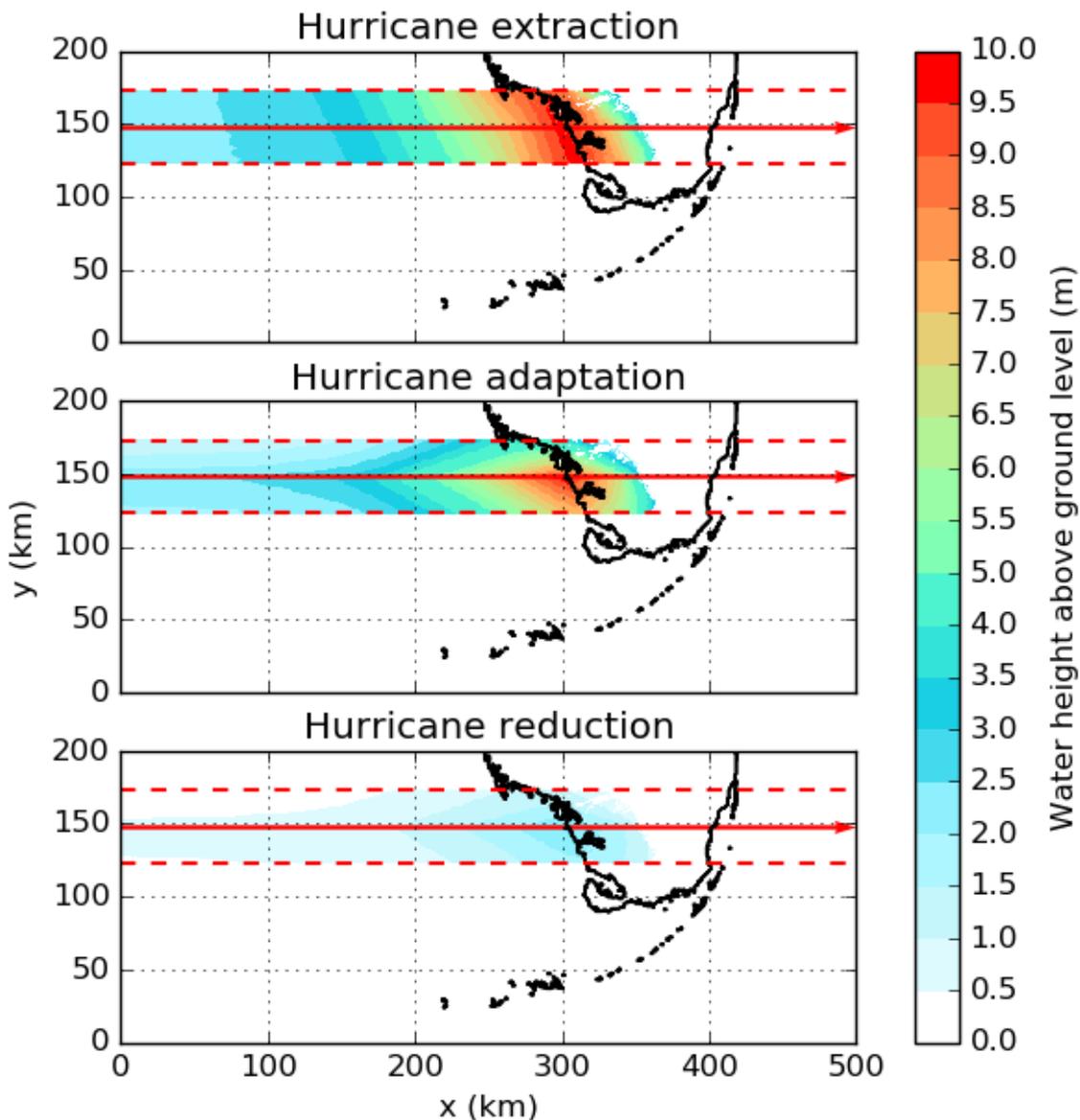
Figure 27: The storm surge peak elevations were modified in three more steps. First, a selection of storm surge peak elevations was made (hurricane extraction), followed by an adaptation of the data that takes the hurricane direction and distance to the hurricane eye into account. At last, the data was multiplied with a reduction factor to match the data to observations.

Subsequently, the storm surge peak values should be adapted such that they represent one hurricane only. As can be seen in the subplot "hurricane extraction" (Figure 27), storm surge levels on both sides of the hurricane centre path are equally high as on the centre of the path (i.e. the arrow). In reality, storm surge decreases with distance from the path of the hurricane centre (see Subsection 2.1.2). Also, storm surge will be higher for onshore winds (the area below the centre path

in Figure 27) than offshore winds (the area above the centre path). To include this behaviour, one needs to decrease the storm surge values on both sides of the hurricane centre. Therefore, the storm surge values were multiplied with different factors for the different hurricane sides. These factors were derived from the high-water profile for Hurricane Camille (1970) in the Northern Gulf of Mexico (see Figure "High water profile for hurricane Camille in the northern Gulf of Mexico, from U.S. Army Corps of Engineers (1970)" from Needham and Keim (2012)).

For instance, the values in the row above the hurricane centre row were multiplied with a factor 0.97 thus decreasing the storm surge elevations in comparison with the hurricane centre row. Then, the values in the row above this row were multiplied with a factor 0.97 multiplied with the same factor 0.97. This process was repeated until the last row within the hurricane radius was reached. The same process was repeated for the rows under the hurricane centre. In this direction, a factor 0.99 was used, causing the storm surge peak values to decrease more slowly in this direction. This approach results in the new storm surge peak distribution (see subplot "hurricane adaptation" in Figure 27).

By means of verification, the maximum storm surge peak elevation by SLOSH were compared to observed surface water elevations (data by NOAA Tides and Currents) near hurricane landfall positions during severe hurricane events. To this end, surface water elevation data near hurricane landfall locations were obtained during Hurricane Irma (2017) and Michael (2018) (see Figure 28 and Figure 29, respectively). During Hurricane Irma, a negative storm surge was observed (i.e. water is driven away from the shore, lowering water levels), followed by a storm surge of approximately 1.5m above the datum. For Hurricane Michael, no negative storm surge was observed, and the storm surge corresponded to 2.5m above the datum, approximately.

As one can see from "hurricane adaptation" in Figure 27, the maximum storm surge peak elevation near the landfall location created by SLOSH is approximately 10m. The difference between the SLOSH output and the observations (2.5m) is too large; it is known that the SLOSH output clearly overestimates the storm surge for an individual hurricane. Therefore, a reduction factor was applied to the SLOSH output that approximates to (2.5m/10m=) 0.25. In doing so, the storm surge peak elevations become more representative (see "hurricane reduction" in Figure 27).

Obviously, one can question whether the SLOSH output is an overestimation of the inundation zone as SLOSH does not account for individual hurricane events. In this research, however, the inundation zone was not adapted any further and was assumed to be a worst-case scenario. It is beyond the scope of this work to reproduce storm surge peak elevations of individual hurricanes.
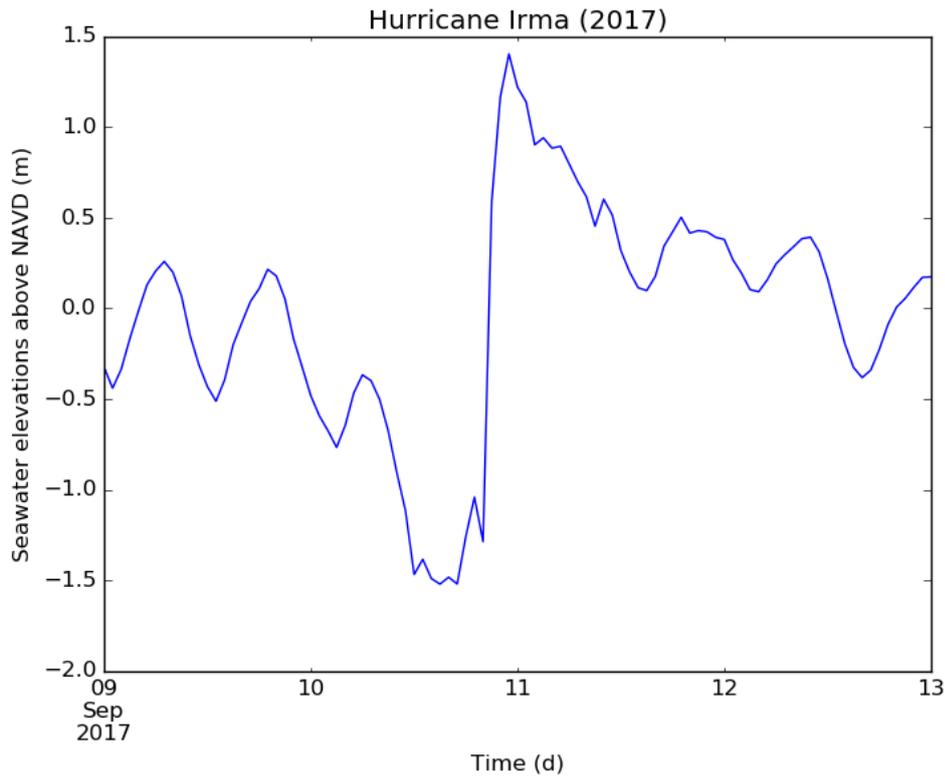
Figure 28: Surface water elevations during Hurricane Irma (2017) in Naples (Florida); a location near the landfall location of the hurricane. The observed data was obtained from the NOAA Tides and Currents station ID 8725110.
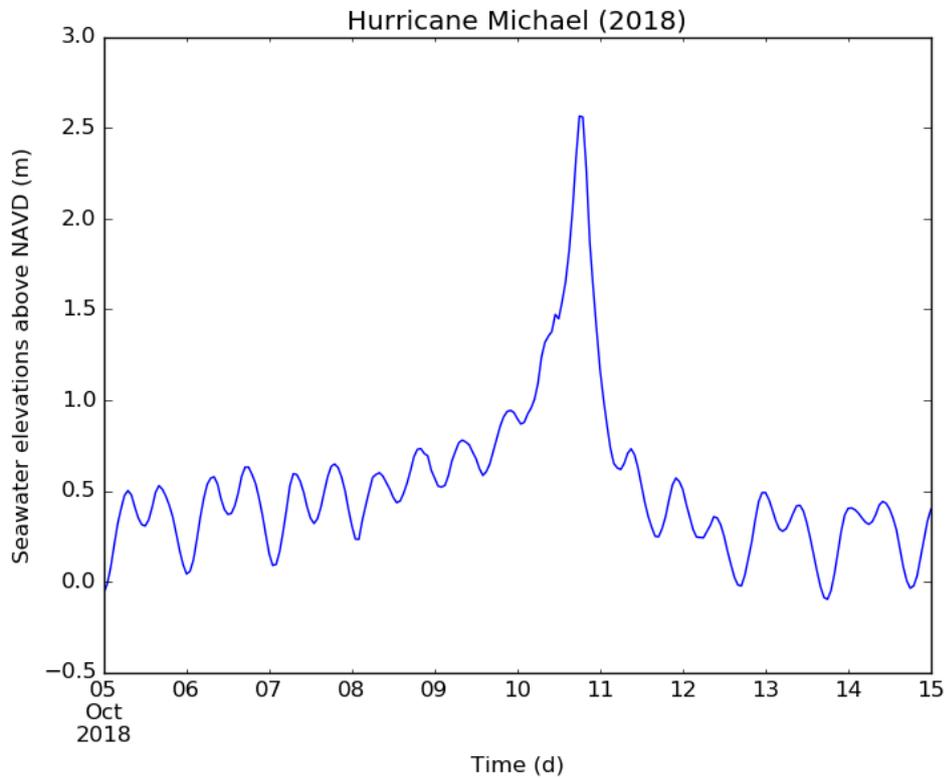
Figure 29: Surface water elevations during Hurricane Michael (2018) in Apalachicola (Florida); a location near the landfall location of the hurricane. The observed data was obtained from the NOAA Tides and Currents station ID 8728690.

3.4.5. Hurricane tool in practice

In this subsection, hurricane-induced storm surge elevations and rainfall are simulated for observation points of the hurricane event presented in Figure 27 ("hurricane reduction"). In Figure 30, the storm surge peak elevations are re-plotted with observation points along the hurricane centre track, including a more specific legend.
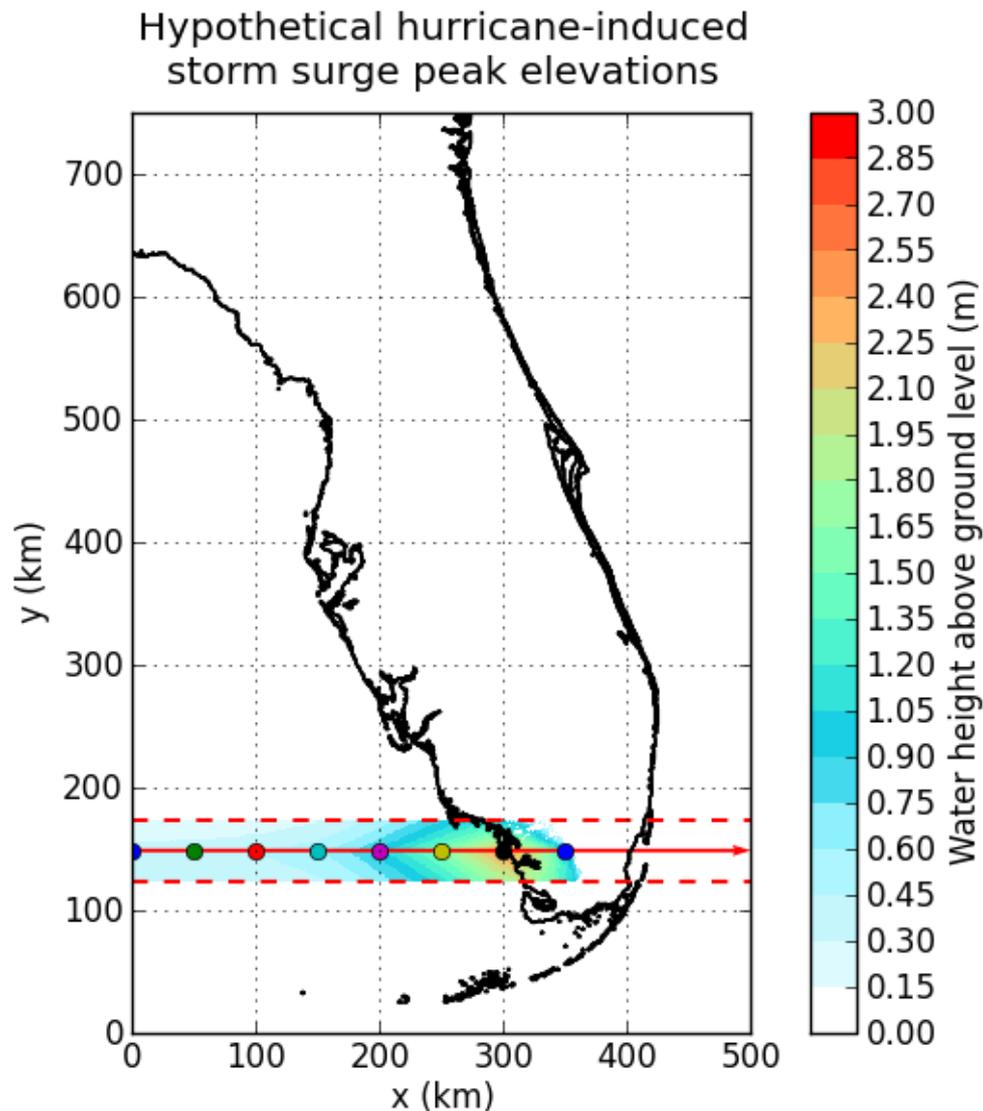
Figure 30: The final storm surge peak elevations for a hypothetical hurricane.

Afterwards, the storm surge hydrograph (see Figure 31) and the storm rainfall (see Figure 32) are plotted for the observation points during the first phase of the hurricane-event (144 hours; 6 days). During this phase, the hypothetical hurricane travels over the whole model domain. After this phase, all storm surge elevations on sea (and rainfall levels) have returned to their pre-hurricane conditions. Storm surge elevations on land, however, need more time to recover to their pre-hurricane state. Therefore, the hurricane-tool simulates the second and last phase of the hurricane-event (±20 days). During this phase, the storm surge elevations on land cease eventually (see Figure 33).
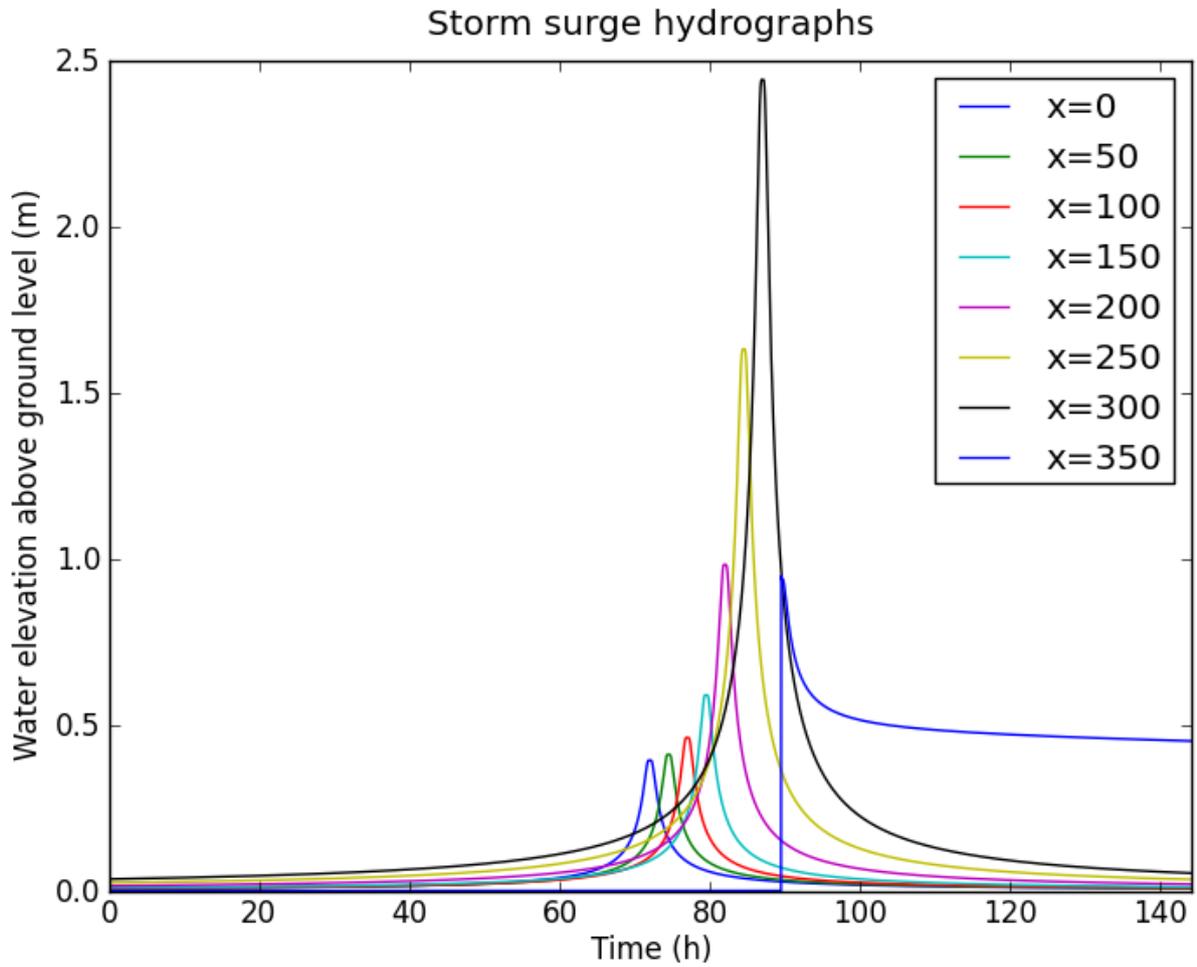
Figure 31: Storm surge hydrographs for observation points (x in km) located on the hurricane centre track during the first-phase of the hurricane event; seven observation points are located on sea, whereas one observation point (x=350 km) is located on land.
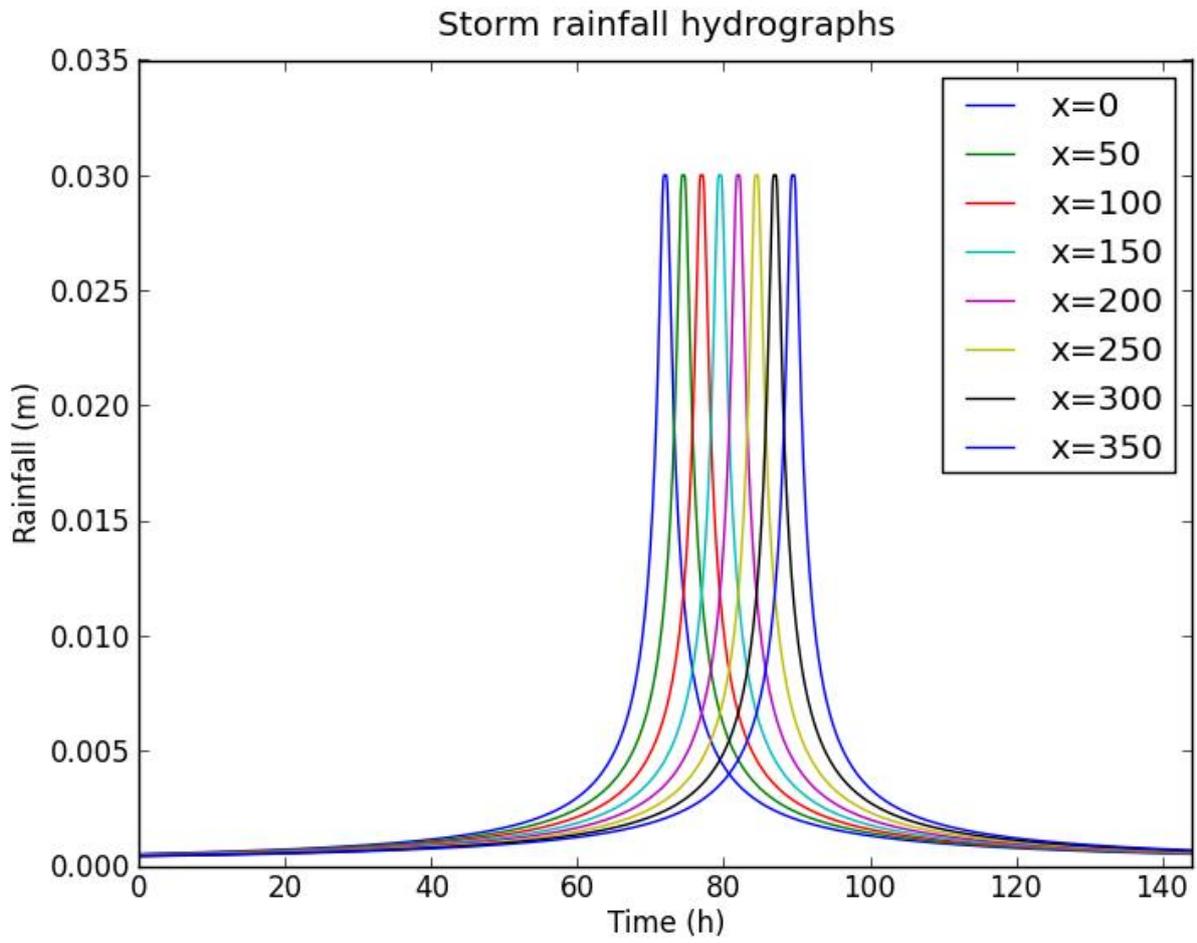
Figure 32: Storm rainfall hydrographs for observation points (x in km) located on the hurricane centre track during the first-phase of the hurricane event.
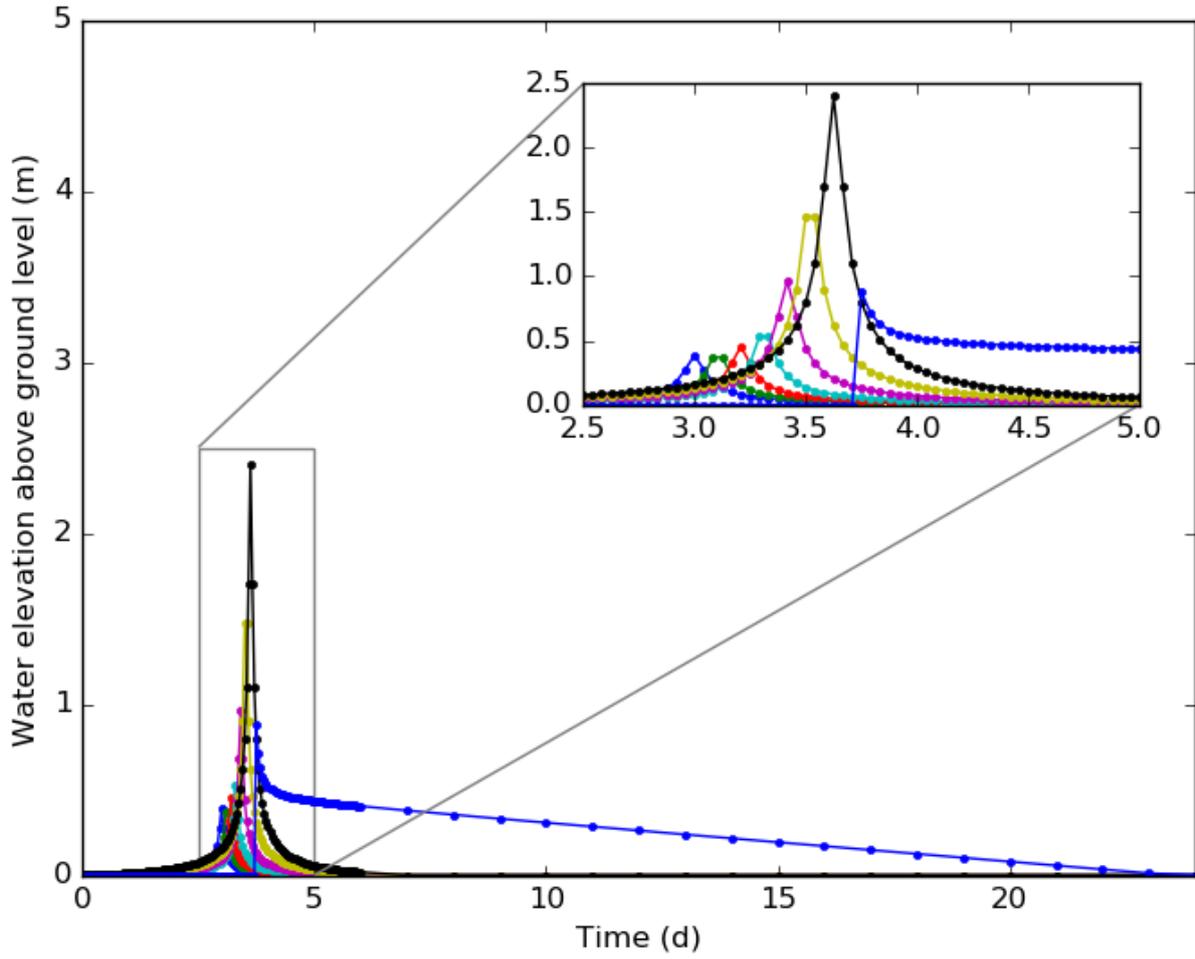
Figure 33: Storm surge hydrographs for observation points located on the hurricane centre track during the first-phase and second phase of the hurricane event; seven observation points are located on sea, whereas one observation point (x=350 km) is located on land.

3.5.   Scenarios and data analysis

To answer the main research question, climate scenarios were developed that covered a variety of hurricane intensities, peak rainfall rates and sea-level rise projections (see Table 11 for an overview). The scenarios are described thoroughly in the subsections below, followed by the data analysis of this study.

The hurricane tool allows for simulation of hurricanes of any direction (i.e. north, east, south, west) and landfall location within peninsular Florida, as long as storm surge peak data (i.e. SLOSH output) is available. Due to time restrictions, however, the scenarios of this research were simulated for one hurricane landfall location and one hurricane direction only: all hypothetical hurricanes made landfall in southern Florida and moved eastward. This area was chosen due to its low hurricane return periods (e.g. 13 to 15 years, see Figure 10) and relatively low elevations (see Figure 11), making the area vulnerable for hurricane-induced storm surge and accompanying saltwater intrusion.

Scenario	Type	Description
1	Hurricane intensity	Saffir-Simpson category 3
2	Hurricane intensity	Saffir-Simpson category 4
3	Hurricane intensity	Saffir-Simpson category 5
4	Rainfall rate	Peak rainfall rate 0.045 m/h
5	Sea-level rise	Projection 0.50 m
6	Sea-level rise	Projection 1.00 m

Table 11: The climate scenarios consist of different hurricane intensities (in terms of Saffir-Simpson category), peak rainfall rates and sea-level rise-projections. The default hurricane intensity is Saffir-Simpson category 5, the default sea-level rise projection is 0.00 m and the default peak rainfall rate is 0.030 m/h.

3.5.1. Hurricane intensity scenarios

The first type of scenarios considers conceptual hurricanes in Saffir-Simpson categories 3 through 5 that make landfall in southern Florida. For each scenario, accompanying data on storm surge peak elevations were obtained from the SLOSH dataset (sf1meow_AGL_e) and adapted in the hurricane-tool (see Section 3.4). The results of these adapted storm surge peak elevations are visualized in Figure 34. As one would expect, the inundation zone corresponds to the hurricane-intensity.

To simulate hurricanes in the transient model, the hurricane tool was used to calculate general head boundary conditions (e.g. storm surge heads, concentrations and densities) for each time-step. An overview of the parameters used in the hurricane-tool calculations are presented in Table 12. Afterwards, the general head boundary conditions are implemented in the transient model to simulate the hurricane event (approximately 26 days). At the end of this period, the inundation levels on land have ceased completely. At last, the transient model has simulated the flushing period of salt out of the groundwater system (approximately 25 years, see Subsection 3.3.2).

Parameter	Value
Hurricane radius of maximum winds	25 km
Hurricane forward speed	20 km/h
Half the hurricane duration	1.25 h
Peak rainfall rate during hurricane	0.030 m/h
Storm surge peak	2.50 m
Sea-level rise projection	0.00 m

Table 12: An overview of the parameters that were used in the hurricane-tool to calculate the storm surge (peak) elevations.
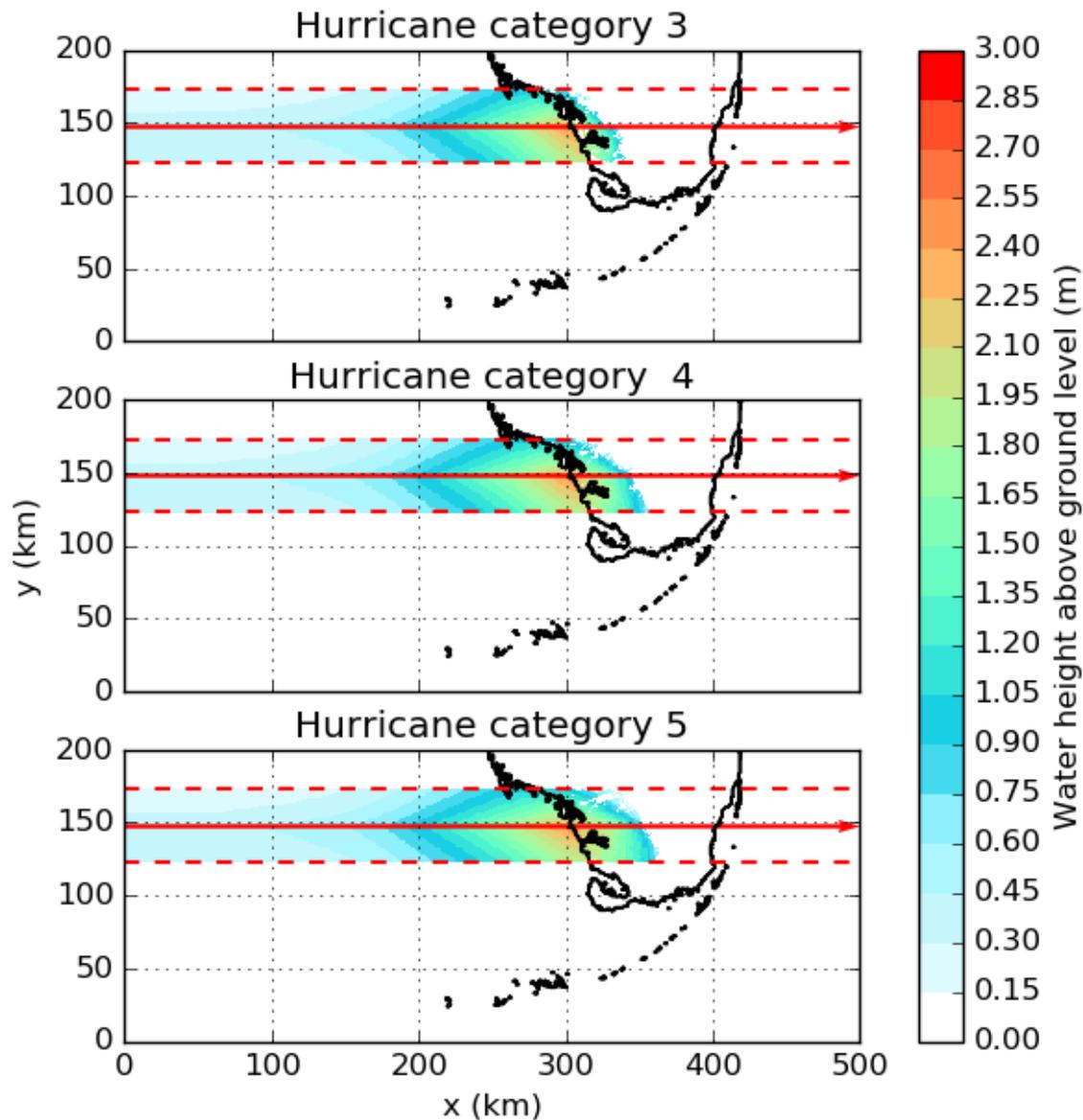
Figure 34: An overview of the adapted storm surge peak elevations of the SLOSH output under the different hurricane intensity scenarios.

3.5.2. Hurricane rainfall scenarios

The second scenario-type considers the category 5 hurricane scenario in combination with an increase of 50% in the peak rainfall rate during the hurricane compared to the default peak rainfall rate of 0.030 m/h (see Figure 35). First of all, the general head boundary conditions are calculated using the hurricane tool. Subsequently, these boundary conditions are implemented in the transient model. During the calculations, the other parameters (see Table 12) are maintained.
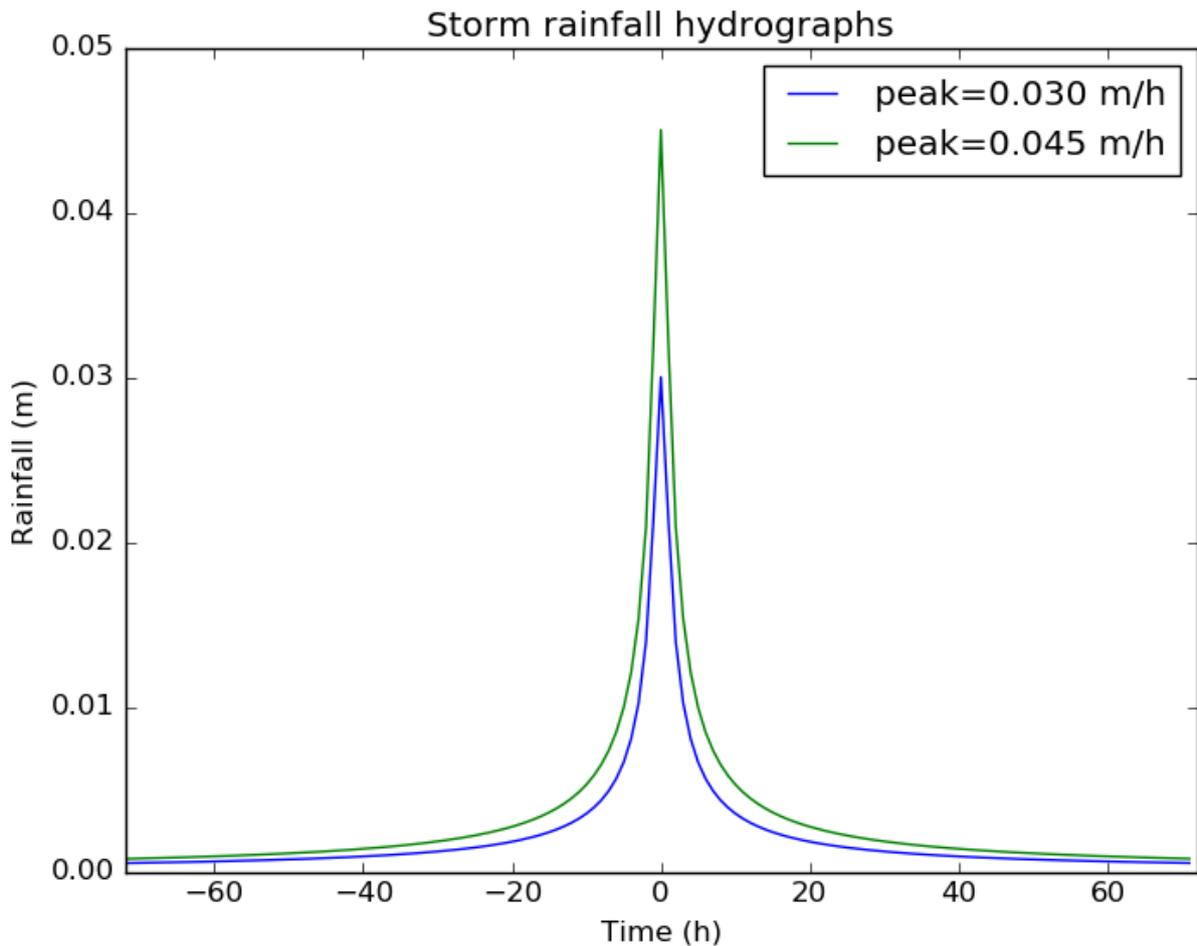
Figure 35: An example of two storm rainfall hydrographs for a hypothetical observation point (see the exponential hydrograph, Equation 16) with different peak rainfall rates during the hurricane.

3.5.3. Sea-level rise scenarios

The last type of scenarios considers the category 5 hurricane that makes landfall in southern Florida in combination with sea-level rise projections of 0.50 and 1.00 m. Using the hurricane tool, the sea-level rise projections were added to the storm surge peak elevations and additional flooding was calculated (see Subsection 3.4.4). The storm surge peak elevations corresponding to the scenarios and the scenario without sea-level rise are visualized in Figure 36.

In the calculations of the general head boundary conditions, the hurricane tool has incorporated the hurricane parameters presented in Table 12. Afterwards, the general head boundary conditions are implemented in the transient-model for each time-step.
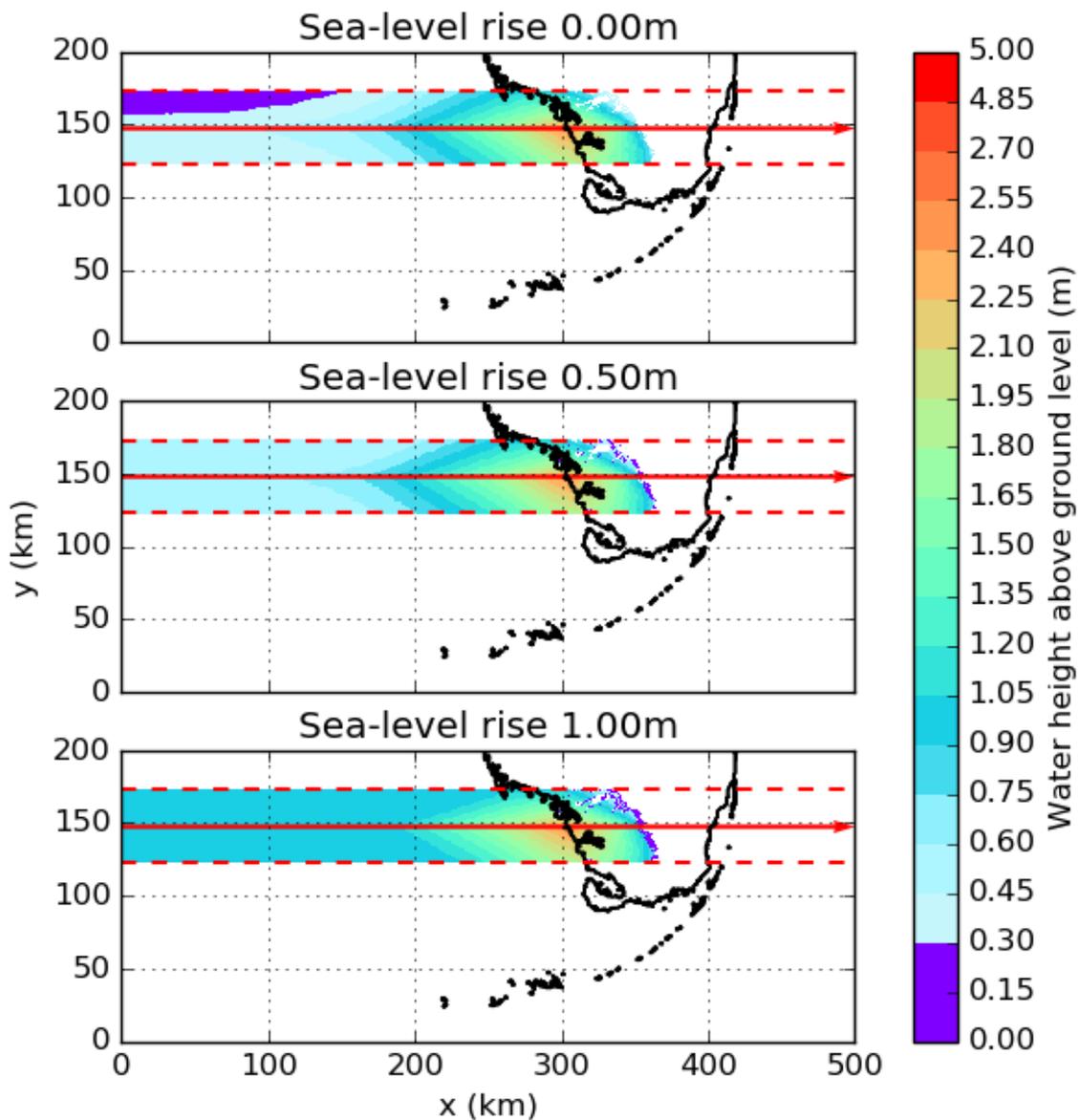
Figure 36: An overview of the adapted storm surge peak elevations of the SLOSH output under the different sea-level rise scenarios. To illustrate the differences between the sea-level rise scenarios, low inundation values are accentuated with purple.

3.5.4. Data analysis

All scenarios were analysed using three groundwater salinization assessment criteria: the solute mass infiltration (kg TDS), the fresh groundwater volume (m^3) and the flushing time (years). During the simulation of the hurricane event and the following 25 years flushing period, the solute mass and the related fresh groundwater (concentrations of ≤1 kg/m^3 and ≤2 kg/m^3) volume are monitored for the whole model domain. Also, the flushing time that is defined as the time required to recover 90% of the salinized groundwater volume (i.e. the fresh groundwater volume decrease) is calculated. By using this approach, the severity of each hurricane scenario can be calculated and compared. A similar approach was used by Yu et al. (2016) to evaluate groundwater salinization processes.

4. Results

This chapter shows the results of the stationary model and the transient model. First, the main result of the stationary model will be presented that provides initial conditions for the transient model. Afterwards, results of the climate scenarios are discussed in terms of the groundwater salinization criteria. To limit model analysis, the climate scenarios are presented for the hurricane-affected subdomains of the model only. These subdomains were easily selected, as the model was divided vertically into four subdomains by the Parallel Krylov Solver.

4.1. Stationary model

The development of the fresh (concentrations of ≤1 kg/m³ and ≤2 kg/m³) groundwater volume inside the complete model domain over time is plotted in Figure 37. The model started under completely saline conditions (i.e. 35 kg/m³) except for the bottom layer at which (relatively fresh-brackish) boundary conditions are implemented. This explains why the fresh groundwater volume does not start at zero. During the 3000 years simulation, saline groundwater was flushed out until the fresh-saline groundwater interface reaches more or less a steady-state (see Figure 38).
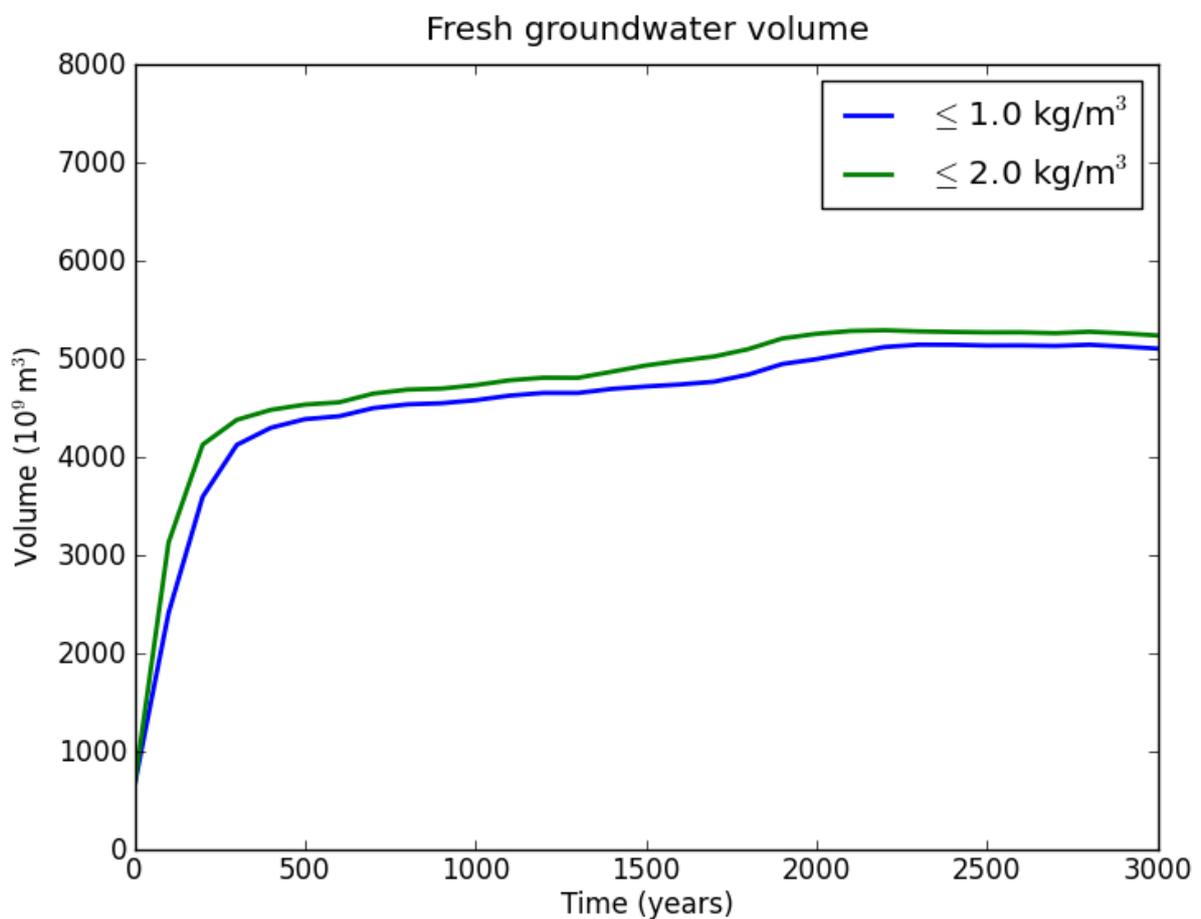
Figure 37: The development of the fresh groundwater volume inside the entire model domain.
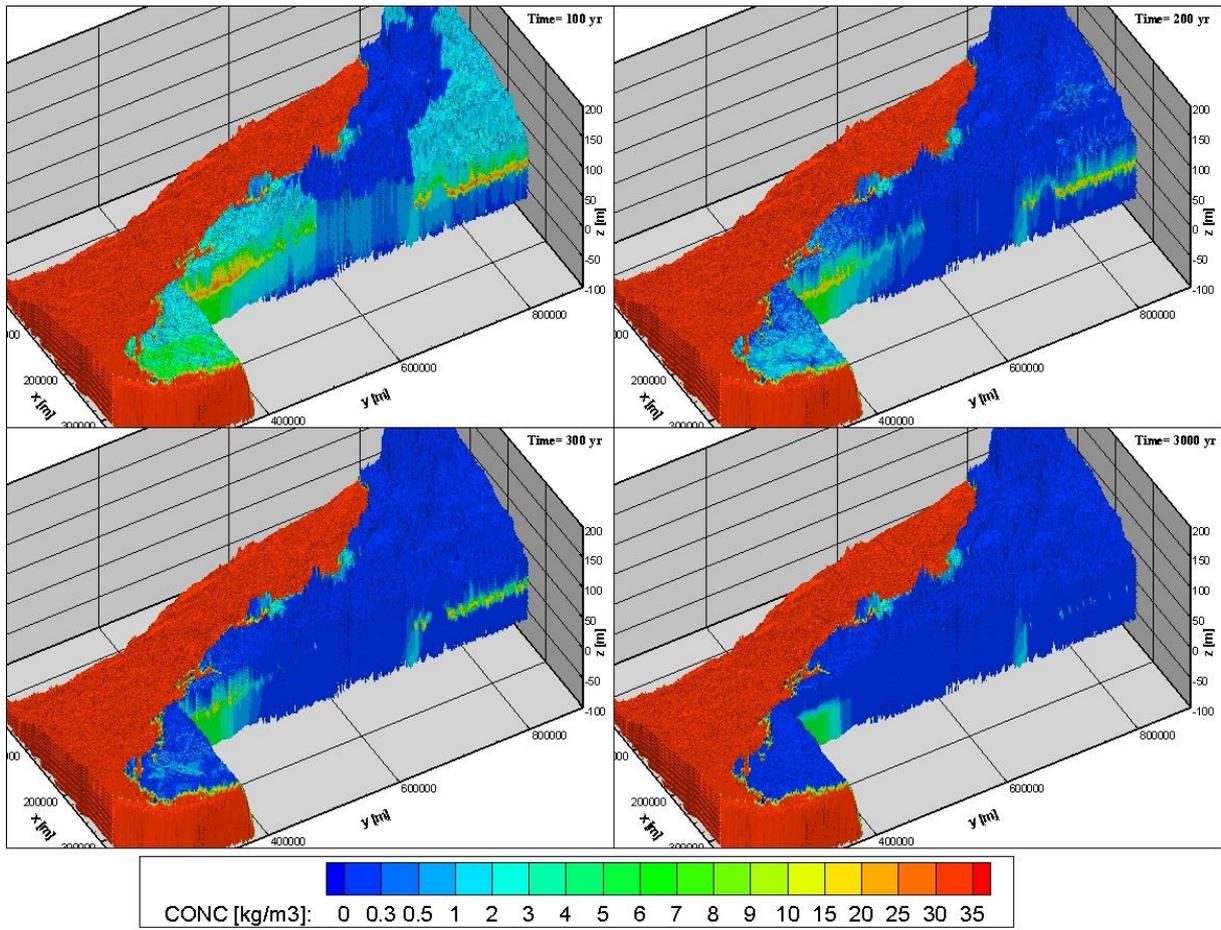
Figure 38: A top view and cross-section of peninsular Florida showing the development of the fresh-saline groundwater distribution for different times of the stationary model run (after 100, 200, 300 and 3000 years).

4.2. Hurricane intensity scenarios

Before analysing the scenarios using the three groundwater salinization assessment criteria, a top view and cross-section of the model are presented to gain a visual impression of the differences between the scenarios. Figure 39 shows a top view of the groundwater concentration in the upper layer (1m thick) right after the storm surge has ceased (after 26 days, see Subsection 3.3.2). The differences between the scenarios are evident: the higher the intensity, the larger the saltwater intrusion extent. This pattern is in accordance with Figure 34: storm surge peak elevations reach further inland for stronger hurricanes. Also, the groundwater concentration appears to be slightly higher (at least locally) for higher hurricane intensity scenarios (compare Figure 39b with Figure 39c). The higher concentrations are most likely due to higher inundation levels: more saline water percolates downward, therefore more saline water mixes with the groundwater and thus the higher the groundwater concentration becomes. In addition, one can observe an abrupt transition from relatively high concentrations (>20 kg/m^3) to lower concentrations at approximately x=315000m. This difference can be explained by the local hydrogeological transitioning of sand into carbonate rocks (limestone) from west to east (see Figure 13). Due to the relatively higher permeability of these carbonate rocks, saline water is flushed out easier than from the sandy subsoil. Therefore, the groundwater concentration is considerably lower further inland.
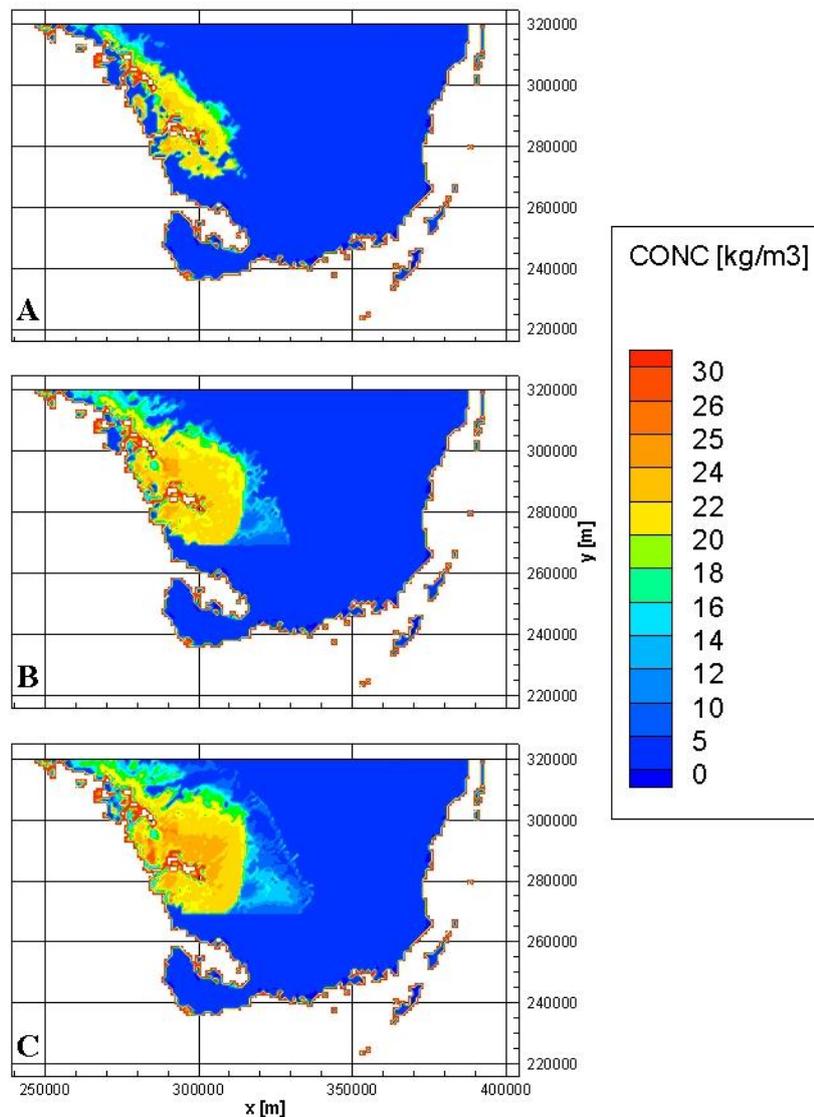
Figure 39: The groundwater concentration is visualized for the hurricane intensity scenarios: subplots A, B and C show the concentration after category 3, 4 and 5 hurricanes, respectively. All subplots represent the concentration of the first layer of the affected Floridan peninsula subzone right after the storm surge has ceased.

Apart from the top view, the groundwater concentration can also be visualized below surface level to gain an impression of the differences between the scenarios with depth. Therefore, a cross-section at the hurricane centre path (y=295000m) is presented for a reference case (Figure 40a) and the different scenarios (Figure 40b, Figure 40c and Figure 40d). Initially, saline groundwater resides in clayey layers (starting at 30m below surface level) and is in equilibrium with fresh groundwater (see Figure 40a). Further inland (x>320000m), the subsoil is formed by highly permeable carbonate rocks and freshwater is encountered only. Also, there are 'columns' of saline water visible that are most probably the results of local groundwater seepage of saline water from deeper clayey layers.

Just like the top view of the groundwater concentration, differences between the scenarios are clearly visible: the higher the intensity, the larger the saltwater intrusion extent. In addition, the effect of the local hydrogeology is evident: further inland, saline groundwater percolates deeper than near the west coast due to high permeability.
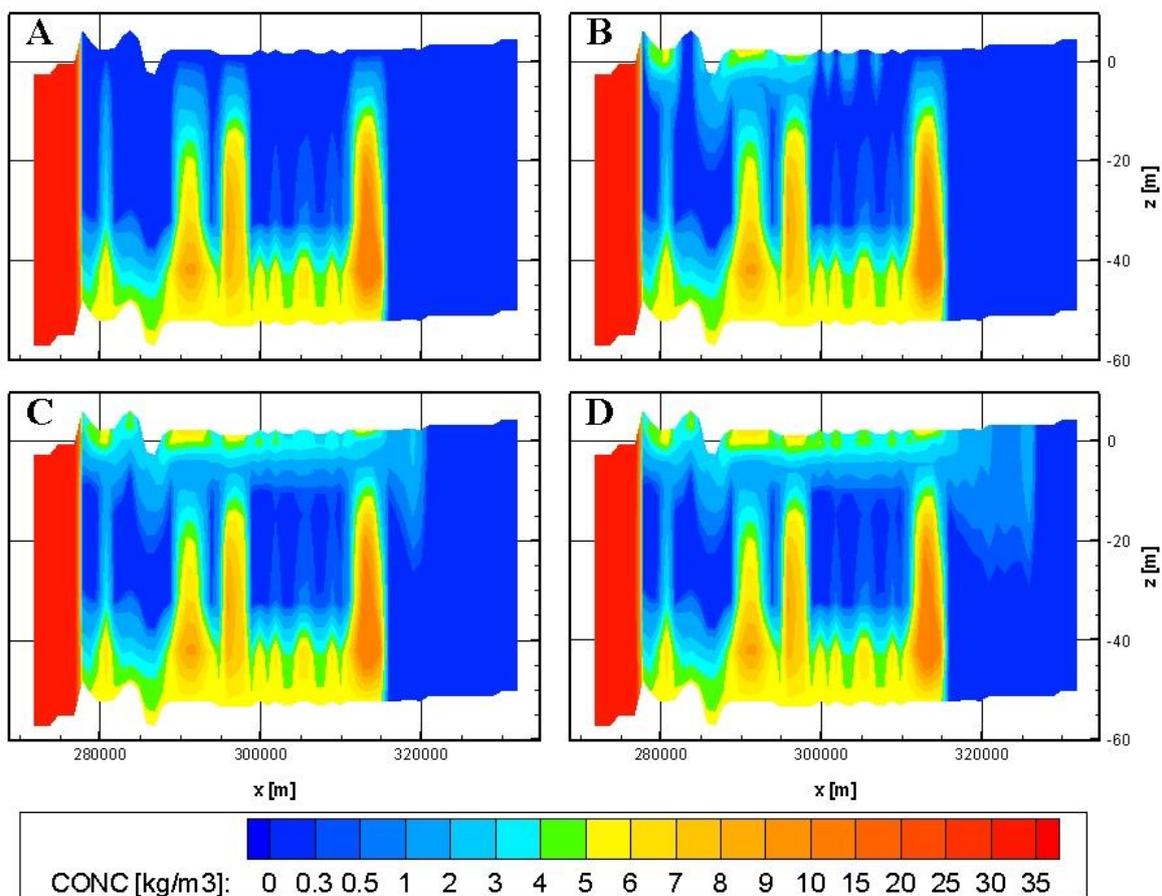
Figure 40: The groundwater concentration is visualized for the hurricane intensity scenarios: subplots A, B, C and D show the concentration of a reference case (i.e. no hurricane) and after category 3, 4 and 5 hurricanes, respectively. All subplots represent the concentration at cross-section y=295000m, 1 year after hurricane landfall.

Figure 39 and Figure 40 represent a spatial overview of the saltwater intrusion extent for the different scenarios, but do not provide any insight into the temporal development of the groundwater concentration. Therefore, the cross-section at y=295000m for the category 5 hurricane scenario is also visualized for several times: right after the storm surge has ceased (26 days), after 1 year, 5 years and 25 years (see Figure 41).
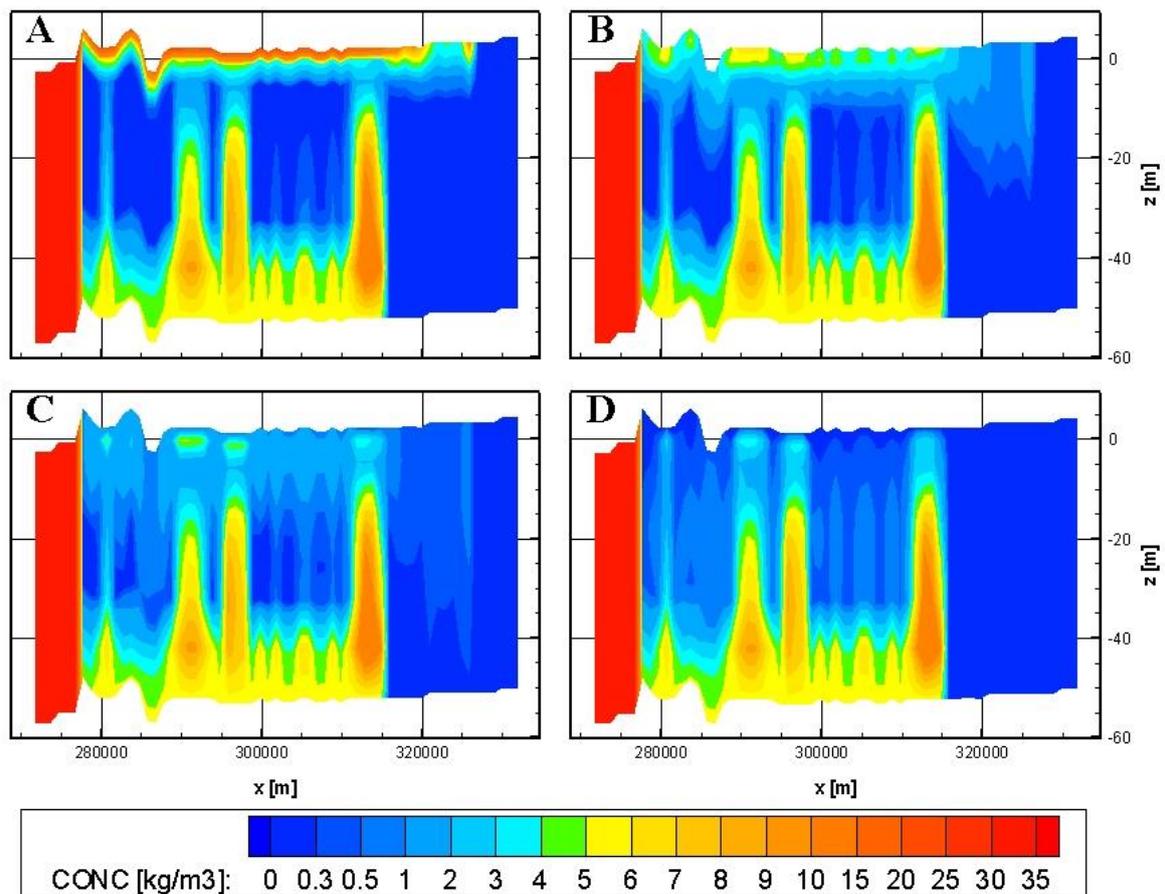
Figure 41: The groundwater concentration after a category 5 hurricane is visualized for different times: subplots A, B, C and D show the concentration right after the storm surge has ceased (26 days), after 1 year, 5 years and 25 years, respectively. All subplots represent the concentration at cross-sections (y=295000m).

The top view and cross-sections provide a visual impression of the differences between the scenarios for certain locations and times only. To gain a further understanding of these differences for the affected subdomains of the model and the simulation period, the scenarios were analysed using three groundwater salinization criteria: the solute mass infiltration (kg TDS), the fresh groundwater volume (m^3) and the flushing time (years) (see Subsection 3.5.4).

The solute mass in the groundwater system of the hurricane-affected area was modelled during the hurricane event and flushing period (see Figure 42). The solute mass started under equilibrium conditions (i.e. the steady-state value from the stationary model) and increased rapidly once the hurricane-induced storm surge arrived, followed by a relatively slow increase (see inset plot Figure 42). After the hurricane event, the solute mass decreased due to advection and hydrodynamic dispersion. After 20 years, the mass was flushed out completely for the category 3 hurricane, whereas the solute mass was not yet flushed out for the category 4 and 5 scenarios. Also, one can observe that the solute mass of the category 3 scenario becomes slightly lower than the original steady-state mass. This behaviour can be explained by the different numerical time discretization of the models: the scenarios were modelled using the transient model (that employs stress-periods up to 1 year) whereas the steady-state value was obtained using the stationary model (stress-periods of 100 years). Therefore, the transient model calculates a more accurate steady-state mass value that deviates from the value of the stationary model. As can be seen from the figure, the scenarios have not yet reached the steady-state value of the transient model.
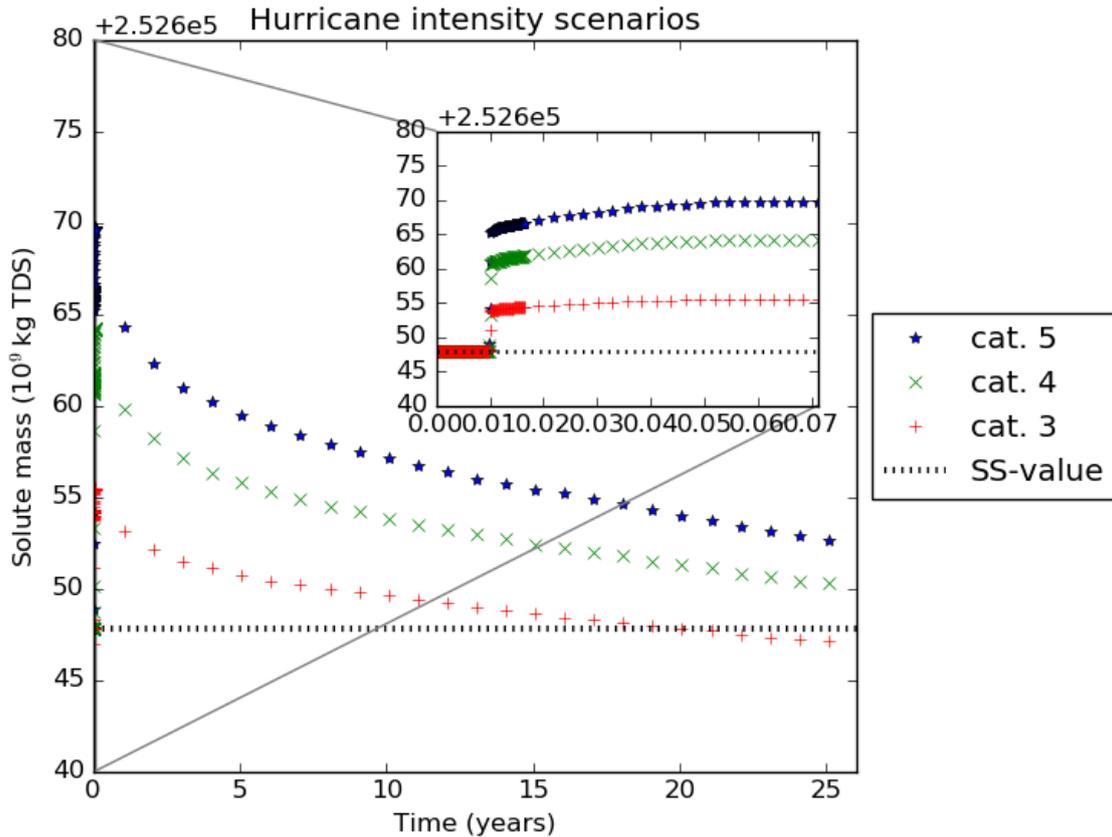
Figure 42: The solute mass infiltration during the hurricane event and flushing period under different hurricane intensity scenarios. The dotted line represents the steady-state value from the stationary model. The data represent the two hurricane-affected subdomains, namely p002 and p003 (see Figure 16).

The fresh (concentrations of ≤1 kg/m^3 and ≤2 kg/m^3) groundwater volumes are visualized in Figure 43 and Figure 44, respectively. During the hurricane-event, the fresh groundwater volume decreased rapidly and reached the lowest value after one year. This time-period of one year represents the lag-period between the hurricane-event and the induced saltwater intrusion; saline water needs time to percolate, diffuse and disperse into the fresh layers of the groundwater system. Therefore, the lowest volume is not observed during the subsequent days after the hurricane event. Subsequently, the groundwater system recovers. Note that the system approaches a new steady-state volume that is slightly different from the original one, likely due to the different numerical time discretization of the models (the stationary and the transient model). These volume differences are relatively small, less than 1‰.

Figure 43: The fresh (≤1 kg/m³) groundwater during the hurricane event and flushing period under different hurricane intensity scenarios. The dotted line represents the steady-state value from the stationary model. The data represent the two hurricane-affected subdomains, namely p002 and p003 (see Figure 16).

Figure 44: The fresh (≤2 kg/m³) groundwater during the hurricane event and flushing period under the different hurricane intensity scenarios. The dotted line represents the steady-state value from the stationary model. The data represent the two hurricane-affected subdomains, namely p002 and p003 (see Figure 16).

In addition, the flushing time differs among the scenarios. For instance, for the fresh groundwater system with concentrations of ≤1 kg/m^3 the category 5 hurricane scenario reaches flushing time most quickly: after approximately 13 years. After 17 years, the category 4 scenario reaches flushing time, whereas the category 3 scenario does not reach flushing time within 25 years. The behaviour can simply be explained by different salinized volumes among the scenarios. The higher the salinized volume (i.e. the category 5 scenario), the earlier 90% of the salinized volume is flushed out and thus the earlier the flushing time is reached. The lower the salinized volume (i.e. the category 3 scenario), the harder and longer it takes before 90% of the salinized volume is flushed out; a lesser extent of salinized groundwater is exposed to freshwater. A similar pattern is observed for the fresh groundwater with concentrations of ≤2 kg/m^3; the flushing time is reached in all scenarios, albeit at different times: in the category 5 scenario after 5 years and in the other scenarios after 7 years. The increase of solute mass and the decrease of the fresh groundwater volume are quantified for the different scenarios in Table 13. In Table 14, the corresponding flushing times are presented.

If one compares Figure 42 to Figure 43 and Figure 44, one finds that the fresh groundwater system has recovered from the hurricane event entirely, whereas the extra solute mass is not yet flushed out for the category 4 and 5 scenarios. This difference can be explained by distinguishing between the upper part of the groundwater system that is relatively fresh (concentration of ≤2 kg/m^3) and the lower part that is relatively brackish (concentration of >2 kg/m^3) under pre-hurricane conditions. For instance, the upper part becomes salinized during the hurricane's direct aftermath, whereas the lower part requires more time to salinize. Subsequently, the upper part is flushed out by advection and hydrodynamic dispersion: groundwater flows from inland's relatively high hydraulic heads to coast's relatively low hydraulic heads where it ultimately ends up in the transition zone. Simultaneously, rainfall flushes the top of the groundwater system. However, the lower part of the groundwater system does not face this fresh groundwater flux directly; fresh rainwater requires time to percolate to lower zones. Therefore, the lower groundwater zone takes more time to recover than the upper part. To conclude, the upper part of the groundwater system with concentrations of ≤2 kg/m^3 may have recovered already, whereas the lower part of groundwater system with concentrations of >2 kg/m^3 may not have recovered yet. In other words, the solute mass is not yet flushed out completely.

Hurricane intensity	Solute mass infiltration (10^{10} kg TDS) change	Fresh groundwater (≤1 kg/m^3) volume (10^9 m^3) change	Fresh groundwater (≤2 kg/m^3) volume (10^9 m^3) change
Category 3	+0.77	-2.00	-1.20
Category 4	+1.64	-4.60	-2.50
Category 5	+2.19	-6.00	-3.20

Table 13: The solute mass and the fresh groundwater volume under different hurricane intensity scenarios.

Hurricane intensity	Solute mass flushing time (years)	Fresh groundwater (≤1 kg/m^3) flushing time (years)	Fresh groundwater (≤2 kg/m^3) flushing time (years)
Category 3	16	Not reached within 25 years	7
Category 4	Not reached within 25 years	17	7
Category 5	Not reached within 25 years	13	5

Table 14: The solute mass flushing time and the fresh groundwater volume flushing time under different hurricane intensity scenarios.

4.3. Hurricane rainfall scenarios

The second type of scenarios represented the two hurricane rainfall scenarios. For both scenarios, the same category 5 hurricane was used as in the hurricane intensity scenarios except for the peak rainfall rate: the adapted peak rainfall rate (0.045 m/h) is slightly larger than the default rate (0.030 m/h). Due to the small differences between these scenarios, the top view and cross-section of the hurricane intensity scenarios represent the hurricane rainfall scenarios as well (see Figure 39 and Figure 40). Therefore, the scenarios were analysed using the groundwater salinization criteria only. First of all, the solute mass over time is visualized for the scenarios (see Figure 45).

Figure 45: The solute mass infiltration during the hurricane event and flushing period under different hurricane rainfall peak rate scenarios. The dotted line represents the steady-state value from the stationary model. The data represent the two hurricane-affected subdomains, namely p002 and p003 (see Figure 16).

The fresh (concentrations of ≤1 kg/m³ and ≤2 kg/m³) groundwater volumes for both scenarios are plotted in Figure 46 and Figure 47. During the first two years after the hurricane event, the higher peak rainfall rate scenario tends to show a slightly higher fresh groundwater volume. Afterwards, the differences between the scenarios minimized and the scenarios became equal. The flushing time was also equal for both scenarios (see hurricane intensity category 5 in Table 14).
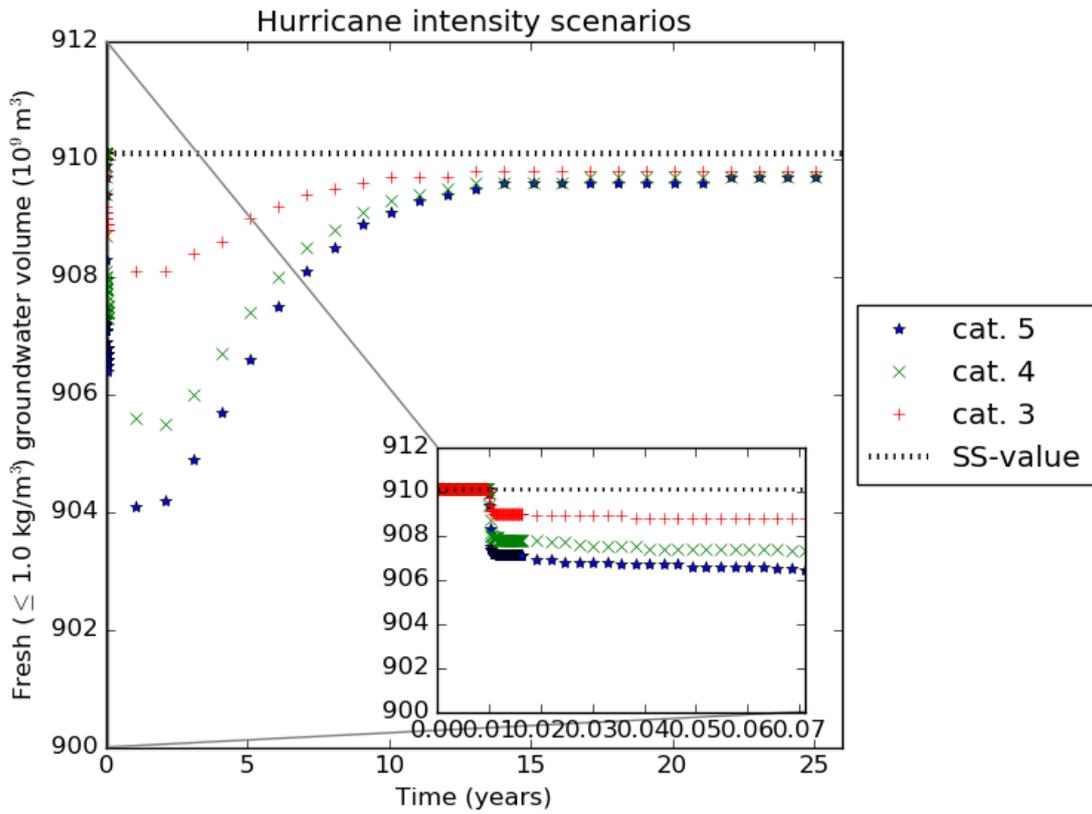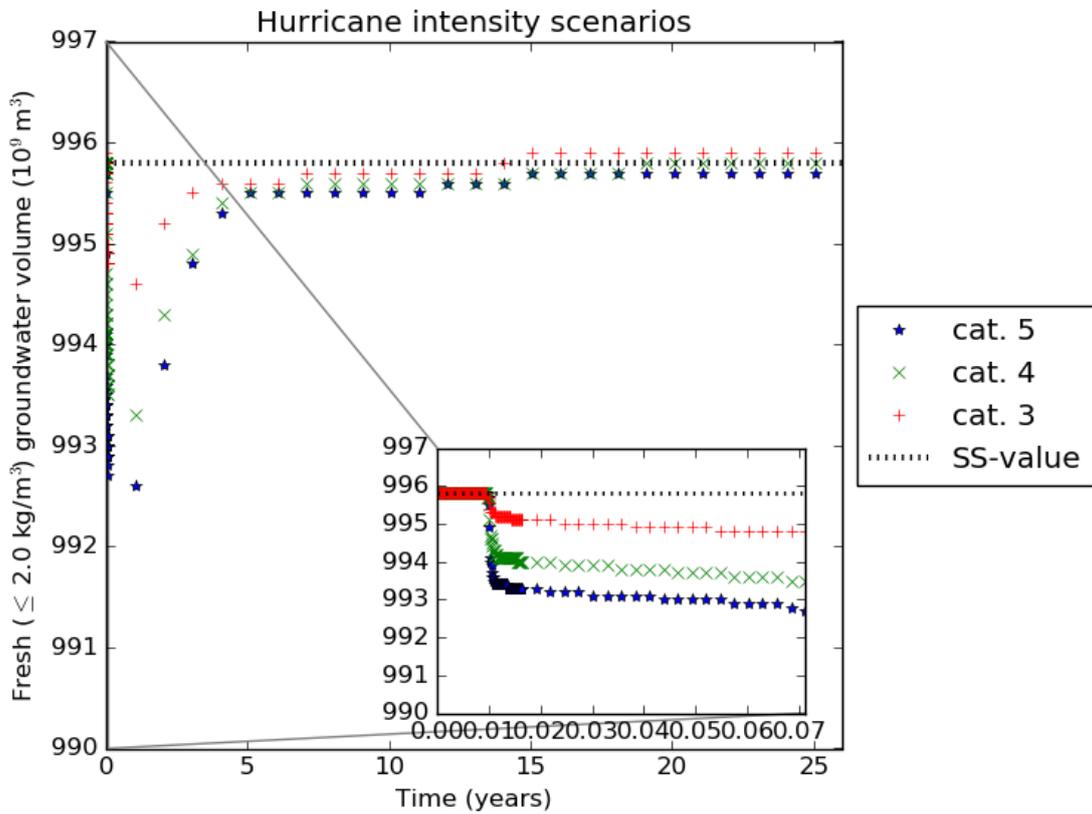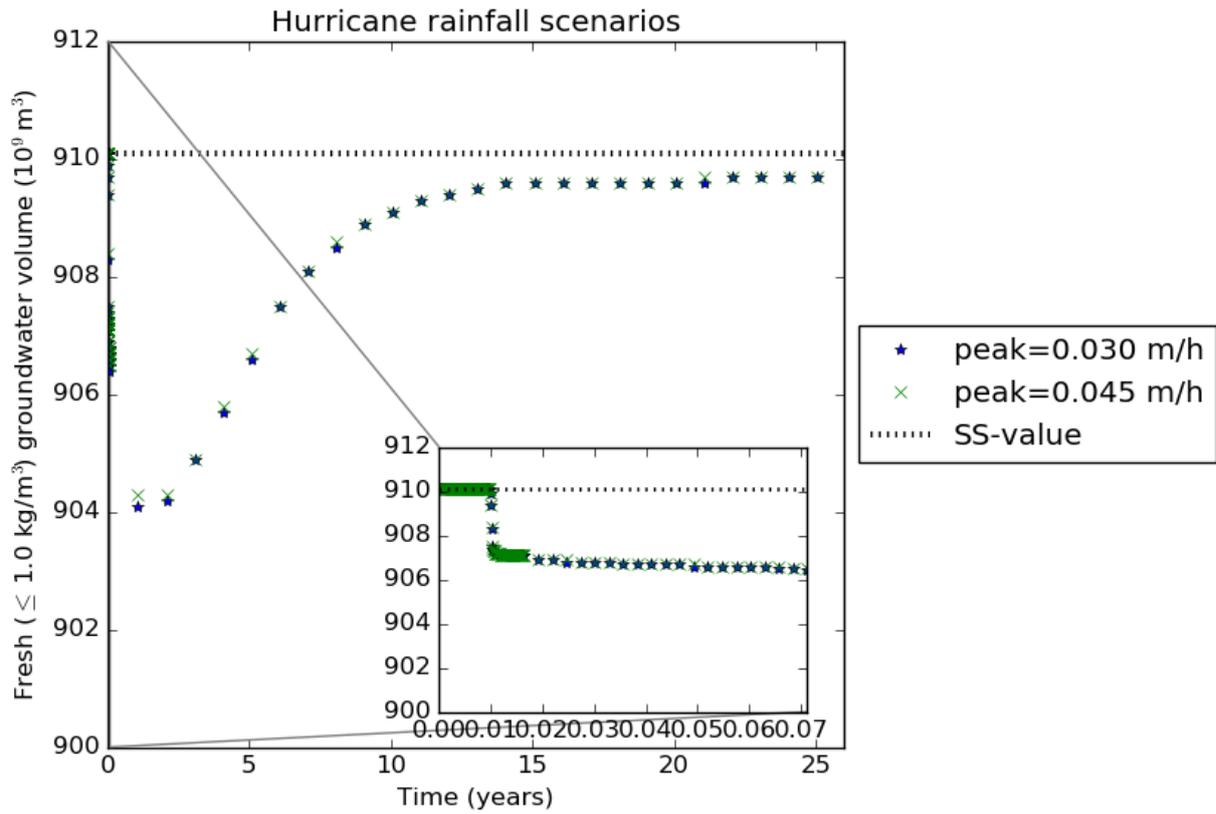
Figure 46: The fresh (≤1 kg/m3) groundwater during the hurricane event and flushing period under different hurricane rainfall peak rate scenarios. The dotted line represents the steady-state value from the stationary model. The data represent the two hurricane-affected subdomains, namely p002 and p003 (see Figure 16).
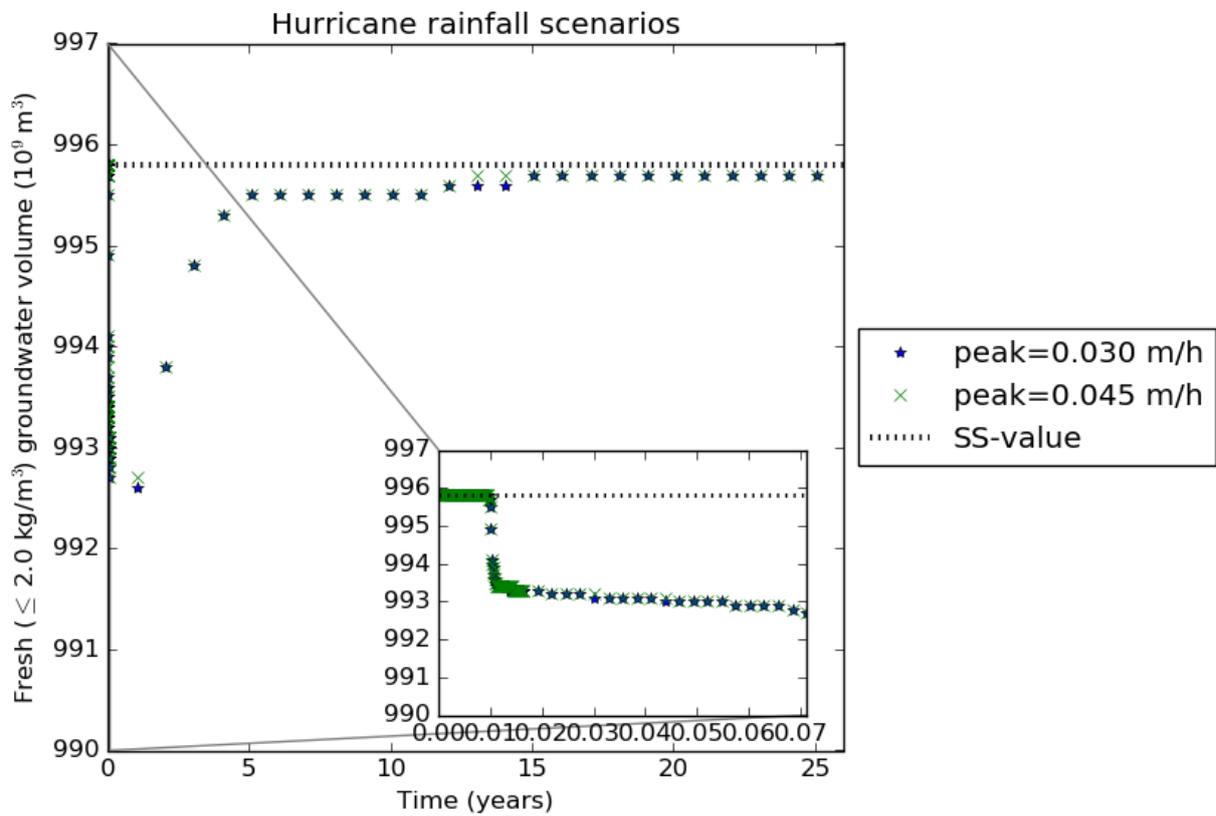
Figure 47: The fresh (≤2 kg/m3) groundwater during the hurricane event and flushing period under different hurricane rainfall peak rate scenarios. The dotted line represents the steady-state value from the stationary model. The data represent the two hurricane-affected subdomains, namely p002 and p003 (see Figure 16).

4.4. Sea-level rise scenarios

The last type of scenarios represented the sea-level rise scenarios. These scenarios simulated a category 5 hurricane in combination with sea-level rise projections of 0.50 and 1.00m. First of all, a top view and cross-section of the model are presented to gain a visual impression of the differences between the scenarios. Afterwards, the scenarios are analysed using the three groundwater salinization assessment criteria.

Figure 48 shows a top view of the groundwater concentration in the upper layer (1m thick) and visualizes the saltwater intrusion extent for the different sea-level rise scenarios. Note that the legend differs from the top view of the hurricane intensity scenarios (Figure 39) to accentuate small differences between the scenarios. The figure shows that for higher sea-level rise projections (slightly) larger saltwater intrusion extents are involved. This pattern is in accordance with Figure 36; storm surge peak elevations reach further inland when sea-level rise is included. The pattern can also be observed in a cross-section of the affected area (see Figure 49).
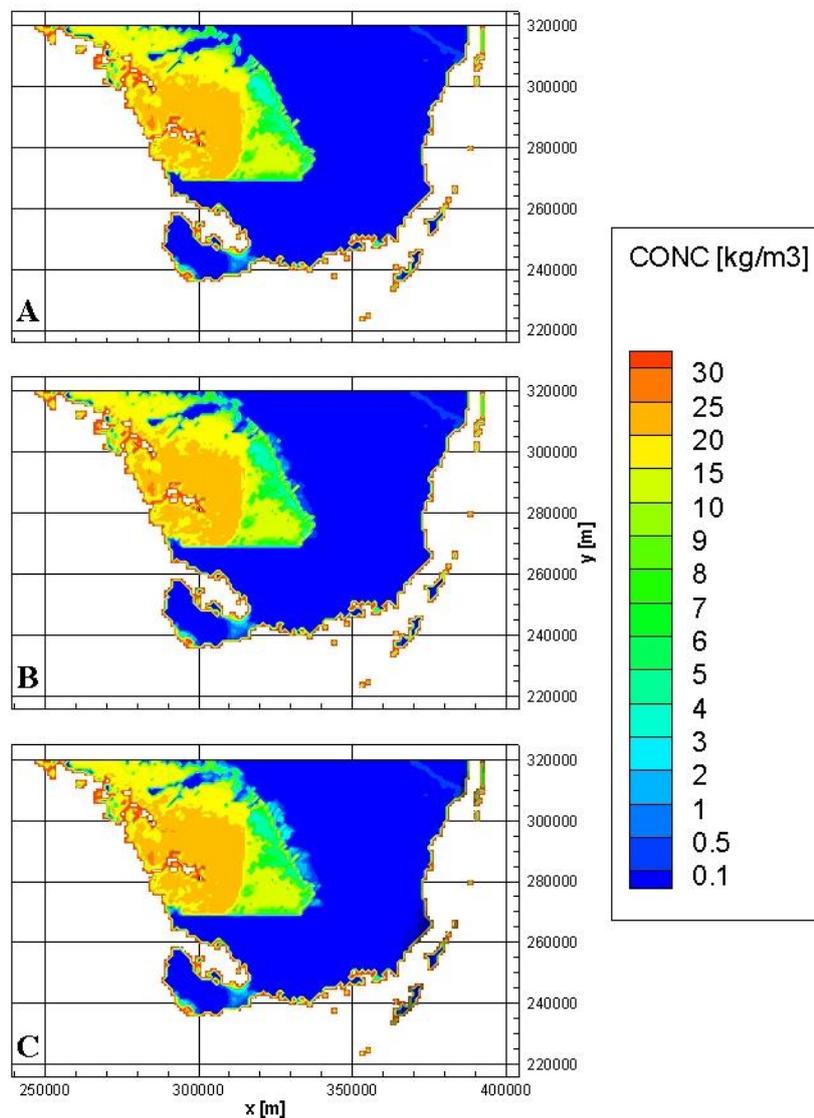
Figure 48: The groundwater concentration is visualized for a category 5 hurricane combined with different sea-level rise scenarios: subplot A shows a reference case with no sea-level rise, subplots B and C represent a sea-level rise of 0.50m and 1.0m, respectively. All subplots represent the concentration of the first layer of the affected Floridan peninsula subzone right after the storm surge has ceased.
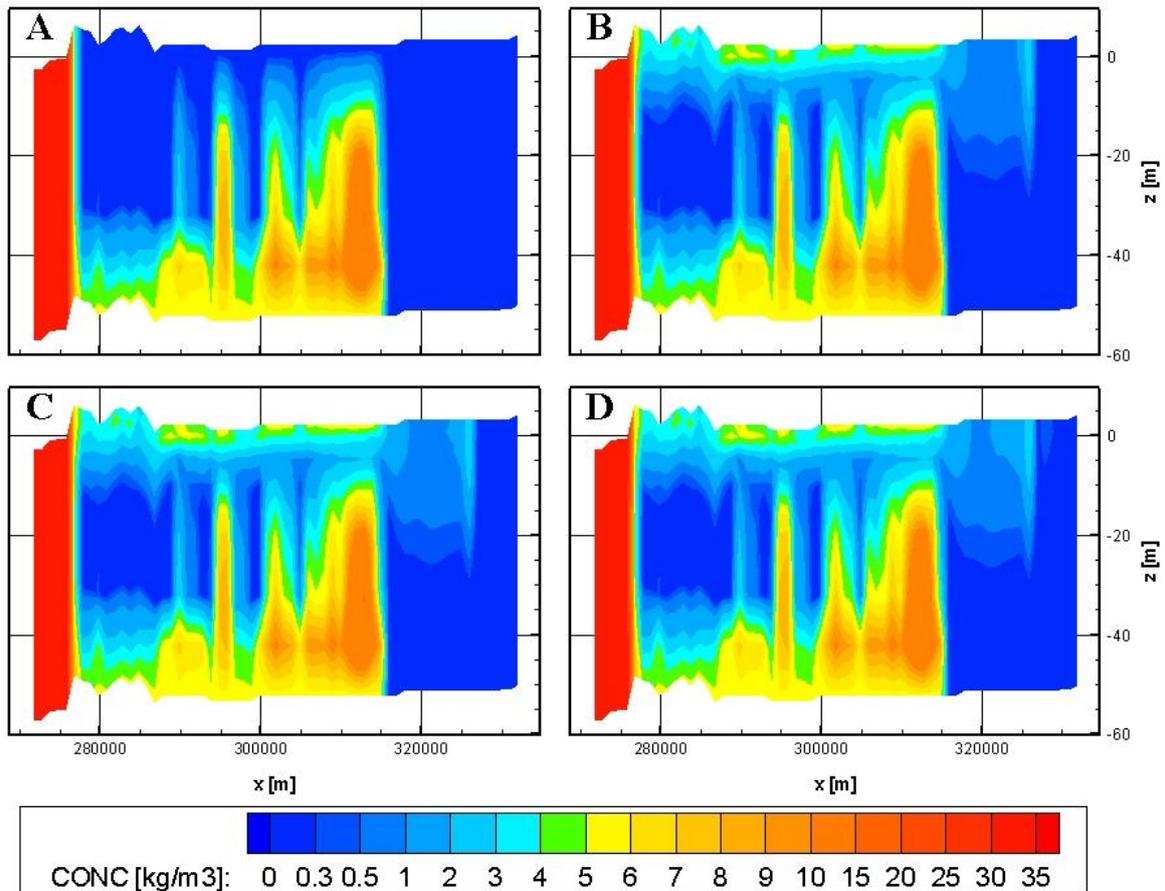
Figure 49: The groundwater concentration is visualized for a category 5 hurricane combined with different sea-level rise scenarios: subplot A shows the concentration of a reference case (i.e. no hurricane), B, C, D show the concentration after a category 5 hurricane combined with a sea-level rise of 0, 0.50 and 1.00m, respectively. All subplots represent the concentration at cross-sections (y=296750m) right after the storm surge has ceased.

To gain a further understanding of the differences for the affected subdomains of the model and the simulation period, the scenarios were analysed using three groundwater salinization criteria.

Figure 50 shows the solute mass of the scenarios and an accompanying scenario excluding sea-level rise. Under all scenarios, the solute mass starts in equilibrium and increases rapidly during the storm surge of the hurricane event. The 1.00m scenario shows the most pronounced effect; the differences between the scenarios however, are relatively small. In the subsequent 25 years, the solute mass decreased, however, the solute mass was not yet flushed out completely for the flushing time was not yet reached.
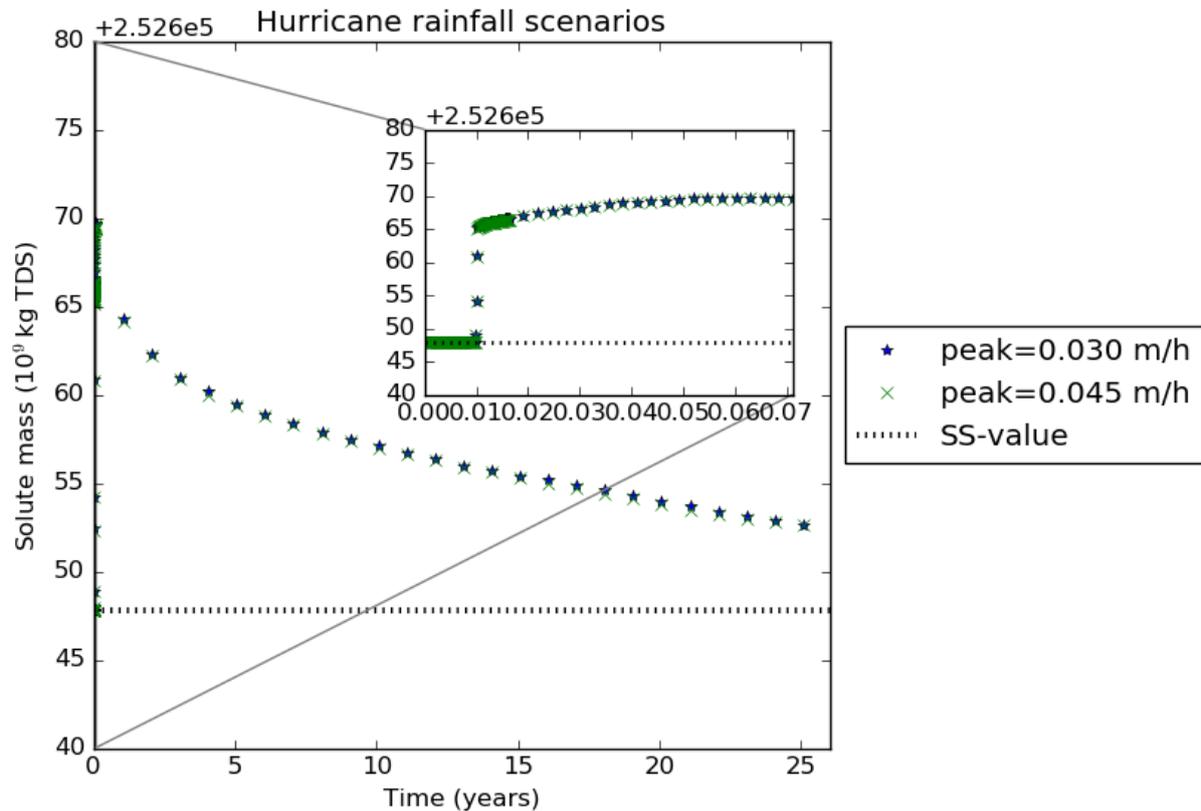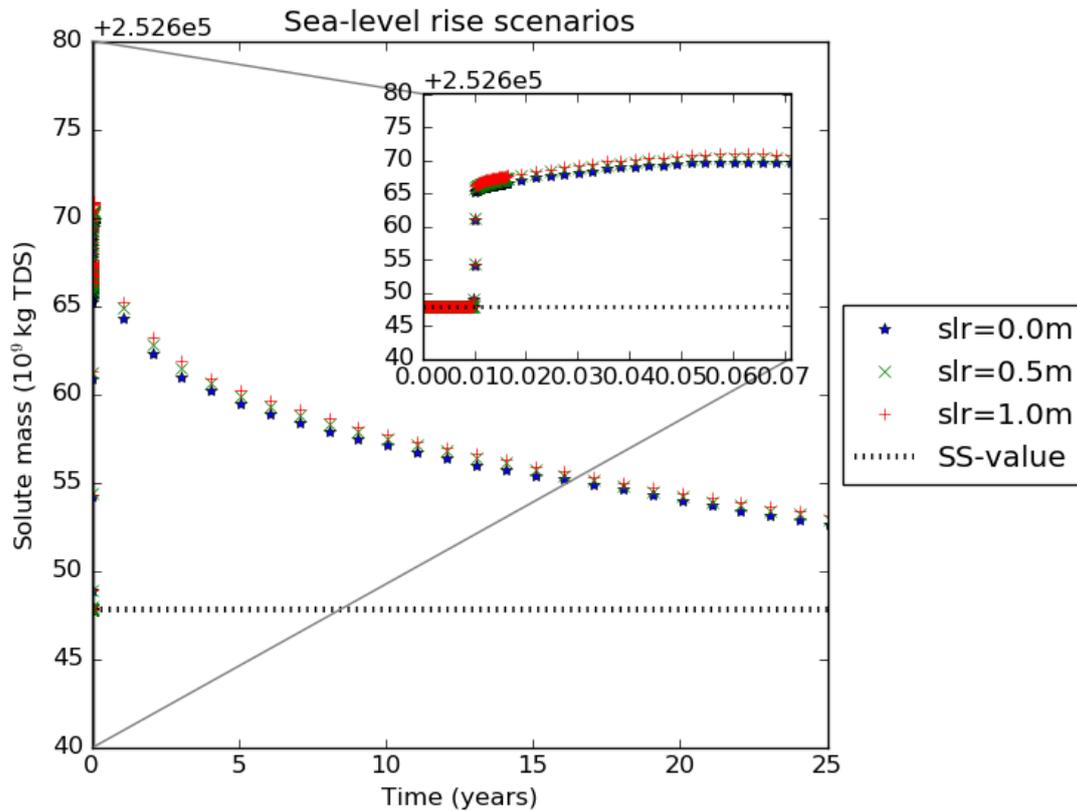
Figure 50: The solute mass infiltration during the hurricane event and flushing period under different sea-level rise scenarios. The dotted line represents the steady-state value from the stationary model. The data represent the two hurricane-affected subdomains, namely p002 and p003 (see Figure 16).

In addition, the fresh groundwater volume was monitored during the model simulation and is plotted in Figure 51 and Figure 52, respectively. For all scenarios, the fresh groundwater volume decreased rapidly during the hurricane event, with the strongest decrease for the 1.00m scenario. However, just like the solute mass, the differences are relatively small. The increase of solute mass and the decrease of the fresh groundwater volume are quantified for the different scenarios in Table 15. Afterwards, the differences between the scenarios diminished and the salinized volume was flushed out equally for all scenarios (13 years for the groundwater system with concentrations of ≤1 kg/m^3 and ±5 years for ≤2 kg/m^3) (see Table 16).
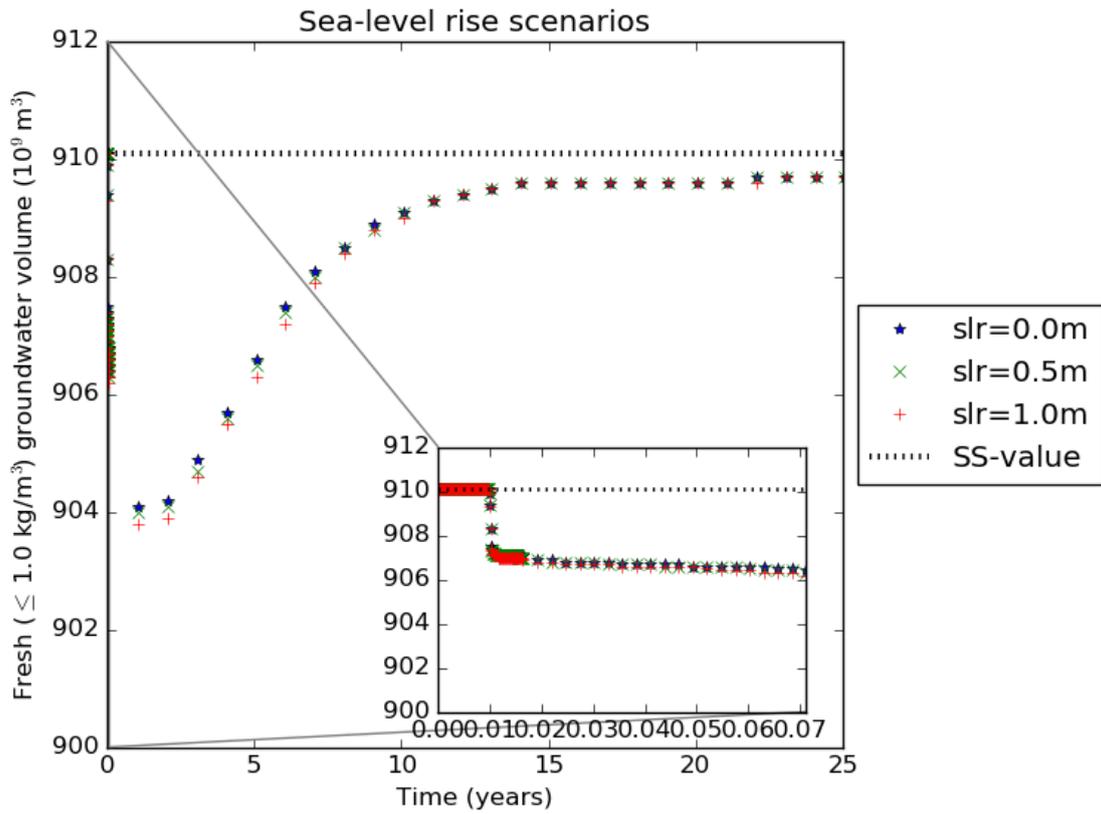
Figure 51: The fresh (≤1 kg/m3) groundwater during the hurricane event and flushing period under sea-level rise scenarios. The dotted line represents the steady-state value from the stationary model. The data represent the two hurricane-affected subdomains, namely p002 and p003 (see Figure 16).
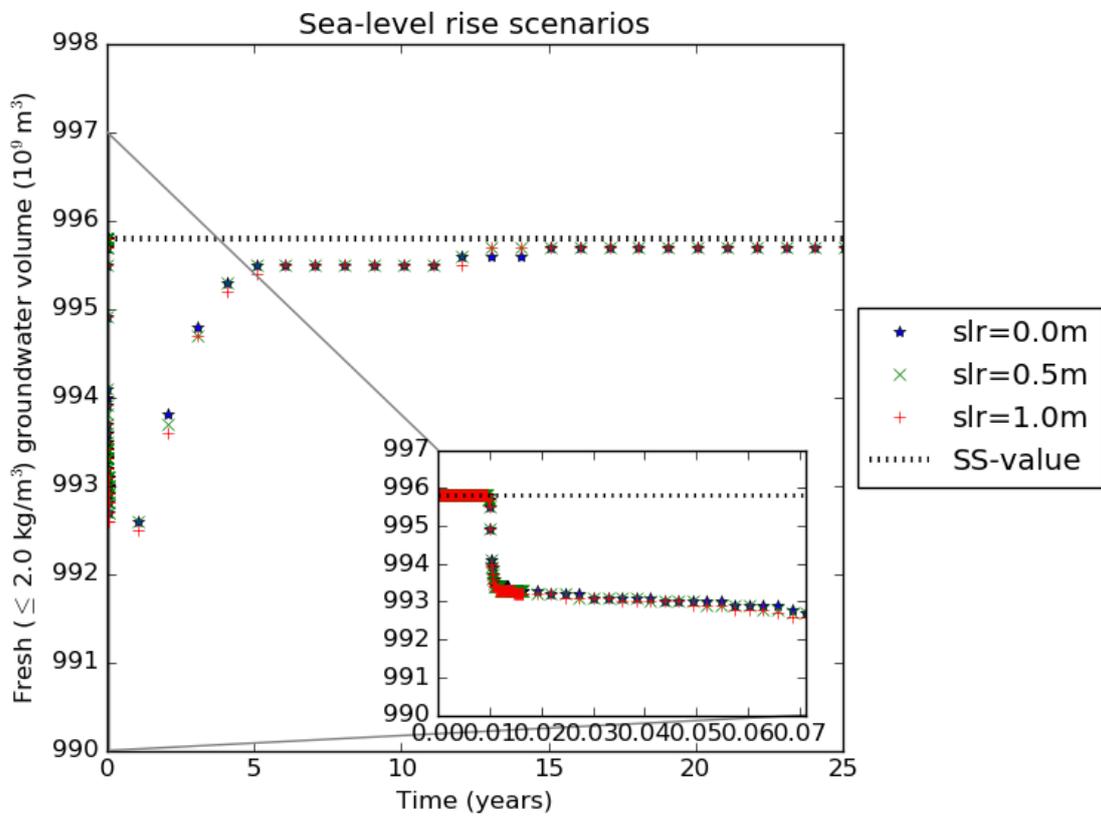
Figure 52: The fresh (≤2 kg/m3) groundwater during the hurricane event and flushing period under sea-level rise scenarios. The dotted line represents the steady-state value from the stationary model. The data represent the two hurricane-affected subdomains, namely p002 and p003 (see Figure 16).

Sea-level rise scenario	Solute mass infiltration (10^{10} kg TDS) change	Fresh groundwater (≤ 1 kg/m^3) volume (10^9 m^3) change	Fresh groundwater (≤ 2 kg/m^3) volume (10^9 m^3) change
SLR = 0.00 m	+21.9	-6.00	-3.20
SLR = 0.50 m	+22.6	-6.10	-3.20
SLR = 1.00 m	+23.1	-6.30	-3.30

Table 15: The solute mass and the fresh groundwater volume under different sea-level rise scenarios.

Sea-level rise scenario	Solute mass flushing time (years)	Fresh groundwater (≤ 1 kg/m^3) flushing time (years)	Fresh groundwater (≤ 2 kg/m^3) flushing time (years)
SLR = 0.00 m	Not reached within 25 years	13	5
SLR = 0.50 m	Not reached within 25 years	13	5
SLR = 1.00 m	Not reached within 25 years	13	6

Table 16: The solute mass flushing time and the fresh groundwater volume flushing time under different hurricane intensity scenarios.

5. Discussion

In this chapter, results of the climate scenarios (hurricane intensities, hurricane peak rainfall rates and sea-level rise projections, see Sections 4.2 to 4.4) will be discussed and compared. For each scenario, hypotheses based on the literature review will be given and tested on the model results. Furthermore, the study's limitations and contributions are considered.

5.1. Hurricane intensity scenarios

The first sub-research question aims to provide knowledge and insight into consequences of hurricane intensity on saltwater intrusion: "How does hurricane-induced saltwater intrusion affect fresh groundwater availability under different hurricane intensities?"

As the largest part of storm surge levels is determined by wind stress, one can expect higher storm surges to occur for higher hurricane intensities (however, this relationship is not that straightforward; other parameters such as hurricane size also play an important role, see Subsection 2.1.3). In turn, higher storm surge levels result in larger inundation zones that lead to more vertical saltwater intrusion, lowering the fresh groundwater availability.

The results of the hurricane-intensity scenarios confirm these expectations. For instance, the higher the intensity, the larger the inundation zone, the more solute mass infiltrates (i.e. the more saltwater intrusion occurs) and the longer the recovery times become (see Figure 42). Consequently, an increase in hurricane intensity leads to a decrease in fresh groundwater volume (see Figure 43 and Figure 44). The differences between the scenarios are most pronounced in the direct aftermath of the hurricane event. In the subsequent years, the differences diminish, and the same steady-state value is reached eventually.

5.2. Hurricane rainfall scenarios

The second sub-research question considers the impact of hurricane rainfall on saltwater intrusion: "How does hurricane-induced saltwater intrusion affect fresh groundwater availability under different hurricane peak rainfall rates?" Therefore, one scenario with a relatively higher peak rainfall rate is simulated and compared to the scenario with the default peak value.

One can expect that higher hurricane rainfall rates lower the concentration levels of the total water head (i.e. the sum of storm surge and hurricane rainfall) as the amount of storm surge remains constant. In turn, a lower inundation concentration involves less saltwater intrusion and a relatively higher fresh groundwater availability. In other words, higher hurricane rainfall rates are expected to increase the fresh groundwater volume.

The results of the scenarios meet the expectations; the fresh groundwater volume differs between the scenarios, but only slightly. For instance, the fresh groundwater volume is slightly higher for the high peak rainfall rate scenario, after one year. After two years, the differences minimize, and the scenarios becomes equal. These small differences can be explained by the relatively small peak rainfall rate increase (from 0.030 to 0.045 m/h) in comparison to the storm surge peak value (for example, 1.0m at x=350km, see Figure 31). Furthermore, the peak rainfall rate was reached for a limited time only and dropped rapidly afterwards. Due to the relatively small contribution of freshwater to the total inundation level (even after the peak rainfall rate increase), the inundation will be a little bit less saline only.

5.3. Sea-level rise scenarios

The third sub-research question concentrates on hurricane-induced storm surge in combination with sea-level rise projections: "How do consequences of hurricane scenarios change when sea-level rise projections are considered?"

Sea-level rise has a potential amplifying effect on inundation zones; the higher the sea-level rise, the further storm surge can move inland (Frazier et al., 2010). In other words, sea-level rise can extend contemporary hurricane-induced storm surge hazard zones to move further inland. In turn,

extended inundation zones amplify vertical saltwater intrusion and reduce the fresh groundwater availability. This amplifying effect is observed in the sea-level rise scenarios: the higher the sea-level rise, the larger the inundation zone, and the more solute mass infiltrates (see Figure 50). However, the differences between the sea-level rise scenarios are relatively small.

5.4.   Comparison climate scenarios

If one compares the climate scenarios to one another, two preliminary conclusions can be drawn. First, the level of saltwater intrusion depends strongly on the climate scenario. For instance, hurricane intensity has the most pronounced effect (i.e. the higher the intensity, the larger the extent of saltwater intrusion; see Figure 42). When sea-level rise is included in the simulations, saltwater intrusion levels increase slightly (see Figure 50). Rainfall increases during the hurricane event have minimal effect (see Figure 45). These results were obtained for one hurricane landfall location and one hurricane direction only: eastward moving hurricanes that make landfall in southern peninsular Florida. For future research, it is recommended to simulate various hurricane directions and landfall locations. Subsequently, one can construct a vulnerability map for the Florida peninsula as a whole for different scenarios.

The second conclusion is that under all climate scenarios, the groundwater system requires a significant amount of time (i.e. more than 10 years) to flush out 90% of the salinized volume. After this flushing period, the system is considered to have recovered from the hurricane-event. However, is this length sufficient before another severe hurricane (i.e. category ≥3) makes landfall? If we consider the return period of 13 to 15 years (Keim et al., 2007), the groundwater system can likely recover in time, before a subsequent hurricane (and related storm surge) will strike the shore. However, the return periods presented by Keim et al. (2007) do not include potential climate change effects (see Figure 10). Climate change projections indicate different hurricane behaviour; hurricanes will strike less frequently but will be more extreme (i.e. higher storm surge; relatively longer flushing period). Therefore, the suggested return period by Keim et al. will probably be affected over time.

Also, climate change can affect the precipitation pattern of Florida (Fiedler et al., 2001). For example, rainfall events are expected to become more intense and more sporadic, leading to worse droughts. As the natural capability of a coastal aquifer to recover from storm surge depends on the amount of infiltrating rainfall, droughts can enlarge the flushing period. For instance, during rainfall events, porewater salinity diffuses into the overlying freshwater, however, without freshwater, porewater salinity levels may continue to rise as a result of evapotranspiration (Steyer et al., 2007). In other words, changing precipitation patterns can lead to relatively longer flushing periods.

To conclude, the return and flushing periods can be affected by climate change. Future research should investigate these potential climate change effects.

5.5. Study limitations

This study involves several limitations that should be addressed as these factors impact the findings of this study. The limitations can be divided into three categories: the approach to calculate hurricane-induced storm surge, the approach to include sea-level rise effects and the hydrogeological model. The limitations are discussed in the following subsections.

5.5.1. Hurricane-induced storm surge

The first type of limitations considers the approach that is used to calculate hurricane-induced storm surge. The inundation levels are estimated using the average of Cialone's basic synthetic hydrograph equation and a linear hydrograph equation (see Equation 18). Cialone's equation, however, is developed for coastal water levels and does not apply for inundation levels on land where different processes such as permeability and saturation apply. Therefore, usage of Cialone's equation on land leads to inaccurate inundation levels. Also, usage of the linear hydrograph equation introduces inaccuracies in the inundation levels. The linear hydrograph equation (see Equation 17) includes the parameter 'recovery time' which is the time before storm surge levels on land have ceased. The recovery time strongly depends on the permeability of the soil and is based on a few groundwater observations only (see Figure 19). Due to the limited amount of analysed observations, the observed permeability of the soil (and thus the recovery time) might deviate from the actual permeability. For instance, if the surface would contain clay, the recovery time would be larger as clay involves a relatively low permeability and groundwater recharge would be less intense. In turn, larger recovery times involve longer inundation periods; basically, the groundwater system is exposed to a salinized volume for a longer time. On the other hand, a low permeable subsurface would lead to less saline water to be infiltrated.

In addition, spatial variations and heights of storm surge peak values along the coast may not be representative of a hurricane. For instance, the peak values are obtained from the SLOSH model output and do not account for individual hurricanes. Therefore, the storm surge peak values are adapted using the approach as explained in Subsection 3.4.4. Despite all adaptations, the storm surge peak values are most likely to differ from accurate storm surge models such ADCIRC or XBeach. Therefore, the input of storm surge peak values for the hydrograph equation may not be accurate.

Apart from this, by means of simplicity, the storm rainfall hydrograph is based on Cialone's hydrograph equation that is meant for storm surge. It is plausible to assume that storm rainfall behaviour does not match seawater behaviour during a storm. However, as rainfall increases have minimal effect (see Section 4.3), the rainfall hydrograph shape will be of minor importance for the results.

To conclude: this research employs simplified storm hydrograph equations with storm surge peak values that may not be accurate. Therefore, the hurricane-induced storm surge projections should be interpreted as a (rough) estimation of the impact of climate scenarios on fresh groundwater availability.

5.5.2. Sea-level rise effects

The second type of limitations considers sea-level rise effects. In this research, sea-level rise projections were directly added to the storm surge peak values. This approach is a simplification; the actual relationship between sea-level rise and storm surge increases may be complex. Using this approach, non-inundated cells become inundated if their surface elevation is lower than the total water head (i.e. surface elevation + layer of water) of an inundated neighbouring cell. The major disadvantage of this method is that valuable information of the SLOSH data is lost. For example, SLOSH includes natural barriers (e.g. levees, houses and forests) in model flow calculations. However, by using this approach, the accuracy of these barriers cannot be maintained anymore, and the quality of the SLOSH data is deteriorated (Maloney and Preston, 2014).

5.5.3. Hydrogeological model

The last type of limitations concerns the hydrogeological model. The model is coarse with cells of 1000m x 1000m and involves the main hydrogeological units only; local surface variations in the unsaturated zone are excluded. A finer model grid would most certainly show different results, for instance, if the unsaturated zone would contain clay locally, the flushing times would be locally considerably higher as clay retains the salinized water (while a clay layer could also limit saline water infiltration from the start anyway).

Furthermore, the flushing times are calculated for a small (yet important) part of the hydrogeological model only: the surficial aquifer system (consisting mainly of sandy material). Different aquifer systems involve other flushing times. For example, carbonate rock aquifers involve (at least locally) a relatively higher permeability; i.e. the salinized groundwater can flow, diffuse and disperse with a relative ease into deeper layers. The same accounts for the fresh groundwater supply; recharge can reach the salinized zones much easier, leading to smaller flushing periods. In addition, as already mentioned, the presence of clay in the aquifer system can also alter the flushing times. Therefore, the results are only applicable for the surficial aquifer system in southern peninsular Florida.

5.6. Study contributions

Model simulations indicate that hurricane intensity has the most pronounced effect on saltwater intrusion and is amplified when sea-level rise projections are considered. Also, the study shows that on average, the coastal groundwater system can recover in time before another hurricane and related storm surge will strike the shore.

The results are in line with similar research on the same study area by Xiao et al. (2019). Xiao et al. explored the effects of storm surge on saltwater intrusion into the surficial aquifer system in coastal east-central Florida. Their research indicates that rapid saltwater intrusion occurs after storm surge. Afterwards, the aquifer required approximately 8 years to recover from the saltwater intrusion.

Climate change can lead to relatively more intense hurricanes and sea-level rise (i.e. longer flushing periods over larger areas). If the accompanying return period becomes smaller than the flushing period, coastal groundwater systems will be put under increasing pressure, due to the fact that salt is accumulated in the subsurface. Then, this research indicates that strategies that mitigate and reverse saltwater intrusion should be considered timely and carefully to protect important freshwater resources. Elsayed and Oumeraci (2018) suggest the best strategy to prevent vertical saltwater intrusion is by constructing coastal barriers (e.g. levees) that can barely be overtopped or breached in combination with an inland subsurface drainage system that absorbs the residual saline water before it can reach the fresh groundwater part of the aquifer. Therefore, it is important to know the locations of these resources, to protect them timely.

6. Conclusion and recommendations

In this section, the sub-research questions and the main research question will be answered. Afterwards, the results are assessed, and the study's limitations and contributions are mentioned.

6.1.   Sub-research question 1

The first sub-research question was: "How does hurricane-induced saltwater intrusion affect fresh groundwater availability under different hurricane intensities?" Model simulations indicate that relatively more saltwater intrusion occurs under relatively higher hurricane intensity scenarios. Furthermore, the higher the intensity, the longer the recovery time of the coastal groundwater system. Simultaneously, hurricane intensity affects the fresh groundwater availability: the stronger the hurricane, the more solute mass infiltrates and the smaller the fresh groundwater volume becomes. The differences between the scenarios are most pronounced in the direct aftermath of the hurricane event. In the subsequent years, the differences diminish, and the same steady-state value is reached eventually.

6.2.   Sub-research question 2

The second sub-research question was: "How does hurricane-induced saltwater intrusion affect fresh groundwater availability under different hurricane peak rainfall rates?" Simulation of the high peak rainfall rate scenario indicates that extra hurricane rainfall only slightly reduces hurricane surge-induced saltwater intrusion. After two years, the difference vanishes, and the scenarios become basically equal. In terms of solute mass infiltration, no pronounced differences are observed.

6.3.   Sub-research question 3

The third sub-research question was: "How do consequences of hurricane scenarios change when sea-level rise projections are considered?" Sea-level rise amplifies hurricane-induced saltwater intrusion: the higher the sea-level rise, the (slightly) larger the inundation zone and the more saline water intrudes into the groundwater system. For both sea-level rise projections, the fresh groundwater availability is lowered. These fresh groundwater volume differences are most pronounced during the first years after the hurricane event. Afterwards, the salinized volume is flushed out equally for all scenarios (>10 years for concentration of ≤1 kg/m^3).

6.4.   Main research question

The main research question was: "How does hurricane-induced saltwater intrusion affect fresh groundwater availability in Florida under different climate scenarios?" This study shows that hurricane intensity has the most pronounced effect on saltwater intrusion and is amplified when sea-level rise projections are considered. Also, the study shows that the surficial aquifer system can recover in time before another hurricane and related storm surge will strike the shore. However, if the return period is shortened due to climate change, the system may not be able to recover in time before another hurricane approaches. In that case, strategies that mitigate and reverse saltwater intrusion should be considered. Due to limitations regarding the hurricane-induced storm surge calculations and the used hydrogeological model, the findings should be used as an indication of the impact of climate scenarios on fresh groundwater availability. Future research should investigate whether the findings of this research can be reproduced with an accurate storm surge model. Furthermore, climate change effects on hurricane return periods for vulnerable areas should be analysed. This all should be done with a more detailed numerical model that represents more accurately the relevant hydrogeological processes. For future research, it is also recommended to simulate various hurricane directions and landfall locations. Subsequently, one can construct a vulnerability map for the Florida peninsula as a whole for different scenarios.

7. References

Alpha, T.R., Galloway, J.P., Tinsley III, J.C., 1997. Karst topography; computer animations and paper model, USGS: Open-File Report 97-536A&B. https://doi.org/10.3133/ofr97536A

Barlow, P.M., 2003. Ground Water in Freshwater-Saltwater Environments of the Atlantic Coast U . S . Department of the Interior. U.S. Geol. Surv. Reston, Virginia Circular 1, 121.

Barlow, P.M., Reichard, E.G., 2010. Saltwater intrusion in coastal regions of North America. Hydrogeol. J. 18, 247–260. https://doi.org/10.1007/s10040-009-0514-3

Baxter, G.P., Wallace, C.C., 1916. Changes in volume upon solution in water of the halogen salts of the alkali metals. II. J. Am. Chem. Soc. 38, 70–105.

Bell, K., Ray, P.S., 2004. North Atlantic Hurricanes 1977–99: Surface Hurricane-Force Wind Radii. Mon. Weather Rev. 132, 1167–1189. https://doi.org/10.1175/1520-0493(2004)132<1167:nahshw>2.0.co;2

Christensen, J.H., Kanikicharla, K.K., Aldrian, E., An, S. Il, Albuquerque Cavalcanti, I.F., de Castro, M., Dong, W., Goswami, P., Hall, A., Kanyanga, J.K., Kitoh, A., Kossin, J., Lau, N.C., Renwick, J., Stephenson, D.B., Xie, S.P., Zhou, T., Abraham, L., Ambrizzi, T., Anderson, B., Arakawa, O., Arritt, R., Baldwin, M., Barlow, M., Barriopedro, D., Biasutti, M., Biner, S., Bromwich, D., Brown, J., Cai, W., Carvalho, L. V., Chang, P., Chen, X., Choi, J., Christensen, O.B., Deser, C., Emanuel, K., Endo, H., Enfield, D.B., Evan, A., Giannini, A., Gillett, N., Hariharasubramanian, A., Huang, P., Jones, J., Karumuri, A., Katzfey, J., Kjellström, E., Knight, J., Knutson, T., Kulkarni, A., Kundeti, K.R., Lau, W.K., Lenderink, G., Lennard, C., Leung, L. yung R., Lin, R., Losada, T., Mackellar, N.C., Magaña, V., Marshall, G., Mearns, L., Meehl, G., Menéndez, C., Murakami, H., Nath, M.J., Neelin, J.D., van Oldenborgh, G.J., Olesen, M., Polcher, J., Qian, Y., Ray, S., Reich, K.D., de Fonseca, B.R., Ruti, P., Screen, J., Sedláček, J., Solman, S., Stendel, M., Stevenson, S., Takayabu, I., Turner, J., Ummenhofer, C., Walsh, K., Wang, B., Wang, C., Watterson, I., Widlansky, M., Wittenberg, A., Woollings, T., Yeh, S.W., Zhang, C., Zhang, L., Zheng, X., Zou, L., 2013. Climate phenomena and their relevance for future regional climate change, in: Climate Change 2013 the Physical Science Basis: Working Group I Contribution to the Fifth Assessment Report of the Intergovernmental Panel on Climate Change. Cambridge University Press, pp. 1217–1308. https://doi.org/10.1017/CBO9781107415324.028

Cialone, M.A., Butler, H.L., Amein, M., 1993. DYNLET1 application to Federal Highway Administration projects.

Conver, A., Sepanik, J., Louangsaysongkham, B., 2008. Sea, lake, and overland surges from hurricanes (SLOSH) basin development handbook v2 . 0 31.

Dorst, N., 2019. National Oceanic Atmospheric Administration (NOAA) Hurricane Research Division (HRD) - What is the average forward speed of a hurricane? [WWW Document]. URL https://www.aoml.noaa.gov/hrd/tcfaq/G16.html (accessed 6.1.19).

Elsayed, S.M., Oumeraci, H., 2018. Modelling and mitigation of storm-induced saltwater intrusion: Improvement of the resilience of coastal aquifers against marine floods by subsurface drainage. Environ. Model. Softw. 100, 252–277. https://doi.org/10.1016/j.envsoft.2017.11.030

Emanuel, K.A., 2013. Downscaling CMIP5 climate models shows increased tropical cyclone activity over the 21st century. Proc. Natl. Acad. Sci. 110, 12219–12224. https://doi.org/10.1073/pnas.1301293110

Fiedler, J., Mays, F., Siry, J., Alvarez, R., Cropper, W., Harwell, M., Jagtap, S., Landsea, C., Letson, D., Parker, C., Shivlani, M., Wanless, H., Winchester, J., 2001. Feeling the heat in Florida: Global warming on the local level. Natl. Resour. Def. Counc. Florida Clim. Alliance. https://doi.org/10.1890/1540-9295(2003)001[0508:FTH]2.0.CO;2

Frazier, T.G., Wood, N., Yarnal, B., Bauer, D.H., 2010. Influence of potential sea level rise on societal vulnerability to hurricane storm-surge hazards, Sarasota County, Florida. Appl. Geogr. 30, 490–505. https://doi.org/10.1016/j.apgeog.2010.05.005

Guo, W., Langevin, C.D., 2002. User's Guide to SEAWAT: A Computer Program For Simulation of Ground-Water Flow, Techniques.

Heath, R.C., 1983. Basic Ground-Water Hydrology., US Geological Survey Water Supply Paper. https://doi.org/10.3133/wsp2220

Holding, S., Allen, D.M., 2015. Wave overwash impact on small islands: Generalised observations of freshwater lens response and recovery for multiple hydrogeological settings. J. Hydrol. 529, 1324–1335. https://doi.org/10.1016/j.jhydrol.2015.08.052

Horsburgh, K., Vries, H. de, Etala, P., Murty, T., Seo, J.-W., Dube, S., Lavrenov, I., Holt, M., Daniel, P., Higaki, M., Warren, G., Cabrera, R., Nirupama, N., Paradis, D., Dandin, P., 2011. Guide to Storm Surge Forecasting.

Hughes, M., 2016. Coastal waves, water levels, beach dynamics and climate change.

Irish, J.L., Resio, D.T., Ratcliff, J.J., 2008. The Influence of Storm Size on Hurricane Surge. J. Phys. Oceanogr. 38, 2003–2013. https://doi.org/10.1175/2008jpo3727.1

Keim, B.D., Muller, R.A., Stone, G.W., 2007. Spatiotemporal patterns and return periods of tropical storm and hurricane strikes from Texas to Maine. J. Clim. 20, 3498–3509. https://doi.org/10.1175/JCLI4187.1

Ketabchi, H., Mahmoodzadeh, D., Ataie-Ashtiani, B., Simmons, C.T., 2016. Sea-level rise impacts on seawater intrusion in coastal aquifers: Review and integration. J. Hydrol. 535, 235–255. https://doi.org/10.1016/j.jhydrol.2016.01.083

Knutson, T.R., Sirutis, J.J., Zhao, M., Tuleya, R.E., Bender, M., Vecchi, G.A., Villarini, G., Chavas, D., 2015. Global projections of intense tropical cyclone activity for the late twenty-first century from dynamical downscaling of CMIP5/RCP4.5 scenarios. J. Clim. 28, 7203–7224. https://doi.org/10.1175/JCLI-D-15-0129.1

Knutti, R., Sedláček, J., 2013. Robustness and uncertainties in the new CMIP5 climate model projections. Nat. Clim. Chang. 3, 369–373. https://doi.org/10.1038/nclimate1716

Kooi, H., Groen, J., Leijnse, A., 2000. Modes of seawater intrusion during transgressions. Water Resour. Res. 36, 3581–3589. https://doi.org/10.1029/2000WR900243

Kossin, J.P., 2018. A global slowdown of tropical-cyclone translation speed. Nature 558, 104–107. https://doi.org/10.1038/s41586-018-0158-3

Kossin, J.P., Hall, T., Knutson, T., Kunkel, K.E., Trapp, R.J., Waliser, D.E., Wehner, M.F., 2017. Extreme storms, in: Wuebbles, D.J., Fahey, D.W., Hibbard, K.A., Dokken, D.J., Stewart, B.C., Maycock, T.K. (Eds.), Climate Science Special Report: Fourth National Climate Assessment, Volume I. U.S. Global Change Research Program. https://doi.org/10.7930/J0J964J6

Kuniansky, E.L., Bellino, J.C., 2016. Tabulated transmissivity and storage properties of the Floridan aquifer system in Florida and parts of Georgia, South Carolina, and Alabama (ver. 1.1, May 2016). U.S. Geol. Surv. Data Ser. 669, 37.

Langevin, C.D., Hughes, J.D., Banta, E.R., Provost, A.M., Niswonger, R.G., Panday, S., 2020. MODFLOW 6 Modular Hydrologic Model version 6.2.0: U.S. Geological Survey Software Release.

Langevin, C.D., Thorne, D.T., Dausman, A.M., Sukop, M.C., Guo, W., 2007. SEAWAT Version 4: A Computer Program for Simulation of Multi-Species Solute and Heat Transport: U.S. Geological Survey Techniques and Methods Book 6, Chapter A22 39.

Lin, N., Emanuel, K., Oppenheimer, M., Vanmarcke, E., 2012. Physically based assessment of hurricane surge threat under climate change. Nat. Clim. Chang. 2, 462–467. https://doi.org/10.1038/nclimate1389

Mabrouk, M., Jonoski, A., Essink, G.H.P.O., Uhlenbrook, S., 2019. Assessing the fresh-saline groundwater distribution in the Nile delta aquifer using a 3D variable-density groundwater flow model. Water (Switzerland) 11. https://doi.org/10.3390/w11091946

Malmstadt, J., Scheitlin, K., Elsner, J., 2009. Florida Hurricanes and Damage Costs. Southeast. Geogr. 49, 108–131. https://doi.org/10.1353/sgo.0.0045

Maloney, M.C., Preston, B.L., 2014. A geospatial dataset for U.S. hurricane storm surge and sea-level rise vulnerability: Development and case study applications. Clim. Risk Manag. 2, 26–41. https://doi.org/10.1016/j.crm.2014.02.004

Marella, R., Berndt, M., 2005. Water withdrawals and trends from the Floridan aquifer system in the southeastern United States, 1950-2000. USGS Geol. Surv. Circ. 1278.

Maslia, M.L., Hayes, L.R., 1988. Hydrogeology and simulated effects of ground-water development of the Floridan aquifer system, Southwest Georgia, Northwest Florida, and southernmost Alabama, Professional Paper. https://doi.org/10.3133/pp1403H

McDonald, M.G., Harbaugh, A.W., 1988. A Modular Three-Dimensional Finite-Difference Ground-Water Flow Model: U.S. Geological Survey, Techniques of Water-Resource Investigation 06-A1 586. https://doi.org/10.1016/0022-1694(70)90079-X

Miller, J.A., 1990. Ground Water Atlas of the United States: Segment 6, Alabama, Florida, Georgia, South Carolina, Hydrologic Atlas. https://doi.org/10.3133/ha730G

Miller, J.A., 1986. Hydrogeologic framework of the Floridan Aquifer System in Florida and in parts of Georgia, Alabama, and South Carolina—Regional Aquifer-system Analysis: U.S. Geological Survey Professional Paper 1403–B. U.S. Geol. Surv. Provessional Pap. 1403-B, 91.

Needham, H., Keim, B.D., 2012. Storm Surge: Physical Processes and an Impact Scale. Recent Hurric. Res. - Clim. Dyn. Soc. Impacts. https://doi.org/10.5772/15925

NHC, 2019a. Sea, Lake, and Overland Surges from Hurricanes (SLOSH) [WWW Document]. URL https://www.nhc.noaa.gov/surge/slosh.php (accessed 10.25.19).

NHC, 2019b. National Storm Surge Hazard Maps—Version 2 [WWW Document]. URL https://www.nhc.noaa.gov/nationalsurge/ (accessed 10.10.19).

NJSGC, 2019. Understanding Storm Surge [WWW Document]. URL http://njseagrant.org/education/resources-for-educators/lesson-plans/understanding-storm-surge/ (accessed 10.23.19).

Oude Essink, G., 2019. Personal communication.

Sherif, M.M., Singh, V.P., 1999. Effect of climate change on sea water intrusion in coastal aquifers. Hydrol. Process. 13, 1277–1287.

Simmons, C.T., Narayan, K.A., Wooding, R.A., 1999. On a test case for density-dependent groundwater flow and solute transport models: The salt lake problem. Water Resour. Res. 35, 3607–3620. https://doi.org/10.1029/1999WR900254

Sobel, A.H., Camargo, S.J., Hall, T.M., Lee, C., Tippett, M.K., Wing, A. a, 2016. Human influence on tropical cyclone intensity. Science (80-.). 353.

Sonenshein, R.S., 1997. Delineation of saltwater intrusion in the Biscayne Aquifer, Eastern Dade County, Florida, 1995, Water-Resources Investigations Report. https://doi.org/10.3133/wri964285

Spechler, R.M., Halford, K.J., 2001. Hydrogeology, Water Quality, and Simulated Effects of Ground-Water Withdrawals from the Floridan Aquifer System, Seminole County and Vicinity, Florida. U.S. Geol. Surv. Water-Resources Investig. Rep. 01, 116.

Steyer, G.D., Perez, B.C., Piazza, S., Suir, G., 2007. Potential consequences of saltwater intrusion associated with Hurricanes Katrina and Rita. US Geol. Surv. Circ. 137–146. https://doi.org/10.3133/cir13066c

Tihansky, A.B., 1999. Sinkholes, west-central Florida. L. Subsid. United States US Geol. Surv. Circ. 1182, 121–140.

Trenberth, K.E., Cheng, L., Jacobs, P., Zhang, Y., Fasullo, J., 2018. Hurricane Harvey Links to Ocean Heat Content and Climate Change Adaptation. Earth's Futur. 6, 730–744. https://doi.org/10.1029/2018EF000825

Trenberth, K.E., Fasullo, J., 2008. Energy budgets of Atlantic hurricanes and changes from 1970. Geochemistry, Geophys. Geosystems 9, 1–12. https://doi.org/10.1029/2007GC001847

van Engelen, J., Oude Essink, G.H.P., Kooi, H., Bierkens, M.F.P., 2018. On the origins of hypersaline groundwater in the Nile Delta aquifer. J. Hydrol. 560, 301–317. https://doi.org/10.1016/j.jhydrol.2018.03.029

van Engelen, J., Verkaik, J., King, J., Nofal, E.R., Bierkens, M.F.P., Oude Essink, G.H.P., 2019. A three-dimensional palaeo-reconstruction of the groundwater salinity distribution in the Nile Delta Aquifer. Hydrol. Earth Syst. Sci. Discuss. 1–36. https://doi.org/10.5194/hess-2019-151

Vermeulen, P., Gehrels, H., Stroet, C.T., Kremers, T., 2001. Modelling the impact of surface water management on water conservation and water quality. IAHS-AISH Publ. 173–182.

Vermeulen, P.T.M., Roelofsen, F.J., Minnema, B., Burgering, L.M.T., Verkaik, J., Janssen, G.M.C.M., Romero Verastegui, B., 2020. iMOD User Manual. Version 5.1.

Vermeulen, P.T.M., Roelofsen, F.J., Minnema, B., Burgering, L.M.T., Verkaik, J., Rakotonirina, A.D., 2018. iMOD User Manual. Version 4.3.

Walsh, K.J.E., Mcbride, J.L., Klotzbach, P.J., Balachandran, S., Camargo, S.J., Holland, G., Knutson, T.R., Kossin, J.P., Lee, T. cheung, Sobel, A., Sugi, M., 2016. Tropical cyclones and climate change. Wiley Interdiscip. Rev. Clim. Chang. 7, 65–89. https://doi.org/10.1002/wcc.371

White, E., Kaplan, D., 2017. Restore or retreat? Saltwater intrusion and water management in coastal wetlands. Ecosyst. Heal. Sustain. 3, e01258. https://doi.org/10.1002/ehs2.1258

Williams, L.J., Kuniansky, E.L., 2016. Revised hydrogeologic framework of the Floridan aquifer system in Florida and parts of Georgia, Alabama, and South Carolina (ver. 1.1, March 2016). U.S. Geol. Surv. Prof. Pap. 1807, 140.

Winston, R.B., 2019a. Online Guide to MODFLOW-2005 [WWW Document]. URL https://water.usgs.gov/ogw/modflow/MODFLOW-2005-Guide/ (accessed 10.25.19).

Winston, R.B., 2019b. ModelMuse Help [WWW Document]. URL https://water.usgs.gov/nrp/gwsoftware/ModelMuse/Help/ (accessed 10.25.19).

Wooding, R.A., Tyler, S.W., White, I., Anderson, P.A., 1997. Convection in groundwater below an evaporating salt lake: 1. Onset of instability. Water Resour. Res. 33, 1219–1228. https://doi.org/10.1029/96WR03534

Xiao, H., Wang, D., Medeiros, S.C., Bilskie, M. V., Hagen, S.C., Hall, C.R., 2019. Exploration of the effects of storm surge on the extent of saltwater intrusion into the surficial aquifer in coastal east-central Florida (USA). Sci. Total Environ. 648, 1002–1017. https://doi.org/10.1016/j.scitotenv.2018.08.199

Xiao, H., Wang, D., Medeiros, S.C., Hagen, S.C., Hall, C.R., 2018. Assessing sea-level rise impact on saltwater intrusion into the root zone of a geo-typical area in coastal east-central Florida. Sci. Total Environ. 630, 211–221. https://doi.org/10.1016/j.scitotenv.2018.02.184

Xu, S., Huang, W., 2014. An improved empirical equation for storm surge hydrographs in the Gulf of Mexico, U.S.A. Ocean Eng. 75, 174–179. https://doi.org/10.1016/j.oceaneng.2013.11.004

Yan, M., Lu, C., Yang, J., Xie, Y., Luo, J., Yu, X., 2019. Impact of Low- or High-Permeability Inclusion on Free Convection in a Porous Medium. Geofluids 2019. https://doi.org/10.1155/2019/8609682

Yang, J., Graf, T., Herold, M., Ptak, T., 2013. Modelling the effects of tides and storm surges on coastal aquifers using a coupled surface-subsurface approach. J. Contam. Hydrol. 149, 61–75. https://doi.org/10.1016/j.jconhyd.2013.03.002

Yu, X., Yang, J., Graf, T., Koneshloo, M., O'Neal, M.A., Michael, H.A., 2016. Impact of topography on groundwater salinization due to ocean surge inundation. Water Resour. Res. 52, 5794–5812. https://doi.org/10.1002/2016WR018814

Zachry, B.C., Booth, W.J., Rhome, J.R., Sharon, T.M., 2015. A National View of Storm Surge Risk and Inundation. Weather. Clim. Soc. 7, 109–117. https://doi.org/10.1175/wcas-d-14-00049.1

Zheng, C., Wang, P.P., 1999. MT3DMS: a modular three-dimensional multispecies transport model for simulation of advection, dispersion, and chemical reactions of contaminants in groundwater systems; documentation and user's guide.

The picture on the cover page depicts hurricane Floyd and is based on data from the NOAA GOES satellite. The image is produced by Hal Pierce and is retrieved from NASA's Precipitation Measurement Missions (PMM). https://pmm.nasa.gov/image-gallery/visualization-hurricane-floyd